## Title

Wetland Restoration as a Climate Solution: Assessing the carbon, greenhouse gas, and biophysical impacts of restoring degraded agricultural peatlands to freshwater deltaic wetlands



## Author

Hemes, Kyle Seewald

## Publication Date

2019

Peer reviewed|Thesis/dissertation

# Wetland Restoration as a Climate Solution: Assessing the carbon, greenhouse gas, and biophysical impacts of restoring degraded agricultural peatlands to freshwater deltaic wetlands

by

Kyle S Hemes

A dissertation submitted in partial satisfaction of the
requirements for the degree of

Doctor of Philosophy
in
Environmental Science, Policy, and Management
in the
Graduate Division
of the
University of California, Berkeley

Committee in charge:
Professor Dennis Baldocchi, Chair
Professor Whendee Silver
Professor Iryna Dronova
Professor Paolo D'odorico

Summer 2019

Wetland Restoration as a Climate Solution: Assessing the carbon, greenhouse gas, and biophysical impacts of restoring degraded agricultural peatlands to freshwater deltaic wetlands



by

Kyle S Hemes

Abstract

Wetland Restoration as a Climate Solution: Assessing the carbon, greenhouse gas, and biophysical impacts of restoring degraded agricultural peatlands to freshwater deltaic wetlands

by

Kyle S Hemes

Doctor of Philosophy in Environmental Science, Policy, and Management

University of California, Berkeley

Professor Dennis Baldocchi, Chair

The biosphere removes nearly a quarter of anthropogenic greenhouse gas emissions each year through biogeochemical processes. These fluxes, along with biophysical exchanges of energy and water, play an important role in local to global climate dynamics and human well-being. With an urgent need to decrease the amount of greenhouse gases in the atmosphere to avoid runaway climate change, much recent work has focused on identifying and quantifying the role that terrestrial ecosystems could play in mitigating climate change. Restoration of coastal and deltaic wetlands, with their often carbon-rich organic soils and high productivity, presents an attractive but largely untested land-based climate mitigation strategy.

The benefits associated with wetland restoration stem from two key areas. First, drained agricultural peat soils can be large greenhouse gas sources. Second, the slow decomposition rates of inundated wetland soil organic matter along with high productivity leads to soil carbon accumulation and protection. While these tenets are generally widely appreciated, they have rarely been tested and measured at the ecosystem scale, over multiple years.

In this dissertation work, I studied the coupled biogeochemical and biophysical impacts of a long-term wetland restoration ecological experiment in the Sacramento-San Joaquin River Delta in California, USA. By continuously measuring greenhouse gas and energy fluxes at the ecosystem scale over a variety of land cover types, including four restored wetlands of various ages and structures, I was able to characterize the carbon, greenhouse gas, and biophysical

impacts of degraded peat soil restoration to freshwater deltaic wetlands.

I find that these restored freshwater deltaic wetlands are highly productive, sequestering carbon in the soil as productivity outpaces ecosystem respiration. This productivity comes at the cost of substantial methane emissions, however, making these wetlands greenhouse gas neutral to sources over a century. Despite this fact, transitions from high-emission degraded peat soil agricultural land uses to restored deltaic wetlands often reduce greenhouse gas emissions overall. Furthermore, I analyze how the biophysical impacts of this restoration activity – the changes to the way the ecosystems exchange heat and water – affect the surface temperature and boundary layer. I find that along with potential biogeochemical benefits, restored deltaic wetlands have an evaporative cooling effect due to rougher, wetter canopies.

These findings shed light on the viability of freshwater wetland restoration as a land-based climate mitigation solution. Restored wetlands should be part of a climate solution, but aren't a 'quick fix'. Ecosystem restoration is a dynamic process, with interannual variability, succession, and disturbance influencing the long-term performance of these ecosystems. Despite the incurred methane emissions in our restored wetlands, the flooded conditions effectively inhibit heterotrophic soil respiration and thus sequester carbon and create soil, refilling the deeply subsided 'islands' that have formed over the past century and a half. Other positive co-benefits, like local to regional biophysical cooling, along with habitat enhancement, must be considered to understand the full potential of restored wetlands as a part of the climate solution.

**Table of Contents**

**List of Figures**

**List of Tables**

**Acknowledgements**

A PhD is never completed in isolation. Especially in the case of field projects that span time and space, many hands and minds went into making this research possible. I would like to thank my advisor, Dennis Baldocchi, for his consistently incisive, upbeat, and supportive mentorship and guidance. I have learned so much from both his way of approaching science, and the excitement and passion he brings to his work every day. I also wish to recognize members of both my qualifying and dissertation committees for guiding and challenging me along the way. I would like to thank all my many lab-mates - undergraduates, graduate students, postdoctoral fellows, researchers, and lab technicians - for their support and collaboration. I especially appreciate the close collaboration and mentorship from postdocs Elke Eichelmann and Sam Chamberlain. None of this work would have been possible without the lab technicians, Joe Verfaillie and Daphne Szutu, who kept so many pieces of this research network running spectacularly.

I have my parents to thank for opening up the world to me, and providing me the opportunities to find myself in this position. To my mother, Lois, for instilling in me a desire to serve, and a strong work ethic with which to do it. And to my father, Joe, for engaging my scientific creativity and love of the natural world.

And finally, I couldn't and wouldn't have done this without the loving and unconditional support of my partner, Simone. She has inspired me to tap into my own inner confidence and persistence that has served me in this PhD process.

I would like to recognize the work of all Berkeley Biometeorology Lab members throughout the years who helped maintain towers and collect and proces data over the lifetime of these sites. We thank the California Department of Water Resources and the Metropolitan Water District of Southern California for collaboration and access to research sites, and the Delta farmers for their cooperation as we made measurements alongside their farm operations.

This work was supported by the California Department of Water Resources (DWR), through a contract from the California Department of Fish and Wildlife, and the United States Department of Agriculture. Funding for the AmeriFlux core sites was provided by the U.S. Department of Energy's Office of Science. Through the Delta Science Fellowship, Kyle was supported during much of this work by the Delta Stewardship Council Delta Science Program and California Sea Grant College Program.

All Delta sites used in this analysis are part of the Ameriflux network, with data available at http://ameriflux.lbl.gov/. Portions of this dissertation have been reprinted from *Geophysical Research Letters*, *Agriculture & Forest Meteorology*, and the *Journal of Geophysical Research: Biogeosciences*.

# 1 Introduction

## *1.1 Land-based climate change mitigation*

Natural and working lands play an important role in terrestrial carbon cycling, with the potential to be a source or a sink of carbon dioxide ($CO_2$) and other greenhouse gases (GHG) (Friedlingstein et al., 2014). The IPCC 5$^{th}$ assessment report states that reversibility of anthropogenic climate change will only be possible with "large net removal of $CO_2$ from the atmosphere over a sustained period" (Myhre et al., 2013), making carbon (C) sequestration by ecosystems a critical component of any climate stabilization pathway. International and sub-national climate change policies and agreements, including the Kyoto protocol (UNFCCC, 1997), the Paris Agreement (UNFCCC, 2015), and California's climate change targets (Nunez and Pavley, 2006), intend to leverage natural and working ecosystems to contribute to mitigation targets. More recently, the IPCC's 1.5°C Special Report outlined the important role that the 'agriculture, forestry and other land use' sector will play in keeping global average temperature within this ambitious target (Rogelj et al., 2018b).

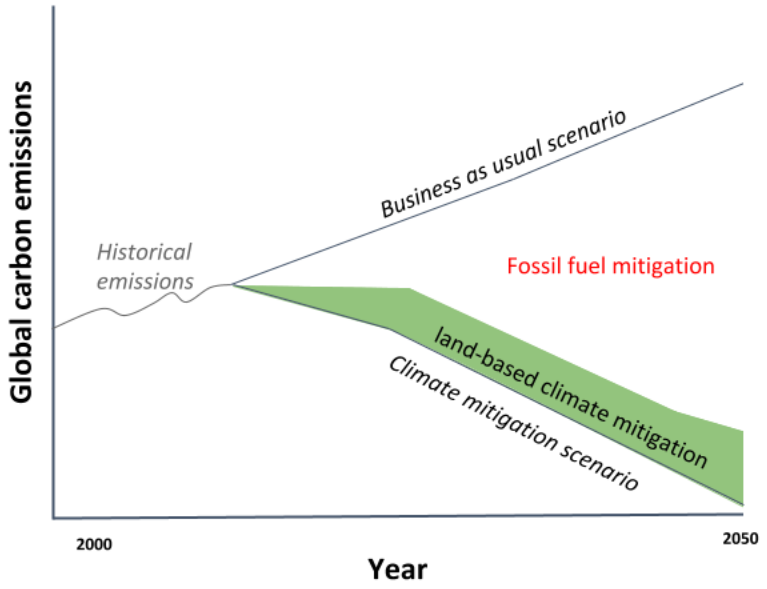


*Figure 1.1: Schematic cartoon of global carbon emissions and potential pathways reliant on land-based climate mitigation*

Despite a flurry of policy intentions and investment in creating and maintaining resilient land-based C sinks, there is an incomplete understanding of the coupled local, regional and global climate impacts and tradeoffs inherent in these proposed land-use changes (Bonan, 2008; Luyssaert et al., 2018; Perugini et al., 2017). Carbon dioxide removal through land cover and

land management changes can serve two purposes: 1) to hasten movement toward C neutrality and stabilize global temperature rise and 2) to remove atmospheric $CO_2$ after an overshoot (Rogelj et al., 2018b).

Many ambitious climate change mitigation scenarios are front-loaded with land-based C sequestration, with 1.5°C pathways featuring substantially more $CO_2$ removal through mid-century than 2.0°C pathways (Rogelj et al., 2018a). Because of this up-front reliance on land-based climate mitigation strategies (Figure 1.1), unintended side effects of these policies have a disproportionate potential to influence support for future mitigation policy. For these reasons, it is imperative to have as complete an understanding as possible of the impacts of these types of strategies.

Land cover and land management change affect climate by altering both the biogeochemical and biophysical processes that govern the exchange of C, water, and energy between the land and atmosphere (Bonan, 2008; Erb et al., 2017). Biogeochemical impacts are caused by changes in exchange rates of C and nitrogen (N) between ecosystems and the atmosphere (Arneth et al., 2010; Tian et al., 2016). These impacts result in emissions that are often long-lived, well-mixed, and global in scale. The GHGs that are most impacted by land cover and land management change are $CO_2$, methane ($CH_4$), and nitrous oxide ($N_2O$), each with different atmospheric lifetimes, potencies, sources and sinks (Table 1.1). Land cover or land management changes that affect multiple GHGs, often in varying magnitudes and directions, make the net climate effect of certain land-based interventions especially challenging to characterize in the long term. Methane, is of special importance, as the recently observed sharp rise in atmospheric concentration along with a negative isotopic trend suggests a surge in biogenic wetland- and agriculture-related $CH_4$ emissions, especially from the tropics (Nisbet et al., 2019, 2016)

| *Greenhouse gas* | *Atmospheric lifetime* | *Global warming potential*[1] | *Sustained global warming potential*[2] | *Major biogenic sources* | *Major biogenic sinks* |
|---|---|---|---|---|---|
| Carbon dioxide ($CO_2$) | > centuries | - | - | autotrophic plant respiration, heterotrophic soil respiration, decomposition, wildfires | vegetation photosynthesis, ocean uptake |
| Methane ($CH_4$) | ~ 12 years | 34 (100-year GWP) | 45 (100-year SGWP) | freshwater wetlands, rice agriculture, ruminants, saturated soil, wildfires, permafrost | upland soils, atmospheric OH reactions |

| | | | | | |
|---|---|---|---|---|---|
| Nitrous oxide ($N_2O$) | ~121 years | 298 (100-year GWP) | 270 (100-year SGWP) | fertilized agriculture, livestock | upland soils |

*Table 1.1: Greenhouse gases most affected by land cover and land management change. [1](Myhre et al., 2013); [2](Neubauer and Megonigal, 2015)*

While biogeochemical impacts of land-based climate mitigation are most often addressed in policy and strategy, biophysical impacts are often overlooked. Biophysical impacts of land cover and land management changes include alterations to surface albedo, the partitioning of available energy between sensible and latent heat, and changes in surface roughness (Burakowski et al., 2017; Mahmood et al., 2014; Perugini et al., 2017; Zhao and Jackson, 2014) (Table 1.2). These biophysical impacts are fixed geographically, potentially reversible as land is restored, and commonly local to regional in scale. At a large enough spatial extent, however, there is evidence that these types of biophysical changes could lead to important continent-scale teleconnections (Laguë and Swann, 2016; Swann and Lague, 2018).

| *Biophysical impact* | *Definition and mechanism* | *Potential local to regional climate impacts* |
|---|---|---|
| surface albedo | shortwave reflectance | higher albedo will result in less available net radiation; lower albedo will result in more available net radiation |
| partitioning of surface energy fluxes | available energy will be partitioned between sensible and latent heat | enhanced latent heat flux can cause an evaporative cooling effect; enhanced sensible heat flux can cause increased air temperature |
| surface roughness | canopy architecture will change friction velocity and roughness | enhanced roughness will promote turbulent heat fluxes (sensible and latent heat flux) away from the surface, and result in a canopy more coupled to the atmosphere |

*Table 1.2: Primary biophysical impacts of land cover and land management change*

A number of land cover changes and land management practices for $CO_2$ removal have been proposed (Erb et al., 2018; Fargione et al., 2018; Griscom et al., 2017), including forest management (Zhao and Jackson, 2014), agriculture soil practices (Paustian et al., 2016) and peatland restoration (Leifeld and Menichetti, 2018). Upper-envelope estimates, depending on the price of C, show that land-based climate mitigation strategies could increase C storage and avoid emissions equivalent to 23.8 Pg $CO_2e$ $yr^{-1}$ globally (Griscom et al., 2017), or more than a fifth of net United States emissions (Fargione et al., 2018) at a fraction of the cost of more technological $CO_2$ removal strategies (Psarras et al., 2017). Many pathways to staying below

1.5°C require large areas of land cover change, especially before mid-century, while other forms of mitigation ramp up (Rogelj et al., 2018b, 2018a).

These 'upper-envelope' estimates of land-based climate mitigation, however, carry large uncertainties, and many strategies are yet to be meaningfully tested on the ground or over long time periods. There is concern that reliance on land-based C sinks, without a realistic accounting of unintended biogeochemical and biophysical feedbacks as well as physical limits, could 'distract' policymakers and the general public from urgently needed decarbonization in the most carbon-intensive sectors of the economy (Anderson et al., 2019; Baldocchi and Panuelas, 2018; Schlesinger and Amundson, 2018). The considerable uncertainty, coupled with political interest, makes observational ecological experiments of land-based climate mitigation strategies all the more valuable as a means to ground-truth the potential of these strategies.

### *1.2 Wetland restoration as a climate mitigation solution*

Coastal and freshwater wetland restoration, as well as peatland restoration, have been identified as priority land-based climate mitigation strategies (Fargione et al., 2018; Griscom et al., 2017; Leifeld and Menichetti, 2018; Moomaw et al., 2018; Paustian et al., 2016). Peatlands alone, while encompassing less than 3% of the global terrestrial land area, harbor nearly a quarter of the global soil carbon stocks (Yu, 2012). In addition to the potential for carbon sequestration in restored coastal wetlands and peatlands, restoration is attractive as a means of climate adaptation to sea level rise and storm surges (Mitsch and Mander, 2018; Moomaw et al., 2018; Windham-Myers et al., 2018).

The benefits associated with wetland restoration for avoided emissions and enhanced C sequestration stem from two key areas. First, drained agricultural peat soils can be large GHG sources (Hatala et al., 2012; Knox et al., 2015; Schrier-Uijl et al., 2014; Veber et al., 2017). As organic-rich soils are drained and exposed to the atmosphere, aerobic respiration leads to large $CO_2$ emissions relative to flooded or saturated conditions that inhibit aerobic respiration. This $CO_2$ source, along with emissions of other potent agricultural GHGs like $CH_4$ and $N_2O$, can cause agricultural peat soils to be significant net emitters. By restoring these subsided lands to managed wetlands, these agricultural emissions can be avoided. Second, the slow decomposition rates of wetland soil organic matter along with high net primary productivity leads to soil carbon accumulation. Maintaining wetland structure and function can protect much of the sequestered C and associated N from organic matter mineralization, leading to the potential for long-term C storage and lower $N_2O$ emissions (Deverel et al., 2016, 2014; Yarwood, 2018).

Estimates of the potential mitigative effects of avoiding peatland and wetland drainage and restoring wetlands are highly uncertain. While the potential extent of this strategy is small compared to many land-based climate mitigation strategies, the magnitude of avoided or removed GHGs tends to be comparatively large. A soil-focused survey found that restoring drained organic soils could avoid and remove 0.3-1.3 Pg $CO_2$-eq $yr^{-1}$ (Paustian et al., 2016). The combined strategies of avoiding coastal wetland and peatland impacts, as well as restoring already degraded systems, could result in mitigation of 2.7 (95% CI: 2.4-4.5) Pg $CO_2$-eq $yr^{-1}$ globally, or 14% of ecosystem-mitigation opportunities to keep global mean warming to less than 2°C, according to an upper-envelope global synthesis of 'natural climate solutions' (Griscom et al., 2017). Due to uncertainty in restored peat wetland $CH_4$ dynamics, this study assumed that enhanced $CH_4$ is completely offset by higher $CO_2$ sequestration. Other work has shown that restoring degraded peatlands could avoid the equivalent of 1.91 Pg $CO_2$-eq globally, but similarly assumed that peatland restoration results in a GHG-neutral ecosystem (Leifeld and Menichetti, 2018). I test these assumptions in Chapter 2 (Hemes et al., 2018a), and in Chapter 3 (Hemes et al., 2019), analyze the multi-year measured net carbon and GHG impact of wetland restoration in what is one of the longest continuous field experiments of this kind of land-based climate mitigation strategy.

### *1.3 Eddy covariance and ecosystem-scale measurements*

Fluxes represent the quantity of energy or mass that passes through a certain area during a certain amount of time. At the ecosystem scale, land-atmosphere fluxes represent important components of the mass balance of soil and vegetation, giving us an integrated approximation of how environmental drivers affect ecosystem physiology (Baldocchi, 2014). The first ecosystem-scale measurements of trace gas exchange were approximated through basic tree measurements (diameter and height) scaled to total biomass through the use of allometric equations (Whittaker et al., 1974). This method is still popular for its low-tech reproducibility, but misses important belowground carbon pools and is limited in its spatial and temporal resolution, due to the high labor intensity of the practice. Chamber-based measurements are effective for understanding fluxes from the leaf to plant scale (Mooney et al., 1971), but can cause measurement artifacts due to the need for an enclosure. Upscaling chamber-based fluxes to the ecosystem scale, especially in complex natural systems, can be challenging due to the limited spatial resolution of this method.

Eddy covariance, with its spatially integrated and nearly continuous measurements, provides the only direct measurement of the mass and energy flux density between land and atmosphere across a large domain (Baldocchi, 2014; Baldocchi et al., 1988). While the method does suffer from challenges closing the energy balance (Leuning et al., 2012; Wilson et al., 2002), in very stable nighttime conditions (Aubinet, 2008), with heterogenous fetches, or in non-ideal terrain

(Aubinet et al., 2003), it has become widespread, open-source and standardized (Baldocchi et al., 2001; Novick et al., 2018).

The heterogeneous and continuous nature of ecosystem GHG emissions requires long-term spatially integrated measurements to fully characterize temporal and spatial variability (Baldocchi, 2003). Even contemporary ecology struggles to measure at temporal and spatial scales that match the processes and underlying mechanisms being observed (Estes et al., 2018). The vast majority of collocated wetland $CO_2$ and $CH_4$ flux measurements to date have been made using chamber methods that sample limited spatial and temporal scales (Bridgham et al., 2006; Frolking et al., 2011; Meng et al., 2016). To directly measure the climatic effects of potential land-based mitigation strategies, both in terms of biogeochemical mass exchange of multiple relevant GHGs and biophysical energy fluxes, eddy covariance is an appropriate method. We complement this 10-20 Hz record with extensive measurements of environmental and meteorological drivers at the tower site (Eichelmann et al., 2018).

### *1.4 Dissertation scope and summary*

In this dissertation work, I studied the coupled biogeochemical and biophysical impacts of a long-term wetland restoration ecological experiment in the Sacramento-San Joaquin River Delta (hereafter, Delta) in California, USA. I employed a network of eight eddy covariance flux towers continuously measuring GHG and energy fluxes at the ecosystem scale over a variety of land cover types, which allowed me to characterize the GHG, C, and biophysical impacts of degraded peat soil restoration to freshwater deltaic wetlands.

In addition to climate change mitigation, restoration is motivated by the need to combat soil subsidence caused by decades of drainage and soil C oxidation in the Delta (Deverel et al., 2016; Deverel and Leighton, 2010; Drexler et al., 2009; Mount and Twiss, 2005; Weir, 1950). Like many river deltas around the world, anthropogenic hydrological modifications exposed C-rich soil to the atmosphere, catalyzing soil oxidation and leading to the sinking of the land surface (Syvitski et al., 2009). Once a 1400 $km^2$ wetland and riparian flood plain draining two of California's largest rivers, the modern Delta is today a series of subsided islands, ringed by levees, and dominated by agricultural land uses like corn, alfalfa, and pasture. Responsible for providing at least a portion of the drinking water to more than two-thirds of Californians (Miller et al., 2008), the Delta is a contested waterscape, characterized by interlinked climate, soil, and water challenges. These complex challenges provide an interesting backdrop to test, at an ecosystem scale, the climatic impacts of freshwater wetland restoration.

In the second chapter (Hemes et al., 2018a), I will analyze the Delta sites in the context of other restored wetlands and peatlands around the world, to understand what I call a 'biogeochemical compromise' – the flooding-induced inhibition of aerobic respiration at the cost of anaerobic emissions of $CH_4$ (Bridgham et al., 2013). I explore how this compromise compares to that of other restored and natural wetlands around the world, and the global wetland modeling implications of this result. I will test the assumption from the literature that restored wetlands or peatlands will be GHG neutral (Griscom et al., 2017; Leifeld and Menichetti, 2018).

In the third chapter (Hemes et al., 2019), I look more broadly across the network of land use types in the Delta to understand the complete, multiyear C and GHG budgets associated with land use conversions from agriculture on degraded peat soil to restored wetlands of various ages and structure. This work will explicitly address the discrepancy in net radiative forcing associated with various conceptualizations of the global warming potential of $CH_4$ and $N_2O$ (Allen et al., 2018, 2016; Neubauer and Megonigal, 2015). The chapter is designed to be relevant for policymakers interested in incentivizing climate mitigation wetland restoration practices in the Delta.

In the fourth chapter (Hemes et al., 2018b), I will go beyond the biogeochemical impacts to assess the biophysical implications of wetland restoration from one of the dominant agricultural land cover types in the Delta, alfalfa. This study will use eddy covariance data to derive aerodynamic surface properties and temperature, with the goal of understanding how commonly-unaccounted for biophysical impacts of novel land use changes like wetland restoration could attenuate or enhance the potential biogeochemical effects at local to regional scales. While these biophysical effects are beginning to be recognized in forest-related landscapes (Anderson et al., 2011; Bonan, 2008; Lee et al., 2011), other land-based climate mitigation strategies like wetland restoration (Fargione et al., 2018; Griscom et al., 2017; Leifeld and Menichetti, 2018) rarely take into consideration these important biophysical feedbacks.

# 2 A biogeochemical compromise: The high methane cost of sequestering carbon in restored wetlands[1]

## *2.1 Abstract*

Peatland drainage is an important driver of global soil carbon loss and carbon dioxide ($CO_2$) emissions. Restoration of peatlands by re-flooding reverses $CO_2$ losses at the cost of increased methane ($CH_4$) emissions, presenting a biogeochemical compromise. While restoring peatlands is a potentially effective method for sequestering carbon, the terms of this compromise are not well constrained. Here, we present fourteen site-years of continuous $CH_4$ and $CO_2$ ecosystem-scale gas exchange over a network of restored freshwater wetlands in California, where long growing seasons, warm weather, and managed water tables result in some of the largest wetland ecosystem $CH_4$ emissions ever recorded. These large $CH_4$ emissions cause the wetlands to be strong GHG sources, while sequestering carbon and building peat soil. The terms of this biogeochemical compromise, dictated by the ratio between carbon sequestration and $CH_4$ emission, vary considerably across small spatial scales, despite nearly identical wetland climate, hydrology, and plant community compositions.

## *2.2 Introduction*

Peatland loss is a globally widespread and important driver of our global soil carbon debt (Sanderman et al., 2017). As carbon (C) rich soil is exposed to the atmosphere through draining and hydrological modification, the organic C is rapidly oxidized. Restoration of drained peatlands to wetlands has been promoted as a climate mitigation tactic, as it can effectively reverse soil loss and prevent further carbon dioxide ($CO_2$) emissions, with numerous hydrologic and habitat co-benefits (Griscom et al., 2017; Leifeld and Menichetti, 2018; Paustian et al., 2016). A review of natural climate solutions suggests that restoring peatlands and avoiding peatland degradation could mitigate emissions of ~1500 Tg $CO_2$eq. $yr^{-1}$ (Griscom et al., 2017), while others estimate that restoring drained peatlands could avoid the equivalent of ~1910 Tg $CO_2$eq. $yr^{-1}$ (Leifeld and Menichetti, 2018).

Restoring drained peatlands comes with a biogeochemical compromise – inhibit aerobic respiration at the cost of anaerobic emissions of methane ($CH_4$), the second most important greenhouse gas (GHG) to anthropogenic radiative forcing (Bridgham et al., 2013; Myhre et al.,

[1] originally published as: Hemes, K.S., Chamberlain, S.D., Eichelmann, E., Knox, S.H., Baldocchi, D.D., 2018. A Biogeochemical Compromise: The High Methane Cost of Sequestering Carbon in Restored Wetlands. Geophys. Res. Lett. https://doi.org/10.1029/2018GL077747

2013). The balance between these two GHG fluxes primarily determines if a wetland is a GHG source or sink (Frolking et al., 2011; Petrescu et al., 2015) and understanding drivers of these fluxes is essential to our understanding of future climate (Poulter and et al, 2017; Z. Zhang et al., 2017). The biogeochemical compromise between C sequestration and $CH_4$ emissions has been previously recognized and documented (Hoper et al., 2008; Petrescu et al., 2015), but remains an 'enigma' that may hinder investment in wetland restoration and creation for a suite of ecosystem services (Mitsch and Mander, 2018). Despite a need for better quantification, the vast majority of collocated wetland $CO_2$ and $CH_4$ flux measurements to-date have been made in mid- to high-latitude biomes, often using chamber methods that sample limited spatial and temporal scales (Bridgham et al., 2006; Frolking et al., 2011; Meng et al., 2016).

For restored peatlands, the terms of the biogeochemical compromise are not well constrained, especially since wetlands are the largest and most uncertain atmospheric $CH_4$ source (Kirschke et al., 2013; Poulter and et al, 2017; Saunois et al., 2016). These uncertainties are particularly high in productive regions with long growing seasons, such as tropical, subtropical, and Mediterranean biomes, where long-term ecosystem-scale measurements are lacking. Recent isotopic analyses have attributed the dramatic rise in global atmospheric $CH_4$ emissions to tropical wetlands, agriculture, or livestock (Kirschke et al., 2013; Nisbet et al., 2016; Schaefer et al., 2016), although other work questions the assumptions of a constant atmospheric hydroxyl sink (Turner et al., 2017; Worden et al., 2017). Long-term, continuous, ecosystem-scale measurement campaigns such as those that we present here fill an important observational gap (Estes et al., 2018) and allow for a better understanding of $CH_4$ emissions and their contribution to overall wetland GHG budgets.

The Sacramento-San Joaquin Delta (hereafter, 'Delta'), in northern California's Central Valley, provides an ideal ecosystem to understand restored peatland ecosystem GHG fluxes. Seven thousand years of organic matter buildup in Delta freshwater marshes produced a carbon-rich peat layer up to 15 meters deep (Drexler et al., 2009; Weir, 1950). Much of this C was removed in merely a century and a half through levee building, drainage, and eventual subsidence – the sinking of the land surface as soil C was exposed to the atmosphere and oxidized to $CO_2$ (Deverel et al., 2016). Wetland drainage and subsidence is not unique to the Delta (Moomaw et al., 2018); many economically and ecologically important river deltas around the world are sinking at rates faster than sea levels are rising (Syvitski et al., 2009). In order to avoid the large $CO_2$ emissions that result from oxidizing drained peat soils (Knox et al., 2015), subsided delta peatlands are currently being re-flooded to harness a multitude of environmental benefits, including nutrient retention, habitat preservation, storm protection, in addition to soil accretion through C sequestration (Himes-Cornell et al., 2018; Paustian et al., 2016). The net climate benefit associated with restoration, however, is highly uncertain (Deverel et al., 2017; Hoper et al., 2008; Neubauer, 2014).

Wetland and peatland restoration comes in many forms. While 'restoration' connotes a return to the original, pre-industrial ecosystem, ecological hysteresis often prevents this outcome (Hoper et al., 2008; Johnson et al., 2017; Suding et al., 2015). Prior to drainage, more than 150 years ago, the Delta was made up of intertidal wetlands where seasonal snowmelt from the Sierra Nevada mountains would alter salinity and create a flood-based disturbance regime (Brown and Pasternack, 2005). In the Delta today, major modifications to hydrologic connectivity, salinity, plant community composition, and soil stocks make it impossible to truly 'restore' these wetlands to their pre-industrial state. This results in 'rehabilitated' wetlands that should be considered novel ecosystems – sharing some common hydrological conditions and plant species with their pre-industrial predecessor, but in no way biogeochemically or ecologically identical.

'Wet' restoration in the Delta engineers a system where freshwater inputs keep the water table above the land surface, features emergent, arenchymous plants, and is distinct from other restoration practices in less productive fens and bogs. Other techniques like 'dry' restoration, which maintains the water table below the surface, or 'moist' ditch rewetting, allow for an oxic zone for $CH_4$ oxidation near the surface, and have been shown to reduce $CH_4$. Largely owing to geography, climate, peat type, and restoration management, there is considerable variability in emissions from restored peatlands (Hoper et al., 2008). We use 'wetland restoration' to refer to management of the water table above the ground surface in an effort to inhibit aerobic soil respiration and maximize soil C accretion.

Here, we report results from continuous wetland ecosystem $CH_4$ and $CO_2$ exchange, spanning fourteen site-years across three restored wetland sites in the Delta. A confluence of factors, including historic peat buildup, long growing seasons, warm weather, and managed water tables result in significant net C sequestration, along with some of the largest wetland ecosystem $CH_4$ emissions recorded. We compare our results with other restored or natural wetlands, for which annual or near-annual ecosystem-scale measurements of $CO_2$ and $CH_4$ are available. We also discuss the scaling of C sequestration and $CH_4$ emissions across these sites of nearly identical meteorology and management, with implications to global $CH_4$ modeling and biological sequestration strategies.

### *2.3 Sites and Data*

The Sacramento-San Joaquin Delta lies at the confluence of two of California's major rivers and formed a historic 1400 $km^2$ freshwater wetland landscape near-sea level (Atwater et al., 1979). In the mid-19$^{th}$ century, the region was diked and drained for agricultural purposes, exposing deep peat soils to oxygen. Today, more than 1700 km of dikes and levees hold back the rivers

and sloughs that make up the modern Delta (Mount and Twiss, 2005). The Delta is critical to California's water storage and transport system; providing at least a portion of the drinking water to two-thirds of Californians through the State Water Project and the Central Valley Project (Miller et al., 2008). The Delta's wetland soils are highly organic with the remaining peat estimated to be 4,000-6,000 years old (Drexler et al., 2007; Weir, 1950).

The sites considered for this study are impounded freshwater wetlands, with managed water tables that create consistent anaerobic conditions. Mediterranean 1 ('East End', Ameriflux ID: US-TW4, 38°6.17'N, 121°38.48'W) is a 323 hectare (ha) wetland restored in 2013, Mediterranean 2 ('Mayberry', Ameriflux ID: US-MYB, 38°2.99'N, 121°45.90'W) is a 121 ha wetland restored in 2010, and Mediterranean 3 ('West Pond', Ameriflux ID: US-TW1, 38°6.44'N, 121°38.81'W) is a 3 ha wetland restored in 1997. The three wetlands, each vegetated primarily with *Typha spp*. and *Schoenoplectus acutus*, differ slightly in their aerial extent, bathymetry, and age, but are all subject to identical meteorological conditions due to their close spatial proximity (< 13 km). More details about the environmental conditions at each site can be found in recent publications (Chamberlain et al., 2018; Eichelmann et al., 2018; Hatala et al., 2012; Knox et al., 2015).

We measured gas concentrations using open-path infrared gas analyzers (LI-7500 or LI-7500A for $CO_2$, $H_2O$, LI-7700 for $CH_4$, LI-COR Inc., Lincoln, NE, USA) that were calibrated every 3-6 months, and three-dimensional wind speed and direction using sonic anemometers (WindMaster Pro 1352, Gill Instruments Ltd, Lymington, Hampshire, England) at a 20 Hz frequency. All instruments were mounted on towers at a height of ~5 meters above the ground and oriented to prevent interference with winds from the dominant direction. Fluxes were calculated from the 30-minute covariance of vertical wind speed and a scalar of interest after applying a series of standard and site-specific corrections (Detto et al., 2010; Hatala et al., 2012; Knox et al., 2015). Coordinate rotations were performed so that mean wind speeds at each 30-minute averaging interval were zero in the cross-wind and vertical directions. Webb-Pearman-Leuning corrections were applied to $CO_2$ and $CH_4$ fluxes to account for air density fluctuations (Chamberlain et al., 2017b; Webb et al., 1980). These density corrections typically account for an adjustment of less than 10% of the daily wetland $CH_4$ flux (Chamberlain et al., 2017b).

Half hourly fluxes were filtered for stability and turbulence, friction velocity, wind direction, and spikes in mean densities, variance and covariance to remove flux data measured during non-ideal conditions. We gap filled fluxes by training Artificial Neural Networks (ANN) using meteorological variables (Moffat et al., 2007; Papale et al., 2006), where training, testing, and validation data was selected from a series of k-means clusters to avoid seasonal or diurnal bias (Mathworks, Inc. 2012). Network architecture with varying levels of complexity were tested,

with the simplest architecture selected for which further increases in complexity yielded less than a 5% reduction in mean standard error (Knox et al., 2015). This entire ANN procedure was repeated to produce 20 separate ANNs, and the median of the 20 ANNs was used to fill gaps in the annual data.

Uncertainty was estimated from both random half-hourly measurement error and ANN gap-filling error. For measured half hours, draws from a Laplace distribution parameterized by the residuals of the ANN predictions (binned by flux magnitude) was used as an estimate of the random error (Moffat et al., 2007; Richardson and Hollinger, 2007). For gap-filled half hours, the variance of the cumulative sum of the 20 ANN predictions was used as a measure of uncertainty (Anderson et al., 2016; Knox et al., 2018). Adding the cumulative and random measurement uncertainties in quadrature results in the total uncertainty reported alongside annual sums of gap filled fluxes (Richardson and Hollinger, 2007).

While the Intergovernmental Panel on Climate Change (IPCC) updated the 100-year global warming potential (GWP) of $CH_4$ from 25 to 34 $CO_2$ equivalents ($CO_2$eq-) in its fifth assessment report (Myhre et al., 2013), other work has pointed out the pitfalls with utilizing such an approach designed for a pulse emission (Frolking and Roulet, 2007; Neubauer, 2014). We calculated annual GHG budgets using the 100-year sustained global warming potential (SGWP) proposed by Neubauer and Megonigal (2015), which better captures the radiative forcing implications of a persistent ecosystem emission. This metric relies on an atmospheric perturbation model and quantifies the balance between $CO_2$ sequestration and sustained $CH_4$ emissions characteristic of wetland ecosystems. Our sequestration calculations ignore allochthonous lateral transport of dissolved organic and inorganic C (unless explicitly reported as in Chu et al. (2015); Jammet et al. (2017)), which for the impounded Delta sites is likely negligible.

Literature values of wetland $CH_4$ and $CO_2$ measurements were compiled from Petrescu et al. (2015) as well as more recently published studies and grouped by latitude and wetland type (Table 2.1). Only annual or near-annual eddy covariance studies measuring both $CO_2$ and $CH_4$, from restored or natural wetlands, in addition to a subtropical inundated pasture (Chamberlain et al., 2017a, 2016) are reported here. Interpolations based on seasonal measurements, where necessary, are detailed in Petrescu et al. (2015). More information can be found in the supporting information and existing literature (Chamberlain et al., 2017a; Chu et al., 2015; Desai et al., 2015; Flanagan and Syed, 2011; Friborg et al., 2003, 2000; Herbst et al., 2013; Holm et al., 2016; Jammet et al., 2017; Krauss et al., 2016; Lee et al., 2016; Long et al., 2010; Mastepanov et al., 2008; Olson et al., 2013; Parmentier et al., 2011; Pugh et al., 2017; Rinne et al., 2007; Sachs et al., 2010, 2008; Shurpali et al., 1993; Tiemeyer, 2013; Zhang et al., 2012; Zona et al., 2009).

| *Climate Zone* | *Site name, location* | *Coordinates* | *Ecosystem description* | *Measurement period* | *gC-$CO_2$ $m^{-2}yr^{-1}$* | *$CO_2$ (S/Y)* | *gC-$CH_4$ $m^{-2}yr^{-1}$* | *$CH_4$ (S/Y)* | Citation |
|---|---|---|---|---|---|---|---|---|---|
| Temperate | Plotnikovo, RUS | 56° 51’ N, 82° 58’ E | Mesotrophic fen | 10 May 1999 - 16 September 1999 | -108.00 | S | 19.52 | S | Friborg et al., 2003 |
| | Spreewald, DEU | 51°53' N, 14°02' E | Treed wetland (marsh) | CO2: 8 April - 23 May 2011; CH4: 2011 | -122.73 | Y | 0.20 | S | Tiemeyer, 2013 |
| | Park Falls, WI, USA | 45° 57' N, 90° 16' W | Mixed forest/wetland (28%) landscape (bog) | 2011-2012 | -80.00 | Y | 0.79 | Y | Desai et al., 2015 |
| | Fäjemyr, SWE | 56° 15’ N, 13° 33’ E | Ombrotrophic bog | 06 Feb – 31 Dec 2008, 20 January – 31 Dec 2009 | -30.00 | S | 2.15 | S | Mastepanov et al., 2008 |
| | Lake Erie, OH, USA | 41°27' N, 82°59' W | Emergent freshwater marsh | March 2011-March 2013 | 14.60 | Y | 50.80 | Y | Chu et al., 2015 |
| | Bog lake peatland, MN, USA | 47° 32’ N, 93° 28’ W | Open ombrotrophic bog | 20 May - 12 Oct 1991 & 1992 | 19.64 | S | 10.88 | Y | Shurpali et al., 1993; 1995 |
| | Bog lake peatland, MN, USA | 47° 32’ N, 93° 28’ W | Open ombrotrophic bog | May-Oct 2009-2011 | -35.27 | Y | 16.30 | Y | Olson et al., 2013 |
| | Burns Bog, Delta, BC, CAN | 49° 07' N, 122° 59' W | Rewetted coastal raised bog | 16 June 2015 - 15 June 2016 | -179.00 | Y | 17.00 | Y | Lee et al., 2016 |

| | | | | | | | | | |
|---|---|---|---|---|---|---|---|---|---|
| | Western Peatland, Athabasca, Alberta, CAN | 54° 57' N, 112° 28' W | Moderately rich treed fen | CO2: Aug 2003 - September 2009; CH4: May - September 2007 | -188.45 | S | 2.40 | S | Flanagan and Syed, 2011; Long et al., 2010 |
| | Siikaneva, FIN | 61°50'N, 24°12'E | Boreal oligotrophic fen | CH4: March 2005-Feb 2006; CO2: 2005 | -42.55 | Y | 9.46 | Y | Rinne et al., 2007 |
| | Lost Creek Wetland, WI, USA | 46°N, 89° W | Shrub wetland (marsh) | CO2: 2000-present; CH4: 2014-present | 0.00* | Y | 51.00 | Y | Pugh et al., 2017 |
| | Skjern Meadows, DEN | 55° 54′ N, 8°24′ E | Restored wetland peatland (marsh) | 2009-2011 | -142.27 | Y | 10.51 | Y | Herbst et al., 2013 |
| Arctic | Zackenberg, GREENLAND | 74°30' N, 21°00' W | Continuous permafrost fen | 01 June - 26 August 1997 | -35.18 | S | 3.00 | S | Friborg et al., 2000 |
| | Kytalyk, RUS | 70°49′ N, 147°29′ E | Wetland tundra | 08 July - 24 August 2007-2009 | -88.36 | S | 2.48 | S | Parmentier et al., 2011 |
| | Lena Delta, RUS | 72°22'N, 126°30'E | Wetland tundra polygons | 11 June- 3 September 2006 | -34.36 | S | 1.21 | S | Runkle et al., 2013; Sachs et al., 2008; 2010; Zhang et al., 2012 |
| | Stordalen, SWE | 68°20' N, 19°03' E | Fen | 1 June 2012 - 31 May 2014 | -66.30 | Y | 21.20 | Y | Jammet et al., 2017 |

| | | | | | | | | | |
|---|---|---|---|---|---|---|---|---|---|
| | Barrow, USA | 71°17' N, 156°35' W | Wet sedge tundra | 12 June - 31 August 2007 | -34.09 | S | 0.74 | S | Zona et al., 2009 |
| Subtropical | Buck Island Ranch, FL, USA | 27°9' N, 81°11' W | Grazed, flooded pasture | April 2013 - March 2015 | -119.00 | Y | 23.45 | Y | Chamberlain et al., 2017 |
| | Pointe-aux-Chene WMA, LA, USA | 29°30' N, 90°26' W | Brackish marsh | May 2012 - Oct 2013 | 170.60 | Y | 11.10 | Y | Holm et al., 2016; Krauss et al., 2016 |
| | Salvador WMA, LA, USA | 29°51'N, 90°17' W | Freshwater marsh | May 2012 - Oct 2013 | -337.00 | Y | 47.10 | Y | Holm et al., 2016; Krauss et al., 2016 |

*Table 2.1: Literature values of wetland mean annual (where there are multiple years reported) $CH_4$ and $CO_2$ eddy covariance measurements compiled from Petrescu et al. (2015), as well as more recently published studies. (S) denotes seasonal measurement interpolated*

### *2.4 Results and Discussion*

Delta wetlands sequestered C at rates of up to 698 g C $m^{-2}$ $yr^{-1}$ (Table 2.2) and accreted ~3 cm of new peat per year. However, building peat soil through uptake of $CO_2$ in these highly productive ecosystems comes at a steep $CH_4$ cost (Table 2.2). In the Delta, we report $CH_4$ fluxes of up to 590.6 mg $CH_4$ $m^{-2}$ $day^{-1}$, with annual sums ranging from 27.7 ± 1.0 to 63.4 ± 1.0 g C-CH4 $m^{-2}$ $yr^{-1}$ (Table 2.2;Figure 2.1). A subtropical Louisiana freshwater marsh (Krauss et al., 2016) as well as a temperate freshwater marsh on Lake Erie (Chu et al., 2015) report annual $CH_4$ flux rates as high as those in the Delta (Figure 2). Recent seasonal measurements from another Lake Erie marsh also demonstrate growing season fluxes up to 158.1 g C-$CH_4$ $m^{-2}$ $yr^{-1}$, presumably due to the input of agricultural effluent (Rey-Sanchez et al., 2017). Despite significant peat accretion and net C sequestration, potent $CH_4$ fluxes make the Delta restored wetlands GHG sources to the atmosphere under most circumstances (Figure 2.1).

| **NEE (g C-$CO_2$ $m^{-2}$ $year^{-1}$)** | | | | | | |
|---|---|---|---|---|---|---|
| Year | 2012 | 2013 | 2014 | 2015 | 2016 | 2017 |
| *Mediterranean 1* | | | | -562.4 ± 38.3 | -553.6 ± 40.6 | -442.1 ± 51.7 |

| | | | | | | |
|---|---|---|---|---|---|---|
| *Mediterranean 2* | -448.6 ± 49.7 | -43.3 ± 65.3 | -300.2 ± 31.0 | -362.7 ± 45.8 | -9.8 ± 38.5 | -467.7 ± 71.6 |
| *Mediterranean 3* | | -565.3 ± 81.7 | -314.5 ± 68.7 | -217.6 ± 77.3 | -411.9 ± 59.0 | -737.5 ± 79.8 |
| | | | | | | |
| **$CH_4$ (g C-$CH_4$ $m^{-2}$ $year^{-1}$)** | | | | | | |
| *Mediterranean 1* | | | | 27.7 ± 1.0 | 34.6 ± 1.0 | 49.3 ± 1.5 |
| *Mediterranean 2* | 63.4 ± 1.0 | 58.8 ± 1.0 | 57.2 ± 0.8 | 58.3 ± 0.9 | 45.7 ± 0.9 | 32.6 ± 1.1 |
| *Mediterranean 3* | | 34.0 ± 2.8 | 48.8 ± 3.2 | 55.7 ± 3.5 | 47.0 ± 2.3 | 38.8 ± 2.2 |
| | | | | | | |
| **SGWP (g $CO_2$ eq. $m^{-2}$ $year^{-1}$)** | | | | | | |
| *Mediterranean 1* | | | | -293.7 ± 151.9 | 176.7 ± 160.5 | 1520.9 ± 210.6 |
| *Mediterranean 2* | 2401.9 ± 191.5 | 3590.8 ± 247.2 | 2546.5 ± 123.0 | 2386.6 ± 175.9 | 2880.3 ± 150.7 | 367.1 ± 271.2 |
| *Mediterranean 3* | | 94.0 ± 343.1 | 1961.7 ± 318.4 | 2752.7 ± 352.7 | 1488.7 ± 255.3 | -229.7 ± 321.2 |

*Table 2.2: Annual sums of carbon dioxide ($CO_2$), methane ($CH_4$), and $CO_2$ equivalent emissions using the 100-year sustained global warming potential (SGWP) for fully vegetated restored wetlands in the Delta, with 95% confidence intervals. Negative values refer to loss from the atmosphere and gain by the ecosystem.*

This biogeochemical compromise is not unique; many wetland sites are net GHG sources over 100-year time horizons, despite sequestering C (Figure 2.1). Only the high latitude temperate and arctic sites that produce very little methane (< 5 g C-$CH_4$ $m^{-2}$ $yr^{-1}$), along with the first fully vegetated year at a Delta wetland (Mediterranean 1, 2015, -293.7 ± 151.9 g $CO_2$ eq. $m^{-2}$ $year^{-1}$) are net GHG sinks (Figure 1). Four of the fourteen Delta site-years are GHG neutral or small sources, including 2013 (94.0 ± 343.1 g $CO_2$ eq. $m^{-2}$ $year^{-1}$) and 2017 (-229.7 ± 321.2 g $CO_2$ eq. $m^{-2}$ $year^{-1}$) at Mediterranean 3, as well as recent years at Mediterranean 1 (2016, 176.7 ± 160.5 g $CO_2$ eq. $m^{-2}$ $year^{-1}$) and Mediterranean 2 (2017, 367.1 ± 271.2 g $CO_2$ eq. $m^{-2}$ $year^{-1}$). The remaining nine Delta site-years were large GHG sources of between 1488.7 ± 255.3 and 3590.8

± 247.2 g $CO_2$ eq. $m^{-2}$ $year^{-1}$. Even transiently flooded subtropical pastures were GHG sources due to large $CH_4$ fluxes, despite being inundated for less than two months of the year (Chamberlain et al., 2017a, 2016). Future scenarios (RCP8.5) project increased maximum global wetland area by up to 13% by the end of the 21st century, largely owing to boreal permafrost thaw, with tropical wetlands responsible for the majority of wetland methane emissions (Z. Zhang et al., 2017). Projecting future wetland $CH_4$ emissions and their response to global change relies on realistic constraints on this biogeochemical compromise across diverse climate and soil conditions.

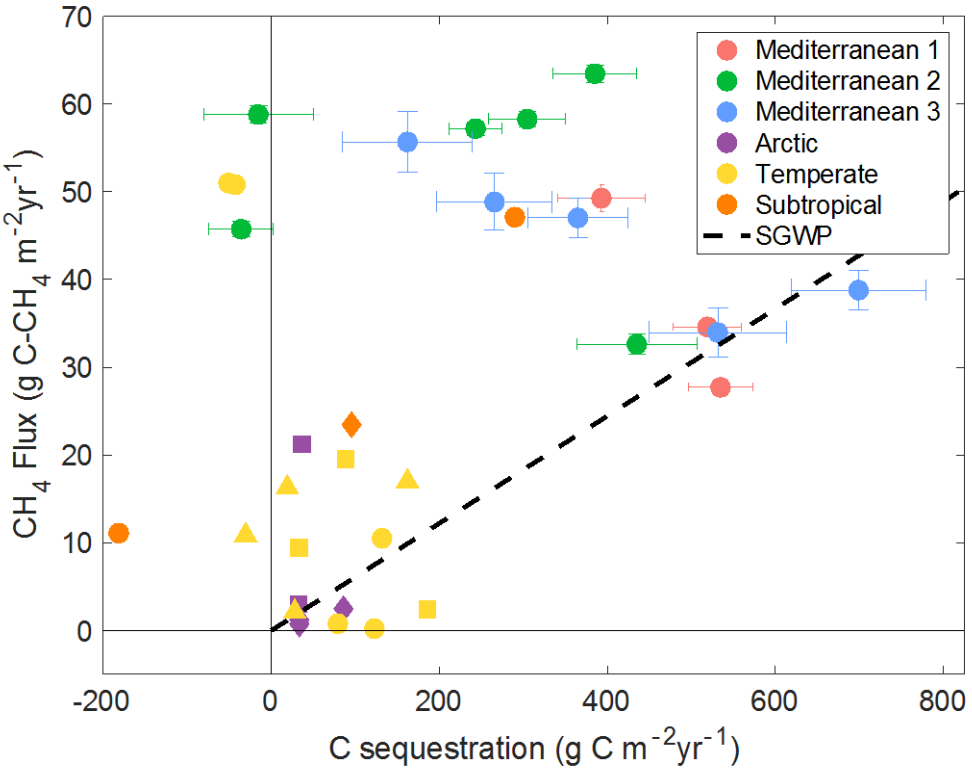


*Figure 2.1: Annual carbon (C) sequestration and methane ($CH_4$) fluxes for all years on record when Delta restored wetlands (Mediterranean 1, 2, and 3; Table 1) were fully vegetated (circles with confidence intervals), along with mean annual ecosystem budgets for other natural and restored wetlands previously reported in the literature, categorized by climate (Table S1). Symbols denote wetland type: circles are marshes, squares are fens, trianglesare bogs, and diamonds are tundra/pasture. The dashed line represents the threshold at which wetlands are a greenhouse gas source or sink given the balance between C sequestration and $CH_4$ fluxes using the 100-year $CH_4$ sustained global warming potential (Neubauer & Megonigol, 2015) of 45. Wetlands to the right of the dashed line are a net greenhouse gas sink.*

The variability of the compromise between building soil and emitting GHGs, determined by the ratio between monthly C sequestration and $CH_4$ emissions, has implications for climate change mitigation strategies that require estimates of this trade-off. While the Delta wetlands acted as GHG sinks during summer periods when high C uptake compensated for $CH_4$ emissions (Figure 2.2), they were often GHG sources on an annual basis (Figure 2.1; Table 2.2). Despite being located within ~13km of each other, experiencing nearly identical meteorological conditions, and sharing a similar species composition, $CH_4$ flux and C sequestration scaled within, but not across wetland sites (Figure 2.2). Both the slope ($1.8 \pm 0.5\%$, $4.0 \pm 0.9\%$, $1.8 \pm 0.5\%$) and/or the intercept ($2.4 \pm 0.5$, $3.3 \pm 0.5$, $3.4 \pm 0.5$ gC-$CH_4$ $m^{-2}$ $month^{-1}$) of these relationships (ordinary least squares, $r^2$ = 54%, 61%, 54%) differ across sites (Mediterranean 1, 2, and 3, respectively), suggesting fundamental differences in the rate at which fixed C is evolved to $CH_4$.

Global $CH_4$ models have historically used a fixed ratio of ecosystem productivity as a proxy for $CH_4$ emissions (Cao et al., 1996; Christensen et al., 1996). Net primary productivity (NPP), for example, integrates factors relevant to $CH_4$ biogeochemistry and has been found to scale linearly with $CH_4$ flux across wetland types (Whiting and Chanton, 2001). Our results suggest that these scaling factors are dynamic (Figure 2.2), even across small spatial scales where important hydrologic, biological, and climatic drivers are controlled. Though some contemporary climate models predict $CH_4$ emissions using mechanistic representations of $CH_4$ biogeochemistry (Poulter and et al, 2017), many global $CH_4$ models still largely rely on estimating $CH_4$ emissions as a fraction of NPP or heterotrophic respiration (Melton et al., 2013). In addition, these two quantities are rarely measured *in situ* at the ecosystem scale without first making assumptions to partition fluxes. Accurately estimating these scaling factors is important, as the estimated ratio between $CO_2$ uptake and $CH_4$ emissions largely determines the modeled $CH_4$ flux strength (Spahni et al., 2011).

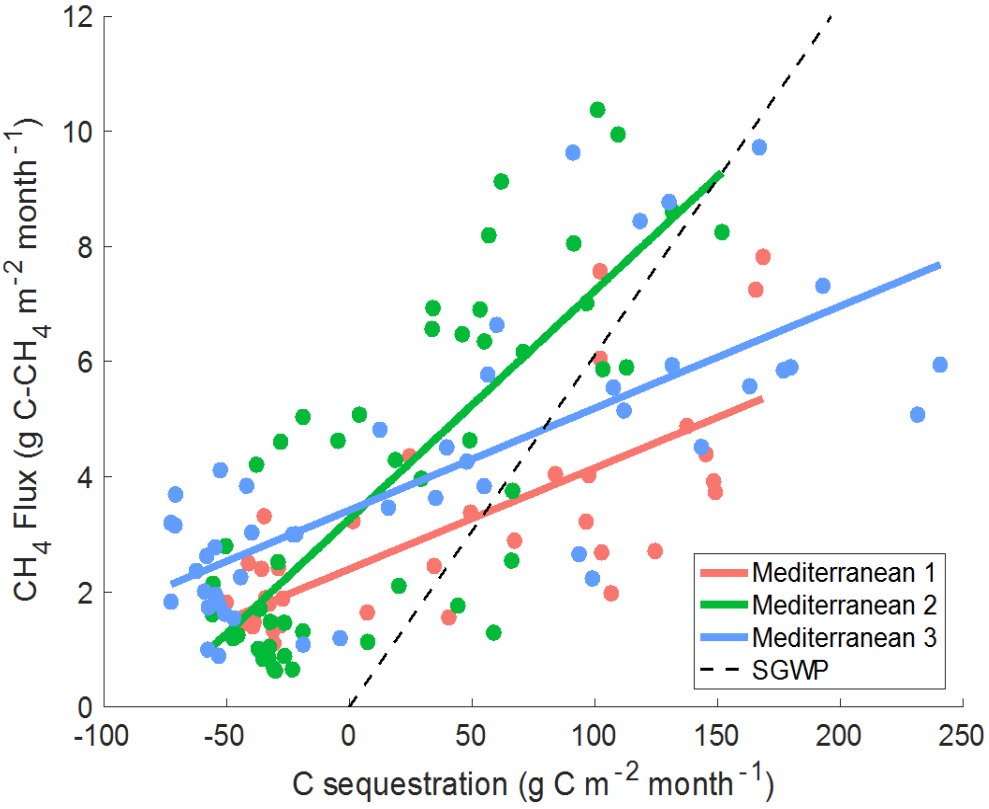


*Figure 2.2: Monthly $CH_4$ emissions and C sequestration at each Delta restored wetland (Mediterranean 1, 2 and 3) for concurrent, fully vegetated observation periods (2015-2017). The black line represents the threshold at which wetlands are a GHG source or sink given the balance between C sequestration and $CH_4$ fluxes using the 100-year $CH_4$ SGWP (Neubauer & Megonigol, 2015) of 45. During months to the right of the dashed line, wetlands were a net GHG sink.*

Wetland restoration can still be an important component of biological climate solutions, but the C sequestration must be realistically weighed against the potential for increased GHG emissions in the short to medium term. Previous work has pointed out that over multi-century to geologic timescales, wetlands commonly exhibit net negative radiative forcing (cooling), due to the short lifetime and dissipating effect of atmospheric $CH_4$ (Frolking et al., 2006; Frolking and Roulet, 2007; Mitsch et al., 2013). Indeed, based on the ratios of C sequestration to $CH_4$ emission over the course of our study, these Delta wetlands would theoretically switch from a GHG source to a sink after 1-2 centuries (Mediterranean 1 and 3) or more than 5 centuries (Mediterranean 2)

(Neubauer, 2014; Neubauer and Megonigal, 2015). This long-term climate benefit notwithstanding, mounting evidence points to the urgency of climate change mitigation to prevent runaway land-atmospheric feedbacks (Arneth et al., 2010; Z. Zhang et al., 2017). Recent methane emissions may be especially important to short-term climate forcing, as the post-2006 uptick in atmospheric $CH_4$ concentrations were associated with an immediate, positive trend in radiative forcing (Feldman et al., 2018).

Our study uses the common practice of assessing the climatic benefits over a 100-year timescale. Even without climate change and sea level rise, assuming a restored wetland will remain intact over longer periods, given social and political drivers of land use change, may not be prudent. Over shorter timescales, more consistent with policy decisions required to mitigate climate change, the relative radiative forcing of $CH_4$ is considerably larger ($CH_4$'s 20-year SGWP is 96) (Neubauer and Megonigal, 2015). Debates related to the timescale at which to judge $CH_4$ emissions extend beyond wetland climate forcing, and also underlie the controversy regarding the climate footprint of natural gas versus coal power (Cathles et al., 2012; Howarth et al., 2011).

Further challenges accounting for wetland impacts on climate stem from a lack of understanding of pre-anthropogenic emissions. Restoring a drained, disturbed wetland back to a state that perfectly matches its pre-anthropogenic natural condition would not result in any net radiative forcing, compared to the pre-industrial 'baseline' (Neubauer, 2014; Roulet, 2000). Due to systemic hydrological changes, intensive management, upstream land use changes, or loss of soil C, many restored wetlands are likely quite different from the pre-anthropogenic wetlands that preceded them. Different types of wetlands may exhibit varying amounts of resiliency to the impacts of climate change (Wu and Roulet, 2014), but with widespread changes, including high-latitude permafrost thaw increasing wetland extent, temperature-driven increases in methanogenesis, alteration to global nutrient cycles, interannual variability in precipitation, and anthropogenic encroachment (Moomaw et al., 2018; Poulter and et al, 2017; Z. Zhang et al., 2017), even the biogeochemistry of 'pristine' wetlands may diverge from a pre-anthropogenic steady state. Understanding restored wetland GHG dynamics with reference to a pre-anthropogenic baseline is a significant challenge, but improved process-based modeling of wetland biogeochemistry (Oikawa et al., 2016a) may allow for prediction of historical ecosystem fluxes when space for time substitutions may not be possible.

Climate change mitigation strategies being proposed today often fail to recognize the important short-term biogeochemical compromise associated with peatland restoration, largely due to limited long-term, ecosystem-scale observations. Our multi-year measurements in highly productive restored freshwater marshes often do not support the assumption that all incurred $CH_4$ emissions will be offset by wetland C sequestration over policy-relevant timescales (Griscom et

al., 2017; Leifeld and Menichetti, 2018). Restoration activities, especially in highly productive systems, must account for the potentially large, induced $CH_4$ flux to avoid unintended climate consequences.

Implementing wetland restoration can still achieve substantial emission reductions when the land use change leads to a net reduction in GHG flux compared to current practices (Schrier-Uijl et al., 2014). In the Delta, large background $CO_2$ efflux from drained, subsided peatlands in some cases results in wetland restoration reducing the net GHG emissions of the parcel (Knox et al., 2015). The choice of GWP metric and timescale by which to weigh the relative radiative impacts of $CH_4$ will greatly affect these determinations (Krauss et al., 2016; Neubauer and Megonigal, 2015). In addition to the potential GHG impact, re-flooding peat soils to a managed wetland also provides an array of environmental co-benefits, including bird and fish habitat, hydrological connectivity, water quality, and even biophysical surface cooling (Himes-Cornell et al., 2018; Paustian et al., 2016). Developing approaches to predict and attenuate restored and created wetland $CH_4$ fluxes will be crucial for implementing climate beneficial restoration strategies (Moomaw et al., 2018; Oikawa et al., 2016a).

Future restoration programs could engineer wetlands by transiently reducing water tables or preferentially restoring wetlands in areas with high alternative electron acceptor pools, as we observed reduced $CH_4$ emissions under such conditions (Figure 2.1). In its initial years (2015 and 2016), a Delta wetland (Mediterranean 1) restored on high iron soils was a small GHG sink or near GHG neutral due to inhibition of $CH_4$ fluxes by microbial iron reduction. These effects may be transient, as three years post-restoration (2017) this site was a GHG source (Chamberlain et al., 2018). In another case, intermittent water table drawdowns over the course of a year inhibited $CH_4$ fluxes enough to make a Delta wetland GHG neutral (Sturtevant et al., 2016) (Mediterranean 3, 2013). Other types of ecosystem disturbance, such as an insect infestation (Mediterranean 2, 2013) and salinization (Mediterranean 2, 2016), had the effect of reducing C sequestration without affecting $CH_4$, leading to large annual GHG emissions (Table 2.2). Our results reveal that disturbance, even in highly managed restored wetlands, can take a significant GHG toll. Sulfate in acid rain (Gauci et al., 2005) and seawater can significantly reduce ecosystem-scale $CH_4$ fluxes (Holm et al., 2016)by introducing a more favorable electron acceptor. Future restoration efforts in coastal and estuarine regions where alternative electron acceptors are present may provide the optimum climate benefit (Kroeger et al., 2017).

Feedbacks associated with a changing climate are likely to amplify the impact of wetland emissions throughout the 21$^{st}$ century (Melton et al., 2013; Z. Zhang et al., 2017). Long-term *in situ* measurements of $CH_4$ emissions from managed and natural wetlands are therefore crucial to constraining global models and understanding GHG emissions associated with planned wetland restoration. Here, we demonstrate the exceptional magnitude of ecosystem-scale $CH_4$ emissions

from Delta restored wetlands with long growing seasons and a history of rapid peat accretion. These restored wetlands do, however, provide a number of important environmental benefits, including accreting soil by sequestering C that will rebuild a subsided land surface and provide levee stability to California's fragile water system. A renewed emphasis on understanding the site-specific variability in productivity scaling relationships, along with expanded ecosystem-scale, *in situ* measurements to validate these relationships across a representative range of climates and wetland types are critical to answering important questions about the biogeochemical compromises implicit in future land use and climate trends.

# 3 Assessing the carbon and climate benefit of restoring degraded agricultural peat soils to managed wetlands[2]

## *3.1 Abstract*

Restoring degraded peat soils presents an attractive, but largely untested, climate change mitigation approach. Drained peat soils used for agriculture can be large greenhouse gas sources. By restoring subsided peat soils to managed, impounded wetlands, significant agricultural emissions are avoided, and soil carbon can be sequestered and protected. Here, we synthesize 36 site-years of continuous carbon dioxide and methane flux data from a mesonetwork of eddy covariance towers in the Sacramento-San Joaquin Delta in California, USA to compute carbon and greenhouse gas budgets for drained agricultural land uses and compare these to restored deltaic wetlands. We found that restored wetlands effectively sequestered carbon and halted soil carbon loss associated with drained agricultural land uses. Depending on the age and disturbance regime of the restored wetland, many land use conversions from agriculture to restored wetland resulted in emission reductions over a 100-year timescale. With a simple model of radiative forcing and atmospheric lifetimes, we showed that restored wetlands do not begin to accrue greenhouse gas benefits until nearly a half century, and become net sinks from the atmosphere after a century. Due to substantial interannual variability and uncertainty about the multi-decadal successional trajectory of managed, restored wetlands, ongoing ecosystem flux measurements are critical for understanding the long-term impacts of wetland restoration for climate change mitigation.

## *3.2 Introduction*

Working lands play an important role in terrestrial carbon (C) cycling, with the potential to be a source or a sink of carbon dioxide ($CO_2$) and other greenhouse gases (GHG) (Canadell and Schulze, 2014). Land management as a $CO_2$ removal strategy could remove up to 6 Gt $CO_2$ $yr^{-1}$ at a lower cost than more energy- and technology-intensive strategies (Psarras et al., 2017), with potential to help counteract society's growing soil C debt (Sanderman et al., 2017). The Intergovernmental Panel on Climate Change (IPCC) 5$^{th}$ assessment report stated that reversibility of anthropogenic climate change will only be possible with "large net removal of $CO_2$ from the atmosphere over a sustained period" (Myhre et al., 2013). Thus, C sequestration by ecosystems is of urgent importance, although limited by physical and ecological constraints (Baldocchi and Panuelas, 2018). Restoring degraded peat soils presents an attractive, but largely untested

[2] originally published as: Hemes, K.S., Chamberlain, S.D., Eichelmann, E., Anthony, T., Valach, A., Kasak, K., Szutu, D., Verfaillie, J., Silver, W.L., Baldocchi, D.D., 2019. Assessing the carbon and climate benefit of restoring degraded agricultural peat soils to managed wetlands. Agric. For. Meteorol. 268, 202–214. https://doi.org/10.1016/j.agrformet.2019.01.017

approach for soil C sequestration and associated climate change mitigation (Griscom et al., 2017; Leifeld and Menichetti, 2018; Paustian et al., 2016).

The benefits associated with wetland restoration for net C sequestration stem from two key areas. First, drained agricultural peat soils can be large GHG sources (Hatala et al., 2012; Knox et al., 2015; Schrier-Uijl et al., 2014; Veber et al., 2017). As organic-rich soils are drained and exposed to the atmosphere, aerobic respiration leads to large $CO_2$ emissions relative to flooded or saturated conditions that inhibit aerobic respiration. Globally, drainage of C-rich peat soils in river deltas has caused subsidence, the sinking of the land surface, as soil C is oxidized to $CO_2$ (Syvitski et al., 2009). This $CO_2$ source, along with emissions of other important agricultural GHG's like methane ($CH_4$) and nitrous oxide ($N_2O$), can cause agricultural peat soils to be large net emitters of GHGs. By restoring these subsided lands to managed, impounded wetlands, these agricultural emissions can be avoided. Second, the slow decomposition rates of wetland soil organic matter compared to high net primary productivity (NPP) leads to soil C accumulation. Maintaining wetland structure and function can protect much of the sequestered C and associated nitrogen from organic matter mineralization, leading to the potential for long-term C storage and lower $N_2O$ emissions (Deverel et al., 2016, 2014; Yarwood, 2018), although there is evidence that C sequestration capacity may not return to its pre-restoration rates (Moreno-Mateos et al., 2017, 2012).

Wetland restoration comes with a biogeochemical compromise, however (Hemes et al., 2018a; Hoper et al., 2008; Petrescu et al., 2015). While flooded wetland systems have the potential to sequester C as NPP outpaces soil respiration, the highly reduced conditions can result in significant $CH_4$ emissions (Bridgham et al., 2013; Dean et al., 2018), often making restored wetlands net GHG sources to the atmosphere over decadal timescales (Hemes et al., 2018a). Due to limited long-term continuous data in restored wetlands of various ages, many future climate scenarios have treated restored wetlands and peatlands as GHG neutral (Griscom et al., 2017; Leifeld and Menichetti, 2018). A recent rise in global atmospheric $CH_4$ concentrations has renewed interest in characterizing the contribution of wetlands to global biogeochemistry and radiative forcing, which is likely around 30% of all anthropogenic and natural $CH_4$ sources (Feldman et al., 2018; Nisbet et al., 2016; Poulter and et al, 2017). Future projections of wetland $CH_4$ emissions suggest that they could play an important role in driving climate change throughout the 21$^{st}$ century (Dean et al., 2018; B. Zhang et al., 2017). Despite this fact, the balance between GHG emissions and C sequestration in wetlands remains an "enigma" (Mitsch and Mander, 2018). Long-term, in-situ, continuous measurements of GHG exchange over these ecosystems are critical to resolve their biogeochemical impact (Hemes et al., 2018a; Petrescu et al., 2015).

The Sacramento-San Joaquin River Delta is a hydrologically critical mosaic of drained and subsided agricultural peat soils that has been undergoing wetland restoration activities in order to

reverse subsidence and accrete soil for up to two decades. This region provides a useful test of the climate impacts of 'wet' restoration on degraded peat soils. Delta GHG budgets have been published for a single growing season, demonstrating that over 2012-2013, a mature wetland was a GHG sink while a younger wetland was a net source of GHG (Knox et al., 2015). During another year at a single restored wetland site (West Pond) in the Delta, Windham-Myers *et al* (2018) report GHG neutrality from combined chamber and eddy covariance measurements. Other studies of wetlands in the Delta have reported net GHG sources, and switchover times (from a source to a sink) of greater than 500 years (Anderson et al., 2016; McNicol et al., 2016).

Drained, subsided agricultural land uses in the Delta have also been individually investigated for GHG and water exchange. Multiyear measurements at a rice paddy (Twitchell Rice) tied large interannual variability in the net C budget to variability in ecosystem respiration ($R_{eco}$) driven by soil temperature (Knox et al., 2016). Teh *et al.* (2011) found an intermittently inundated pasture (Sherman pasture) in the Delta to be a large source of $N_2O$ emissions (2.4 ± 1.3 g $N_2O$-N $m^{-2}$ $yr^{-1}$) and a modest source of $CH_4$ (1.6 ± 1.4 g $CH_4$-C $m^{-2}$ $yr^{-1}$ to 9.5 ± 3.4 g $CH_4$-C $m^{-2}$ $yr^{-1}$) during 2007-2008. The same pasture was a modest GHG source over 2009-2010 (Hatala et al., 2012). Corn and alfalfa represent other dominant and water-intensive land uses in the Delta (Anderson et al., 2018; Eichelmann et al., 2018) that have important GHG implications. Concurrent observations of ecosystem-scale GHG exchange at both restored wetlands and drained agricultural peat soils in close proximity allows for a space-for-time assessment of the climatic effect of land use conversion.

Here, we synthesized 35 site-years of continuous $CO_2$ and $CH_4$ flux data from a mesonetwork of eddy covariance towers in the Delta to compute C and GHG budgets at agricultural sites with drained, degraded peat soils and a chronosequence of four freshwater deltaic restored wetlands. We also integrated $N_2O$ chamber measurements from two of the agricultural sites. Our study sites represent a suite of dominant and potential future land uses in the Delta region, and differ climatically and ecologically from other studied restored wetlands and peatlands, many of which are in northern high-latitude climates. Our study aimed to address the hypothesis that land use change from agriculture on drained, degraded peat soils to freshwater, deltaic restored wetlands, will result in a net GHG benefit over multi-decadal timescales, while accreting soil and sequestering C from the atmosphere into the ecosystem. Along with climate benefits, these ecosystem services have the potential to halt and reverse soil subsidence and protect the fragile hydrological network through which water is transported across California. Further, we assessed what specific land use transitions optimize GHG emission reductions, and quantified the impact of a set of global warming potential (GWP) metrics on this determination.

## *3.3 Materials and Methods*

### *3.3.1 Site characteristics*

The Sacramento–San Joaquin River Delta was once a vast 1400 $km^2$ wetland and riparian zone fed by two of California's largest rivers (Atwater et al., 1979; Cloern and Jassby, 2012). Since drainage in the mid-19th century (Weir, 1950) much of the land surface has been subsiding dramatically, losing close to 200 Tg C due to drainage-induced oxidation of the peat soils (Drexler et al., 2009). A series of dikes and levees protect the subsided 'islands' by holding back the rivers and sloughs that deliver at least a portion of the drinking water to more than two-thirds of Californians through the State Water Project and the Central Valley Project. Generally, wetland soils are highly organic while agricultural soils exhibit a mixed layer of degraded oxidized peat and mineral soil on top with a deep peat horizon below (Miller et al., 2008). Historically, mixed alluvium mollisols formed adjacent to major rivers, while organic histosols were found where fluvial deposition was less pronounced (Atwater et al., 1979; Chamberlain et al., 2018; Deverel and Leighton, 2010). The ten sites considered in this study, described in detail in Table 3.1, are located on Twitchell, Sherman, and Bouldin Islands, and are composed of four restored wetlands and six agricultural sites that make up most of the dominant land uses in the Delta region. Individual study sites have been described in previous work and will be summarized here for brevity (Chamberlain et al., 2018; Eichelmann et al., 2018; Hatala et al., 2012; Knox et al., 2015; Oikawa et al., 2016b). These sites are all part of the Ameriflux network (http://ameriflux.lbl.gov/) through which publicly available data and site information are available.

The Sherman wetland (Ameriflux ID: US-Sne; 263 ha) was restored from Sherman pasture in November of 2016 and was still in the process of establishing a fully vegetated canopy at the time of this study. East End restored wetland (US-Tw4; 303 ha) was constructed in late 2013 after being under continuous corn cultivation. Since the initial flooding, the wetland had filled in with tule *(Schoenoplectus acutus)* and cattail (*Typha* spp.) and represented an early-intermediate stage of restoration, with limited patches of open water. Mayberry restored wetland (US-Myb; 121 ha) was constructed in 2010 on Sherman Island, and represented an intermediate stage of restoration, with a similar species mix. With a water level as deep as 2 meters in open-water channels, Mayberry wetland was the most heterogeneous of the four restored wetland treatments. Additionally, rising salinity levels in the wetland caused lowered productivity between 2014-2016. West Pond restored wetland (US-Tw1; 3 ha) was constructed in 1997 on Twitchell Island (Miller et al., 2008). Our eddy flux measurements began in summer 2012. West Pond, which was dominated by tall, emergent tule and cattail, represented a mature restored wetland and had no open water patches.

All restored wetland sites have undergone 'wet' restoration, a specific type of restoration in which the water table is actively managed to keep the wetland impounded year-round, preventing tidal, seasonal, or geomorphological input of sediment that natural wetlands would have received. Differing bathymetry and pumping schemes, as well as seasonal drought, cause slight variations in the water depth and quality at the four restored wetlands studied. Regenerative tule and cattail seeding was performed at select sites to promote canopy establishment. Due to the widespread modifications throughout the Delta, these novel ecosystems may be more accurately understood of as 'rehabilitated' wetlands - sharing common hydrological conditions and species with their pre-industrial predecessor, but in no way biogeochemically or ecologically identical (Hemes et al., 2018a).

The agricultural sites included most of the dominant agricultural land uses in the Delta region: rice, pasture, corn, and alfalfa. Twitchell rice (US-Twt; *Oryza sativa*) was actively measured between 2009-2017 and planted on degraded, subsided peat soil (Knox et al., 2016). Sherman pasture (US-Snd), active between 2007-2015 (2010-2015 used in this study), was a pepperweed-dominated (*Lepidium latifolium L.*) pasture on the subsided peat soil that became Sherman wetland (Hatala et al., 2012; Teh et al., 2011). Corn (*Zea mays*) was measured during 2012-2013 on Twitchell Island on the location that became East End wetland in 2014, and during 2017 on Bouldin Island (US-Bi2) which contained higher soil C than the Twitchell corn site. Alfalfa (*Medicago sativa* L.) shares a perennial life-cycle strategy with the dominant wetland species and represents one of the largest water users in California (Hanson et al., 2007). This study incorporated data from alfalfa sites on Twitchell and Bouldin islands. Twitchell alfalfa (US-Tw4) was a seven year-continuously planted alfalfa field, previously planted in corn (Baldocchi and Sturtevant, 2015; Oikawa et al., 2016b). The site was sub-irrigated, harvested between 5 and 7 times a year, beginning in mid-March, and periodically grazed with sheep. Rapid leaf area index (LAI) changes (between ~1-3) due to an intensive harvest schedule greatly affected the GHG fluxes. Bouldin alfalfa (US-Bi1) was planted on a higher C soil than that on Twitchell Island, and was measured since August 2016 (Table 3.1).

| **Site (Ameriflux ID and DOI)** | **Location** | **Years included** | **Percentage of missing data $CO_2$/$CH_4$ (%)** | **Land Use history** | **Measurement height / canopy height* (m)** |
|---|---|---|---|---|---|
| **Sherman wetland (US-Sne; 10.17190/AMF/1418684)** | Sherman Island. 38.037 N, -121.755 W | 2017 | 50.2 / 42.8 | 263 ha wetland restored from pasture mid-2016 | 5.4 / 2.0 |

| | | | | | |
|---|---|---|---|---|---|
| **East End wetland (US-Tw4; 10.17190/AMF/1246151)** | Twitchell Island. 38.103 N, -121.641 W | 2014-2017 | 43.6 / 39.9 | 323 ha wetland restored from corn late 2013 | 4.9 / 2.2 |
| **Mayberry wetland (US-Myb; 10.17190/AMF/1246139)** | Sherman Island. 38.050 N, 121.765 W | 2011-2017 | 35.3 / 38.5 | 121 ha wetland restored in 2010 | 5.1 / 3.4 |
| **West Pond wetland (US-Tw1; 10.17190/AMF/1246147)** | Twitchell Island. 38.107 N, -121.647 W | 2013-2017 | 62.2 / 62.1 | 3 ha wetland restored in 1997 | 4.5 / 2.6 |
| **Twitchell Rice (US-Twt; 10.17190/AMF/1246140)** | Twitchell Island. 38.109 N, -121.653 W | 2010-2016 | 49.1 / 50.0 | Paddy rice (*Oryza sativa*) | 3.18 / 0.9 |
| **Sherman Pasture (US-Snd; 10.17190/AMF/1246094)** | Sherman Island. 38.037 N, -121.754 W | 2010-2014 | 36.5 / 51.8 | Restored to Sherman wetland 2015-2017 | 3.2 / 0.4 |
| **Twitchell Corn (US-Tw2; 10.17190/AMF/1246148)** | Twitchell Island. 38.105 N, -121.643 W | May 2012 – May 2013 | 44.9 / n/a | Corn (*Zea mays*), restored to wetland late 2013 | 5.15 / 2.76 |
| **Bouldin Corn (US-Bi2; 10.17190/AMF/1419513)** | Bouldin Island. 38.109 N, -121.535 W | April 2017 – April 2018 | 46.2 / 57.1 | Corn (*Zea mays*) | 5.1 / 2.6 |
| **Twitchell Alfalfa (US-Tw3; 10.17190/AMF/1246149)** | Twitchell Island. 38.115 N, -121.647 W | 2014-2017 | 42.9 / n/a | 30 ha Alfalfa (*Medicago sativa* L.) since 2010 | 2.9 / 0.7 |

| | | | | | |
|---|---|---|---|---|---|
| **Bouldin Alfalfa (US-Bi1)** | Bouldin Island. 38.100 N, -121.500 W | 2017 | 47.6 / 65.1 | Alfalfa (*Medicago sativa* L.) | 3.9 / 0.5 |

*Table 3.1: Site characteristics. *For agricultural sites, approximate maximum canopy height.*

### *3.3.2 Eddy Covariance Measurements and processing*

The heterogeneous and continuous nature of ecosystem GHG emissions requires long-term spatially integrated measurements to fully characterize temporal and spatial variability (Baldocchi, 2003). We used the eddy covariance technique (Baldocchi et al., 1988) to capture continuous, long-term exchange of $CO_2$, $CH_4$, $H_2O$, and energy fluxes between the landscape and the atmosphere, along with measurements of environmental drivers (Eichelmann et al., 2018). Fluxes were measured by sampling a suite of sensors at a frequency of 10 (before ~2015) or 20 Hz, using open-path infrared gas analyzers (LI-7500 or LI-7500A for $CO_2$ and $H_2O$, LI-7700 for $CH_4$, LiCOR Inc., Lincoln, NE, USA) that were calibrated every 3-6 months in the lab. Sonic anemometers measured sonic temperature and three-dimensional wind speeds at 20 Hz (WindMaster Pro 1352 or 1590, Gill Instruments Ltd, Lymington, Hampshire, England). The instrument setup (sampling rate, sensor separation, fetch and sensor height) was designed to minimize spectral loss (Detto et al., 2010). Typical cospectra exhibited slopes that closely match the idealized slope from Kaimal *et al* (1972). The main complication affecting the interpretation of our fluxes was the relative lack of homogeneity of the footprint of the restored wetlands, a mosaic of open water and vegetation (Eichelmann et al., 2018; Hemes et al., 2018b). Energy balance closure for many of these sites has been reported before and is adequate; non-closure at the wetland sites with large tracts of open water (Sherman, East End, and Mayberry wetlands) is due to the inability to capture the vertical and horizontal spatial variability in water column storage of the flux footprint, an important component of the energy balance (Eichelmann et al., 2018; Hemes et al., 2018b).

Trace gas and energy fluxes were calculated using the 30-minute covariance of turbulent fluctuations in vertical wind velocity and scalar of interest after applying a series of standard corrections and site-specific factors (Detto et al., 2010; Hatala et al., 2012; Knox et al., 2015). Coordinate rotations were performed so that mean wind velocities at each 30-minute averaging interval were zero in the cross-wind and vertical directions. To account for air density fluctuations sensed by the open path $CH_4$ and $CO_2$ sensors, the Webb-Pearman-Leuning corrections were applied (Chamberlain et al., 2017b; Webb et al., 1980). To remove flux data measured over non-ideal conditions, half hourly fluxes were filtered for stability and turbulence,

friction velocity, wind direction, spikes in mean densities, variances and covariances, and sensor window obstruction.

To integrate yearly C and GHG budgets we gap filled fluxes by training an Artificial Neural Network (ANN) using measured meteorological variables (Dengel et al., 2013; Moffat et al., 2007; Papale et al., 2006). Training, validation, and testing data was selected from a series of k-means clusters to avoid seasonal or diel bias using Matlab 2017b software (Mathworks, Inc. 2012). Network architecture with varying levels of complexity were tested, with the simplest architecture selected for which further increases in complexity yielded less than a 5% reduction in mean standard error (Knox et al., 2016, 2015). This entire ANN procedure was performed 20 times, producing 20 separate ANNs. The median prediction of the 20 ANNs was used to fill gaps in the annual data.

Due to measurement periods not aligning with calendar years in the case of the two corn sites, we 'wrapped' a few months of the following year's fluxes onto the previous year to achieve an annual calendar year timeseries and budget. This assumes that there is little interannual variability at a single corn site, which is reasonable considering the intensive management and precision farming practices employed. In addition, the wrapped fluxes were from early season (January to April) when the fields are largely fallow. For Bouldin corn, we appended fluxes from the first four months of 2018 to the 2017 record, which did not start until late April of that year. For Twitchell corn, we wrapped just over four months of 2013 to the 2012 record, which began in early May, 2012. The tower was moved ~1 km in May of 2013 to make way for construction of East End wetland. To calculate the remaining two weeks necessary to get an annual sum, we extended the ANN predictions using meteorological data from the displaced tower site. These meteorological inputs do not differ significantly due to the close spatial proximity.

To investigate component fluxes at each site, we partitioned NEE into ecosystem respiration ($R_{eco}$) and gross primary productivity (GPP) using ANNs to predict daytime $R_{eco}$ from nighttime measurements, when photosynthesis is inactive. The residual of NEE and daytime $R_{eco}$ is the GPP. This method, while data-driven and avoiding assumptions of functional relationships between environmental drivers and component fluxes, does have drawbacks. It assumes that nighttime $R_{eco}$ generally functions similarly to daytime $R_{eco}$, and has been shown to overestimate GPP and $R_{eco,}$ potentially due to its inability to capture the Kok effect (Heskel et al., 2013; Oikawa et al., 2016b). For a global comparison analysis, we produced monthly sums from Fluxnet 2015 daily subset data (http://fluxnet.fluxdata.org/), excluding data with NEE quality control of less than 70%, and considering only months with complete daily data.

### *3.3.3 Carbon and greenhouse gas budgets*

Net ecosystem carbon balance (NECB) was computed from the integrated annual sum of NEE (C-$CO_2$), and $CH_4$ (C-$CH_4$), as measured by continuous eddy covariance after quality control and gap filling as described above. For agricultural sites, removed, harvested biomass was added to the C budget. As the harvested crops of the Delta are commodities, the fate of their removed biomass is challenging to track with precision. Much of it may contribute to livestock feed, in which case it could partly result in enteric fermentation and additional $CH_4$ emissions. We follow a conservative approach and convert the removed biomass into $CO_2$ emissions for the purposes of the field-scale GHG accounting. A life-cycle accounting approach would more fully integrate the GHG fate of harvest, potentially resulting in larger GHG emissions at decadal timescales due to the decomposition of this biomass.

Harvest values were determined based on field-level farmer records where possible (Table 3.2). Rice harvest was taken from Knox *et al.* (2016), assuming dry rice grain contains 43% C. Harvest from the 2016 growing season, for which no record exists, was assumed to be the mean of the previous six years. Removed biomass from pasture was not quantified and assumed to be zero. Including it would make the pasture site a larger emission source. Twitchell corn harvest was from farmer records (Knox et al., 2015). Bouldin corn and alfalfa records were taken from farmer records, assuming 44% C dry matter, with corn harvested at 65% moisture and alfalfa at 88% moisture. For Twitchell alfalfa, we established annual relationships (linear least squares regression) between days since harvest and C sequestration measured from eddy covariance data to estimate total removed biomass at each cutting, and for each year. The mean value (693.1 ± 263.2 g C $m^{-2}$ $yr^{-1}$) falls between the upper and lower range given by the farmer.

Wetland NECB was composed primarily of photosynthetic inputs of $CO_2$ minus both autotrophic and heterotrophic respiration outputs of $CO_2$ and efflux of microbial $CH_4$. Because the wetlands were impounded, with little current and outflow, allochthonous lateral transport of dissolved C was not measured, and assumed to be negligible. In other more natural wetland systems, this lateral import and export of carbon is certainly an important component of the C balance (Chu et al., 2015; Krauss et al., 2018). By measuring NEE using the eddy covariance method, the dominant C inputs and outputs are measured continuously, and integrated over an entire footprint. At sites with negative NECB, the residual C was considered stored in the system.

To understand the impact of $N_2O$ emissions on the GHG budget, continuous measurements of $N_2O$ were conducted by an automatic flux chamber system installed in parallel at both the Bouldin corn and Bouldin alfalfa sites. Nine automated flux chambers (Eosense, Inc., Dartmouth, NS, Canada) were connected to a multiplexer, which dynamically signaled chamber deployment and routed gases to a Cavity Ring-Down Spectroscopy gas analyzer (Picarro, Santa

Clara, CA, USA). Only one chamber was measured at a time, and each measurement took approximately 13 minutes. To reduce over- or under-estimation from individual chamber down-time, $N_2O$ flux measurements were estimated using linear interpolation between consecutive measurements for each chamber. Fluxes were then averaged across all chambers over the measurement period (January 2017-January 2018 for Bouldin alfalfa; June 2017-June 2018 for Bouldin corn) to calculate annual $N_2O$ flux (Anthony et al., in prep).

GHG budgets were computed from the integrated annual sum of NEE and emissions of $CH_4$, weighted according to GWP. Traditional GWP metrics were designed for a pulse emission but have been widely applied to ecosystems and are the common standard in climate and emission accounting policies like California's Cap and Trade system and the Kyoto Protocol. The ease and transparency with which these metrics can be applied have afforded them widespread adoption, despite well-documented inadequacies (Allen et al., 2016; Balcombe et al., 2018). Sustained global warming (and cooling) potential (SGWP) metrics account for the sustained nature of ecosystem emissions and differentiate between the effects of uptake and emission of important short-lived climate pollutants (SLCPs) (Neubauer and Megonigal, 2015). This SGWP metric has been applied to wetland sites previously (Hemes et al., 2018a; Krauss et al., 2016; Neubauer and Megonigal, 2015). We chose the IPCC AR5 GWP (without climate change feedbacks) for $CH_4$ of 28 $CO_2$eq and for $N_2O$ of 265 $CO_2$eq (Myhre et al., 2013), and the SGWP for $CH_4$ of 45 $CO_2$eq (Neubauer and Megonigal, 2015), as these lie at the lower and upper end of commonly utilized cumulative 100-year warming potential metrics (Balcombe et al., 2018).

The GWP* metric has been shown to better track the temperature impacts of the integrated radiative forcing associated with SLCPs, which achieve steady state long before the conventionally assessed 100-year timeframe (Allen et al., 2018, 2016). Modeling of the GWP* metric provides a compelling alternative to adopting a standard but arbitrary amortization period like 100 years, as is necessary with GWP and SGWP metrics. To calculate GWP*, we used the method of Allen *et al.* (2016) where changes in $CH_4$ ($\Delta CH_4$) were accounted for instead of the magnitude of $CH_4$ (assuming a GWP of 28 $CO_2$eq). Mean grouped land use (wetland, corn, pasture, and alfalfa) $CO_2$ and $CH_4$ fluxes were used as inputs, with interannual variability as measured from our eddy covariance sites. We ran a Monte Carlo simulation (n=1000) to capture the variability in switchover times due to the interannual variability in fluxes and present a mean year since restoration with a range of uncertainty (± 1 standard deviation) as the switchover time. Switchover time is defined as the length of time after which the positive radiative forcing due to increases in $CH_4$ emissions at a restored wetland is overtaken by the cumulative negative radiative forcing due to $CO_2$ uptake; when cumulative GHG emissions reach zero.

### *3.3.4 Uncertainty and error propagation*

Uncertainty associated with annual NEE and $CH_4$ sums was estimated from both random half-hourly measurement error and ANN gap-filling error. For measured half hours, draws from a Laplace distribution parameterized by the residuals of the ANN predictions (binned by flux magnitude) was used as an estimate of the random error (Moffat et al., 2007; Richardson and Hollinger, 2007). For gap-filled half hours, the variance of the cumulative sum of the 20 ANN predictions was used as a measure of uncertainty (Anderson et al., 2016; Knox et al., 2018). Adding the cumulative and random measurement uncertainties in quadrature resulted in the total uncertainty reported as 95% uncertainty intervals alongside annual sums. This uncertainty describes how well, given the missing data and random error associated with the method, we are able to predict a single year's NEE or $CH_4$. It does not consider any systematic errors intrinsic to the measurement technique and gap filling method.

We also calculated the mean annual sum of a specific site, across all years observed, or across a single land use type, across all site-years observed, to determine the average NEE or $CH_4$ fluxes (Table 1). Uncertainty for this quantity is reported as a standard error of the multiple annual sums, which considers the number of years measured (Table 1). In the case of Twitchell corn, Bouldin corn, and Bouldin alfalfa, where there is only a single site-year of data and thus no interannual standard error, we report the annual ANN and random error, which is commonly less than the error associated with interannual variability. Calculating uncertainty around mean site and land-use NECB, GWP, and SGWP values was done by adding, in quadrature, the standard error of the component fluxes (NEE, $CH_4$, and harvest, where applicable). Multi-year site and land-use mean NECB, GWP and SGWP therefore are reported with propagated uncertainty that represents how well we are able to predict this mean value based on the limited annual measurements we have, and not the measurement error, which tends to be much lower than error associated with year to year variation.

For sites with multiple years of harvested biomass, we take the interannual standard error. When only a single year of harvest was available (Twitchell corn, Bouldin corn, and Twitchell alfalfa), we assumed a standard deviation that is 23% of the measured harvested carbon. This error percentage was estimated from the difference between yield reported by the farmer, and that computed from field-level biomass samples taken near peak biomass at Bouldin corn. Because only one single year of $N_2O$ chamber fluxes exist at two sites, we have no estimate of variation in multiyear sums, and thus exclude this in the error propagation at those two sites. All uncertainties are conservatively rounded up to the nearest whole number.

## *3.4 Results and Discussion*

### *3.4.1 Wetland land cover types*

The wetlands exhibited regular seasonal variations in $CO_2$ flux, with net $CO_2$ uptake (negative NEE) during the growing season and net respiration (positive NEE) during the winter months (Figure 3.1a, Figure 3.10 with confidence intervals). Except for the initial year after restoration, cumulative sums of NEE were neutral or negative (Figure 3.2), indicating net annual uptake of $CO_2$ by the restored wetlands. Cumulative sums reach up to -704 ± 72 g C-$CO_2$ $m^{-2}$ $yr^{-1}$ (West Pond, 2017; mean ± annual 95% uncertainty) with site averages of -321 ± 202, -223 ± 79 and -454 ± 89 g C-$CO_2$ $m^{-2}$ $yr^{-1}$ (mean ± interannual standard error) at East End, Mayberry and West Pond wetlands, respectively (Table 3.2).

Succession and disturbance caused large variation in NEE, and modulated the typical annual cycle of the established wetlands. The initial year after flooding, for which data exists at Sherman, East End, and Mayberry wetlands, were neutral to net sources. At that time, vegetation has not yet established and respiration from recently flooded soil contributed to a positive NEE for these three site-years of 201 ± 101 (Table 3.2; mean ± interannual standard error). Sherman Wetland was a net $CO_2$ source during the 2017 growing season due to sparse vegetation throughout the measurement footprint (Figure 3.2a). Similarly, East End's inaugural 2014 growing season was characterized by net emissions of $CO_2$ as wetland vegetation slowly established, making the site a source of GHG (Figure 3.2b). Mayberry wetland, restored in 2010, also experienced insect infestation (2013) and salinity stress (2015-2016), which reduced $CO_2$ uptake to near neutrality in those years (Figure 3.2c). West Pond wetland, the most mature site (restored in 1997), exhibited perennial uptake (Figure 3.2d) but lags other sites with a delayed green-up in the spring due to a thick layer of dead biomass that competes for photons and delays emergence (Eichelmann et al., 2018; Goulden et al., 2007) (Figure 3.9a).

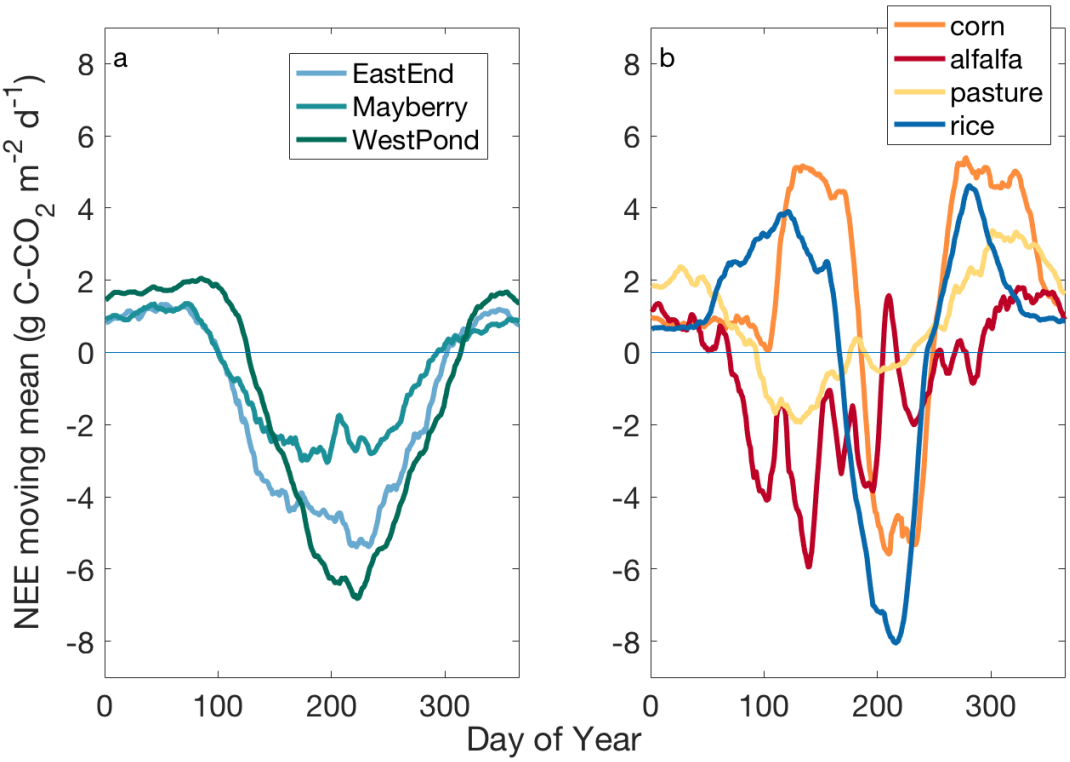


*Figure 3.1: Mean annual (10 day moving mean) net ecosystem exchange (g C-$CO_2$ $m^{-2}$ $day^{-1}$) for a. wetland sites and b. agricultural sites for all complete site-years on record. Full timeseries for wetland sites and agricultural sites in Supplement (Supplemental Figures 3.8, 3.9), as well as mean annual cycle with 95% uncertainty intervals (Supplemental Figures 3.10, 3.11).*

Despite interannual variability, Delta wetlands were generally larger $CO_2$ sinks than other restored wetlands in the literature, especially those in cooler temperate and boreal climates. A rewetted bog in British Columbia was a modest $CO_2$ sink (-179 ± 26.2 gC-$CO_2$ $m^{-2}$ $yr^{-1}$) 8 years after rewetting (Lee et al., 2016), while a restored wetland in Denmark, 7-9 years after rewetting, took up between -53 ± 8 and -268 ± 40 gC-$CO_2$ $m^{-2}$ $yr^{-1}$ (Herbst et al., 2013). Another Danish restored riparian zone with periodic inundation was a net source of $CO_2$ (220 g $CO_2$eq $m^{-2}$ $yr^{-1}$) 12 years after rewetting (Kandel et al., 2018). Mean uptake across all mature, vegetated wetland site-years in the Delta (not including initial years at Sherman, East End or Mayberry wetlands) was -386 ± 55 gC-$CO_2$ $m^{-2}$ $yr^{-1}$ (Table 3.2). The high productivity in the Delta, driven by long growing seasons, warm temperatures, large macrophyte vegetation (~3 m tall), and managed water levels that inhibit aerobic soil respiration, came at a cost. Flooding also caused large $CH_4$ emissions during the growing season when soil and water temperatures were high and carbon from photosynthetic uptake was exuded into the rhizosphere (Figure 3.3).

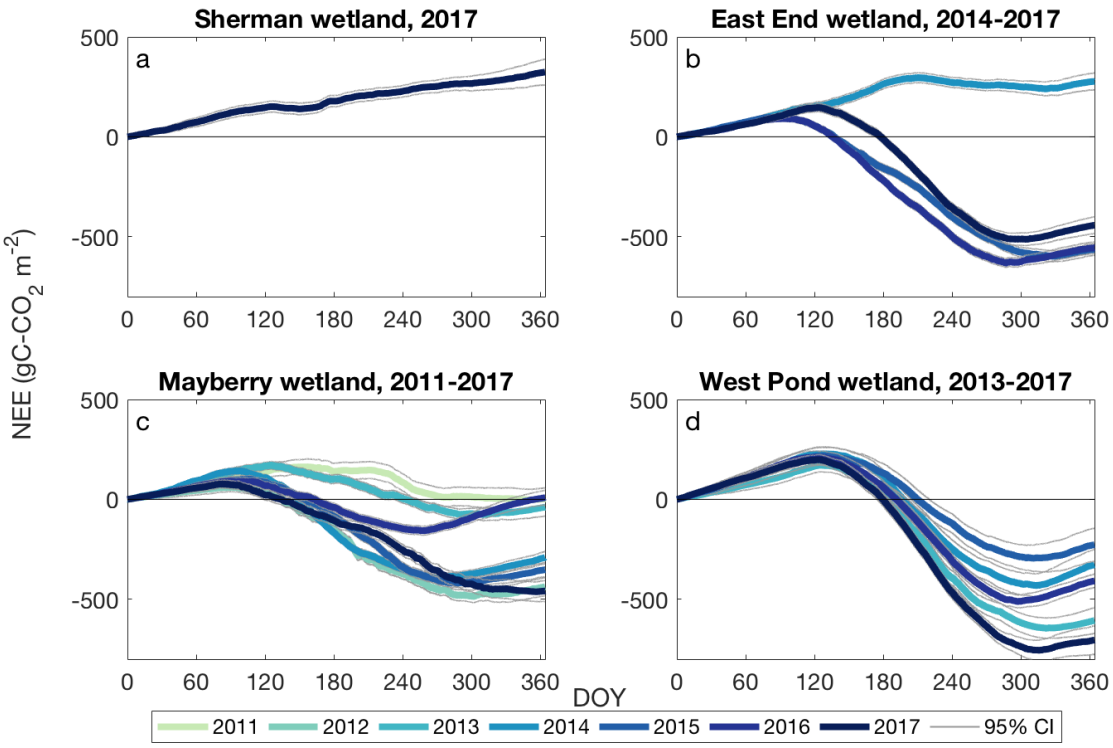


*Figure 3.2: Wetland site cumulative annual net ecosystem exchange ($gC\text{-}CO_2\ m^{-2}\ s^{-1}$), with 95% uncertainty interval error bars from ANN and random error, in grey.*

Delta wetland sites are among the highest $CH_4$ emitters across similarly measured wetlands around the world (Hemes et al., 2018a). $CH_4$ fluxes peaked in the summer and fell off throughout the winter as water temperatures decreased and GPP ceased (Figure 3.3, Figure 3.8b). Cumulative annual sums at the wetland sites ranged from 16 ± 1 to 63 ± 2 g $C\text{-}CH_4\ m^{-2}\ year^{-1}$ (Figure 3.3; mean ± annual 95% uncertainty), with an average across all wetland sites of 44 ± 4 g $C\text{-}CH_4\ m^{-2}\ year^{-1}$ (mean ± interannual standard error).

Interannual variability, however, caused nearly two-fold differences in annual $CH_4$ sums. Recent work points to potential redox controls on methanogensis driving interannual variability, including iron reduction in the years directly following restoration on alluvial soils, before significant peat soil accretion can dominate the soil redox environment (Chamberlain et al., 2018), and inadvertent temporary water table drawdowns creating oxidized conditions. Drivers of methane variability are diverse, scale dependent, and site specific (Sturtevant et al., 2016), although recent empirical modeling approaches can capture a large degree of the variability in these flooded systems (Oikawa et al., 2016a).

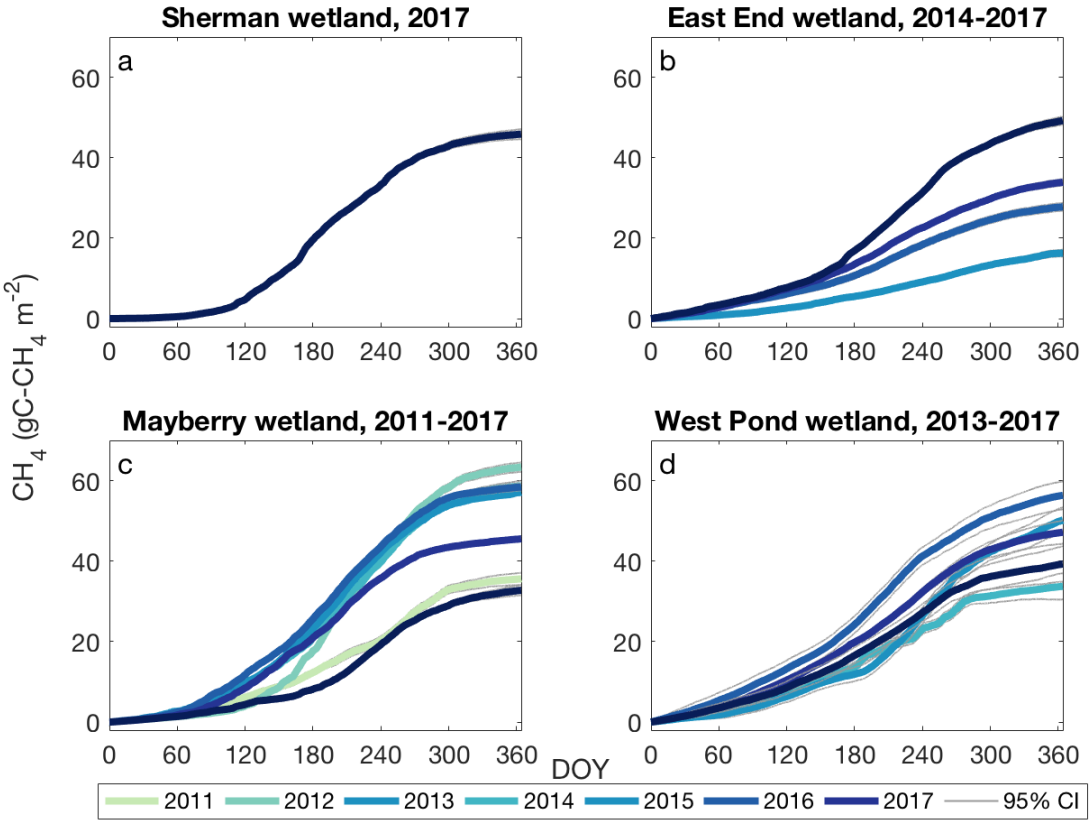


*Figure 3.3: Wetland site cumulative annual methane flux (gC-$CH_4$ $m^{-2}$ $s^{-1}$), with 95% uncertainty interval error bars from ANN and random error, in grey.*

### *3.4.2 Agricultural land cover types*

Agricultural land use types in the Delta included both annual (rice, pasture, and corn) and perennial crops (alfalfa) that underwent very different lifecycles and management practices, largely driving variation in biogeochemical cycling (Figure 3.1b). Rice, which was flooded for the winter and growing season, exhibited net $CO_2$ uptake during the flooded growth stages, when soil respiration was largely inhibited by anaerobic conditions (Figure 3.4a). Winter flooding (for bird habitat) kept winter respiration low, until spring pre-harvest drainage caused a spike in $CO_2$ efflux. Similarly, a $CO_2$ efflux spike in the fall occurred during drainage for harvest and before the field was reflooded (Figure 3.1b, Figure 3.4a). Depending on the size of these $CO_2$ emissions in comparison with uptake during the growing season, rice was a net $CO_2$ source or sink, with cumulative annual sums that ranged from 547 ± 42 to -313 ± 59 g C-$CO_2$ $m^{-2}$ $year^{-1}$ before considering harvested biomass removal (Figure 3.4a; mean ± annual 95% uncertainty). The rice site emitted an average of 12 ± 2 gC-$CH_4$ $m^{-2}$ $year^{-1}$ (mean ± interannual standard error), which accounted for ~10% of its mean $CO_2$ emissions over the study period. A $CH_4$ efflux spike occurred in the fall as the field was drained before harvest (Figure 3.9b), accounting for a large portion of the annual $CH_4$ sum.

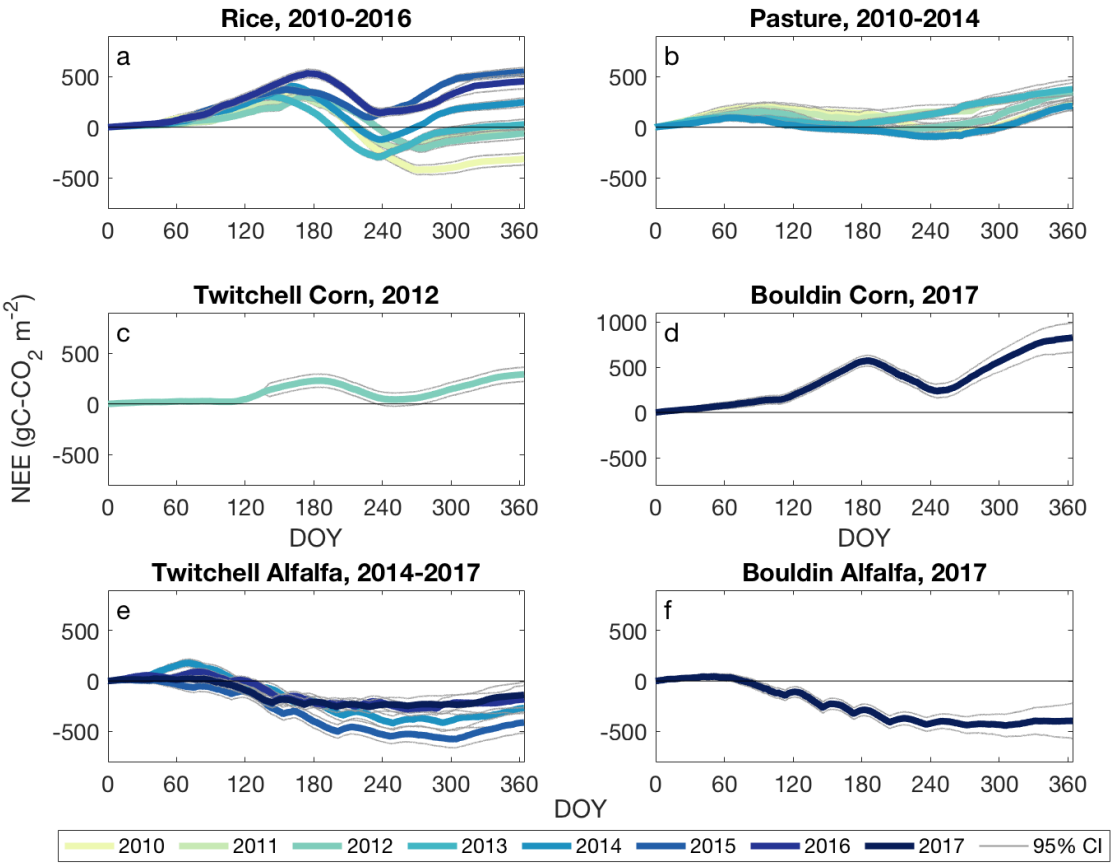


*Figure 3.4: Agricultural site cumulative annual net ecosystem exchange (g C-$CO_2$ $m^{-2}$ $s^{-1}$), with 95% uncertainty interval error bars from ANN and random error, in grey. Sums are computed before considering removed biomass from harvest.*

Pasture was intermittently grazed, on subsided land with lower soil C stocks and periodic inundation (making it unfit for cropland). It contained the least amount of aboveground biomass, and thus exhibited low net uptake during the growing season (Figure 3.1). This uptake occurred in late spring, when invasive pepperweed was in growth stages. Over the hot, dry summer, growth trailed off, although pepperweed was able to tap subsurface irrigation or shallow groundwater due to the heavily subsided island. Large efflux spikes often corresponded to fall precipitation, when otherwise dry soil layers were moistened and microbial activity was catalyzed (Hatala et al., 2012) (Figure 3.9a). All years of data for the pasture site (2010-2014) resulted in a mean $CO_2$ source of 306 ± 36 g C-$CO_2$ $m^{-2}$ $yr^{-1}$ (mean ± interannual standard error; Fig 4b). Periodic anaerobic conditions from standing water after winter precipitation events evolved 9 ± 2 gC-$CH_4$ $m^{-2}$ $yr^{-1}$ (mean ± interannual standard error) over the study period, accounting for a small portion of the pasture site's C budget (Table 1).

A single year of fluxes at two different corn sites (Twitchell corn, 2012-2013 and Bouldin corn, 2017-2018) showed strong growing season uptake during a two-month period (July-August) of rapid biomass accrual with large net respiration during other times of the year, except during flooding (December-February for bird habitat) in the winter (Figure 3.1b). The Twitchell corn site respired less and also took up less $CO_2$ as compared to Bouldin corn, but both underwent peak uptake between DOY 200 and 250. The efficient C4 photosynthetic pathway of corn, achieving high LAI very rapidly, led to a relatively short period of net C uptake compared to the perennial wetlands or alfalfa crops. Despite high maximum uptake, the corn sites were net sources of $CO_2$ on an annual basis, even before accounting for harvested biomass emissions, of $292 \pm 37$ and $826 \pm 84$ g C-$CO_2$ $m^{-2}$ $yr^{-1}$, respectively (mean ± annual 95% uncertainty; Figure 3.4c,d). We measured low $CH_4$ emissions at Bouldin corn, primarily occurring during the flooded winter period, of $2 \pm 1$ gC-$CH_4$ $m^{-2}$ $yr^{-1}$ (Figure 3.9b).

Alfalfa, a perennial crop, exhibits a much longer growing season than the annual crops, but is harvested multiple times a year, explaining the 5-6 periods of reduction in uptake during growing season cuttings (Figure 3.1b). Successive harvests resulted in incrementally lower uptake throughout the growing season. Before accounting for harvested biomass emissions, Twitchell alfalfa, planted on lower C soil, was a mean $CO_2$ sink of $-249 \pm 61$ g C-$CO_2$ $m^{-2}$ $yr^{-1}$ (mean ± interannual standard error), while Bouldin alfalfa was a $CO_2$ sink of $-396 \pm 90$ g C-$CO_2$ $m^{-2}$ $yr^{-1}$ (Figure 3.4e,f), with negligible $CH_4$ emissions ($1 \pm 3$ g C-$CH_4$ $m^{-2}$ $yr^{-1}$; mean ± annual 95% uncertainty; Table 1).

### *3.4.3 Carbon and GHG budgets*

To assess the potential for restored wetlands to sequester C compared to the drained agricultural land uses, we computed multi-year NECB. Except for the first year of restoration at Sherman wetland and East End wetland, NECB for the wetland sites was consistently neutral to negative, supporting our hypothesis that wetlands sequester C from the atmosphere and store it in accreted, organic soil (Figure 3.5). This accretion of C in wetland soils is confirmed by 4,000-6,000 years of historic peat buildup (Drexler et al., 2007; Weir, 1950), as well as recent accretion measurements at West Pond. Simulations suggest accretion of ~3 cm $yr^{-1}$ with rates up to 9 cm $yr^{-1}$ in some locations (Deverel et al., 2014; Miller et al., 2008).

Agricultural sites, on the other hand, were consistently neutral to net C sources, losing C to the atmosphere, mostly in the form of ecosystem $CO_2$ respiration and harvested biomass, which we considered a $CO_2$ emission upon removal from the field (Table 1). This net loss of C from the landscape (Figure 3.5) is consistent with observations of significant subsidence of agricultural lands in the Delta (Deverel et al., 2016; Weir, 1950). In the case of perennial alfalfa, biomass

removed from the site through harvest turns the site from a net sink to a net source of C. On the other hand, productivity would likely not be as high without the periodic harvests, which promote rapid biomass regeneration.

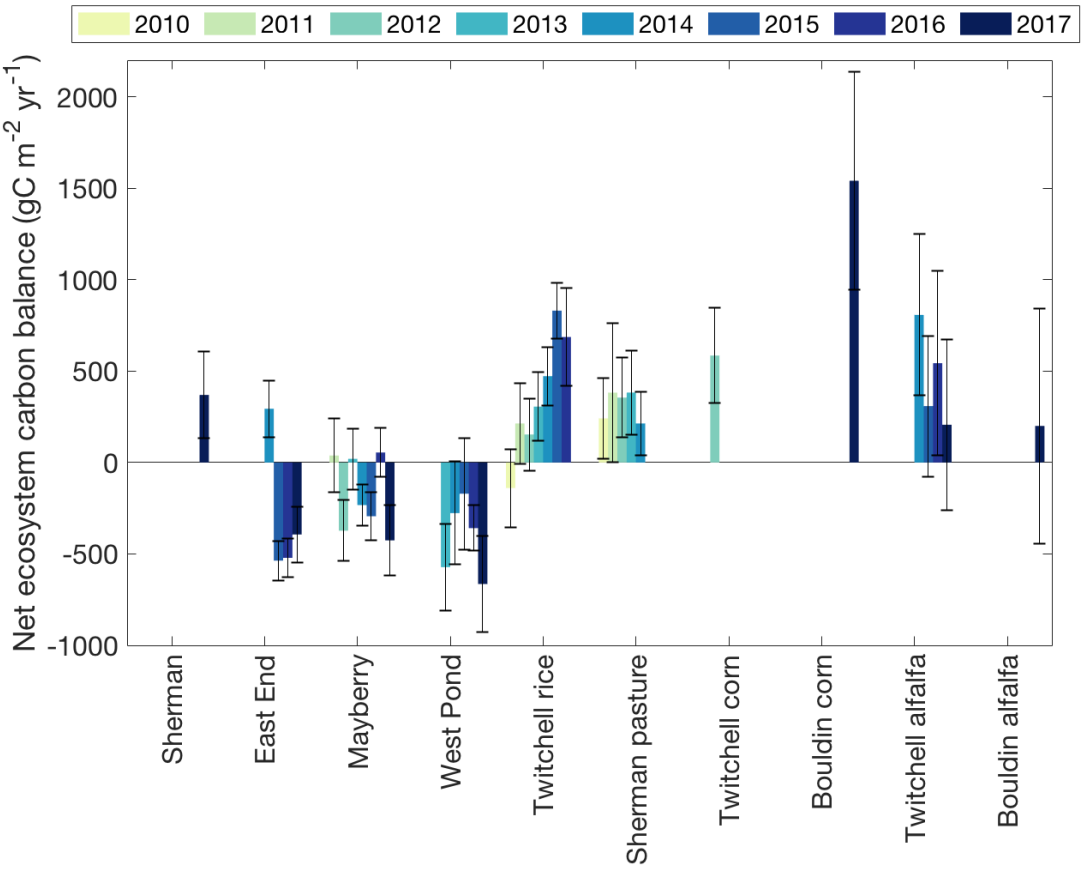


*Figure 3.5: Total annual net ecosystem carbon balance (g C $m^{-2}$ $yr^{-1}$) for each full year at each site. Includes C-$CO_2$, C-$CH_4$, and C removed as harvested biomass from the agricultural sites. Error bars represent 95% uncertainty intervals of the ANN and random error.*

Taking all wetland site-years across the various successional stages, we derived a combined emission factor (using GWP-28) of 620 ± 292 g $CO_2$eq $m^{-2}$ $yr^{-1}$ (mean ± propagated standard error) in the Delta (Table 3.2). This grows to 1785 ± 328 g $CO_2$eq $m^{-2}$ $yr^{-1}$ when using SGWP-45 metric for $CH_4$. These values are not necessarily representative of future wetland emissions, as they are influenced greatly by the initial year after restoration, which is a large source. Mature, vegetated wetlands (excluding initial years after restoration) emitted, on average, 333 ± 230 g $CO_2$eq $m^{-2}$ $yr^{-1}$, using the GWP-28. For each individual site, annual $CO_2$eq emissions were positive for all land uses studied, regardless of GWP metric (Table 3.2). East End and West Pond

wetlands were nearly neutral (13 ± 782 and 32 ± 357 g $CO_2$eq $m^{-2}$ $yr^{-1}$) assuming a GWP-28, while the recently or often disturbed wetlands, like Sherman and Mayberry, were in some cases larger emitters (2901 ± 124 and 1060 ± 337 g $CO_2$eq $m^{-2}$ $yr^{-1}$, respectively) than certain agricultural land uses. When the long-term radiative forcing impacts of $CH_4$ were given more weight due to their sustained nature, as with the SGWP-45 metric, the wetland GHG budgets increased and were, in some cases, larger than agricultural land uses with low $CH_4$ emissions. Agricultural sites were all net sources of $CO_2$eq, even before addition of the $N_2O$ contribution, which was applied for the two sites at which it was measured, using the GWP-265 metric. The corn and rice sites were larger sources than the pasture and alfalfa sites, regardless of the GWP metric.

| *Site* | *$CO_2$* | *$CH_4$* | *Harvest* | *NECB* | *GWP* | *SGWP* | *GWP w/ $N_2O$* |
|---|---|---|---|---|---|---|---|
| | g C-$CO_2$ $m^{-2}$ $yr^{-1}$ | g C-$CH_4$ $m^{-2}$ $yr^{-1}$ | g C $m^{-2}$ $yr^{-1}$ | | g $CO_2$eq $m^{-2}$ $yr^{-1}$ | | |
| | | | | | $CH_4$ GWP-28 | $CH_4$ GWP-45 | $CH_4$ GWP-28; $N_2O$ GWP-265 |
| *Sherman wetland* | 323 ± 34* | 46 ± 1* | n/a | 370 ± 34* | 2901 ± 124* | 4111 ± 128* | - |
| *East End wetland* | -321 ± 202 | 32 ± 7 | n/a | -290 ± 202 | 13 ± 782 | 852 ± 846 | - |
| *Mayberry wetland* | -223 ± 79 | 50 ± 5 | n/a | -173 ± 79 | 1060 ± 337 | 2385 ± 402 | - |
| *West Pond wetland* | -454 ± 89 | 45± 4 | n/a | -409 ± 89 | 32 ± 357 | 1228 ± 404 | - |
| *all wetland sites* | -282 ± 73 | 44 ± 4 | n/a | -238± 74 | 620 ± 292 | 1785 ± 328 | - |
| *all vegetated site-years* | -386 ± 55 | 47 ± 4 | n/a | -339 ± 55 | 333 ± 230 | 1565 ± 272 | - |

| | | | | | | | |
|---|---|---|---|---|---|---|---|
| *Twitchell rice* | 126 ± 115 | 12 ± 2 | 222 ± 14 | 360 ± 116 | 1735 ± 428 | 2059 ± 433 | - |
| *Sherman pasture* | 306 ± 36 | 9 ± 2 | - | 315 ± 36 | 1460 ± 146 | 1700 ± 168 | - |
| *Twitchell corn* | 292 ± 37* | - | 293 ± 68* | 585 ± 77* | 2143 ± 281* | 2143 ± 281* | - |
| *Bouldin corn* | 826± 84* | 2 ± 1* | 712± 164* | 1541± 184* | 5719 ± 674* | 5777 ± 675* | 6595 ± 674** |
| *Twitchell alfalfa* | -249 ± 61 | - | 715 ± 150 | 466 ± 162 | 1709 ± 591 | 1709 ± 591 | - |
| *Bouldin alfalfa* | -396 ± 90* | 1 ± 3* | 595 ± 137* | 200 ± 164* | 775 ± 607* | 808 ± 619* | 915 ± 607** |

*Table 3.2: Mean annual component GHG fluxes, harvest, net ecosystem carbon balance (NECB), GHG budget using global warming potential (GWP-28), sustained global warming potential (SGWP-45), and including $N_2O$ (GWP-265, for the two sites for which it was measured). Uncertainty in component GHG fluxes and harvest is reported with standard error of annual sums (*or in the case of a site with a single year record, error from ANN and random error). NECB and GHG budget uncertainty is reported as propagated standard errors. 'All wetland sites' include all complete wetland site years. 'All vegetated site-years' excludes the first year of restoration at Sherman, East End, and Mayberry wetlands, before vegetation established. The symbol 'n/a' indicates that a field is not applicable to a particular site, while '-' indicates that a value was not measured, and is assumed to be de minimis. **Due to only a single year of $N_2O$, no uncertainty in interannual variability of annual sums was included.*

Beyond restored Delta wetlands, where freshwater inputs keep the water table above the land surface, long-term, continuous, ecosystem-scale accounting of GHG impacts of restored wetlands are limited. Due to geomorphology, climate, wetland type, and restoration strategy, there is considerable variability in emissions from restored peat wetlands (Hoper et al., 2008). A multiyear chamber study of the GHG budgets at a seven-year old restored freshwater bog in Ireland reported a significant net reduction in the GWP at the rewetted and colonized wetland site compared to a drained control, despite a net positive GWP at most revegetated sites (Wilson et al., 2016b). A rewetted British Columbia peat bog was nearly neutral using GWP-28 after almost a decade of re-wetting (Lee et al., 2016). A Dutch peatland landscape study found that agricultural drained peatlands could be returned to sinks of GHG and C within 15 years of rewetting (Schrier-Uijl et al., 2014), while a different restored wetland, 7-9 years after rewetting ranged from a large GHG sink to a small GHG source, both assuming GWP-25 (Herbst et al., 2013). Lack of consistent application of GWP values, as well as different ages and paces of succession, make comparisons between restored wetlands challenging. While our wetland sites

are consistently C sinks, their GHG budgets are all positive due to large $CH_4$ emissions (Table 3.2). In many cases, however, drained peat soil agricultural sites are equivalent or larger GHG sources.

Our continuous ecosystem-scale wetland and agricultural measurements capture the net impact of the dominant two GHGs - $CO_2$ and $CH_4$. In the wetlands, redox states that support partial denitrification and evolution of $N_2O$ are not common (Wilson et al., 2016a, 2016b), unless high $NO_3^-$ inputs inhibit nitrous oxide reductase enzyme activity (Tiedie, 1988). Weekly ebullition chamber and dissolved $N_2O$ measurements at Mayberry wetland confirmed that the contribution of $N_2O$ to radiative forcing was negligible, compared to the other two GHGs (McNicol et al., 2016). In Denmark, a rewetted temperate riparian wetland's annual $N_2O$ emissions accounted for 7% of its overall GHG budget, although this could have been partially stimulated by the periodic inundation (Kandel et al., 2018).

At the agricultural sites, $N_2O$ is not negligible due to nitrogen fertilization and fluctuating redox dynamics favorable to $N_2O$ evolution during irrigation or precipitation (Firestone and Davidson, 1989). Using an array of nine automatic chambers co-located with our eddy covariance measurements at Bouldin corn and Bouldin alfalfa, we measured annual sums of 3.28 ± 0.12 g $N_2O$ $m^{-2}$ $yr^{-1}$ and 0.51 ± 0.07 g $N_2O$ $m^{-2}$ $yr^{-1}$ (mean ± standard error), respectively (Anthony et al., in prep). Using the 100-year GWP of 265 g $CO_2$eq, radiative forcing due to $N_2O$ accounted for 13% and 15% of these agricultural sites' annual GHG budget, or 868 and 136 g CO2eq $m^{-2}$ $yr^{-1}$ (Table 3.2). A literature review by Deverel et al. (2017) estimates that agriculture $N_2O$ in the Delta amounts to between 262 – 974 g $CO_2$ eq $m^{-2}$ $yr^{-1}$. IPCC Tier 1 emission factors for $N_2O$ are on the order of 609 g$CO_2$eq $m^{-2}$ $yr^{-1}$ (Wilson et al., 2016a). $N_2O$ emissions of this order of magnitude warrant further continuous measurements of this important GHG.

### *3.4.4 Climatic impact of restoration*

Conversion from a large GHG source land use type, like Bouldin corn, to a restored wetland, always yields an emission reduction over a 100-year timescale, no matter the GWP metric used (Table 3.3). Other land use conversions, like those from pasture to wetland, will conditionally yield a net emission reduction, depending on the biogeochemical performance and management of the specific restored wetland, as well as the GWP metric considered. Conversion from Twitchell corn and Twitchell alfalfa are similar – if transitioning to a restored wetland like East End or West Pond, emission reductions are achieved, no matter the GWP metric. If transitioning to a wetland like Mayberry, the GWP metric chosen will determine if emission reductions are achieved. Conversion from agricultural systems that are net GHG sinks, like Bouldin alfalfa (and only small net sources after harvest is considered), may in some cases yield emission increases over a 100-year timescale according to these metrics. If considering the agricultural sites' $N_2O$

burden, which we omitted from Table 3.3 as it was not measured consistently across sites, potential emission reductions from wetland restoration would increase.

| ***GWP 28*** | *Sherman Pasture* | *Twitchell Corn* | *Bouldin Corn* | *Twitchell Alfalfa* | *Bouldin Alfalfa* |
|---|---|---|---|---|---|
| *Sherman* | 1441 ± 191 | 759 ± 307 | -2818 ± 685 | 1193 ± 604 | 2126 ± 619 |
| *East End* | -1448 ± 795 | -2130 ± 831 | -5707 ± 1032 | -1696 ± 980 | -762 ± 990 |
| *Mayberry* | -400 ± 367 | -1083 ± 439 | -4660 ± 754 | -649 ± 680 | 285 ± 694 |
| *West Pond* | -1428 ± 385 | -2110 ± 454 | -5687 ± 763 | -1677 ± 690 | -743 ± 704 |
| *Twitchell Rice* | 274 ± 449 | -408 ± 509 | -3985 ± 797 | 26 ± 728 | 960 ± 741 |
| ***SGWP 45*** | *Sherman Pasture* | *Twitchell Corn* | *Bouldin Corn* | *Twitchell Alfalfa* | *Bouldin Alfalfa* |
| *Sherman* | 2411 ± 211 | 1968 ± 308 | -1667 ± 687 | 2402 ± 604 | 3303 ± 632 |
| *East End* | -849 ± 863 | -1291 ± 892 | -4926 ± 1082 | -857 ± 1032 | 44 ± 1049 |
| *Mayberry* | 684 ± 436 | 242 ± 490 | -3393 ± 785 | 676 ± 715 | 1576 ± 738 |
| *West Pond* | -472 ± 437 | -914 ± 491 | -4549 ± 786 | -480 ± 715 | 420 ± 739 |
| *Twitchell Rice* | 359 ± 465 | -84 ± 516 | -3718 ± 802 | 350 ± 732 | 1251 ± 756 |

*Table 3.3: Matrix of emission reductions (blue) or increases (red) in a theoretical land use transition from agricultural (columns) to flooded land uses (rows) in g $CO_2$ eq $m^{-2}$ $yr^{-1}$assuming a GWP of 28 (upper; Myhre et al., 2013) and a SGWP of 45 (bottom; Neubauer & Megonigol, 2018). Emissions from $N_2O$ not included, as these were only measured for two site-years. Uncertainty is reported as propagated standard error of component $CO_2$, $CH_4$, and harvest, where applicable.*

In systems that produce considerable SLCPs, like the restored wetlands studied here, the timescale of analysis can influence the apparent climate impact of the land use change. Much previous work in natural wetlands has shown that despite $CH_4$ emissions, over multi-century timescales natural wetlands tend to have a net biogeochemical cooling effect (Frolking and Roulet, 2007; Roulet, 2000; Roulet et al., 2007). Over time, the cumulative removal of $CO_2$, an

extremely long-lived GHG, vastly outweighs the short-lived $CH_4$ warming effect. Discrepancies between GWP metrics utilized to equate $CH_4$ with $CO_2$ greatly affect if and when emission reductions are achieved and the quantity of those net reductions (Table 3.3). The debate continues about how to best account for SLCPs like $CH_4$ in the context of land-use changes, technology assessments, and mitigation scenarios at the national scale (Allen et al., 2018; Balcombe et al., 2018; Neubauer and Megonigal, 2015). Recent $CH_4$ emissions may be especially important to short-term climate forcing, as the post-2006 uptick in atmospheric $CH_4$ concentrations were associated with an immediate, positive trend in radiative forcing (Feldman et al., 2018). On the other hand, emerging metrics, like GWP*, emphasize the change in SLCPs' flux rate over the cumulative emissions, due to the short atmospheric lifetime of these gases (Allen et al., 2016).

With a simple GWP* model based on $\Delta CH_4$, we assess the 'switchover time' for which restored Delta wetland ecosystems transition from a source to a sink, e.g., when the positive radiative forcing associated with $CO_2$ respiration and $CH_4$ emissions is overtaken by the negative radiative forcing of $CO_2$ removal (Figure 3.6). We also compute how many years it takes for wetland restoration to begin to accrue net GHG benefits to the atmosphere – this occurs when the cumulative wetland GHG emissions (black line) and the cumulative $CO_2$ emissions of the agricultural land use (orange, yellow, pink lines) cross (Figure 3.6). Using these conventions, we compare the avoided emission trajectories of a land use transition from agriculture to a restored wetland, for three cases relevant to the Delta. Due to the abrupt change in NEE after the initial year of restoration, we model the initial year based on the mean and standard deviation of NEE and $CH_4$ emissions from year one at Sherman, East End, and Mayberry wetlands. Subsequent years are assigned the emission factor for NEE and $CH_4$ from fully vegetated wetlands, which excludes the initial year at those same sites (Table 3.2).

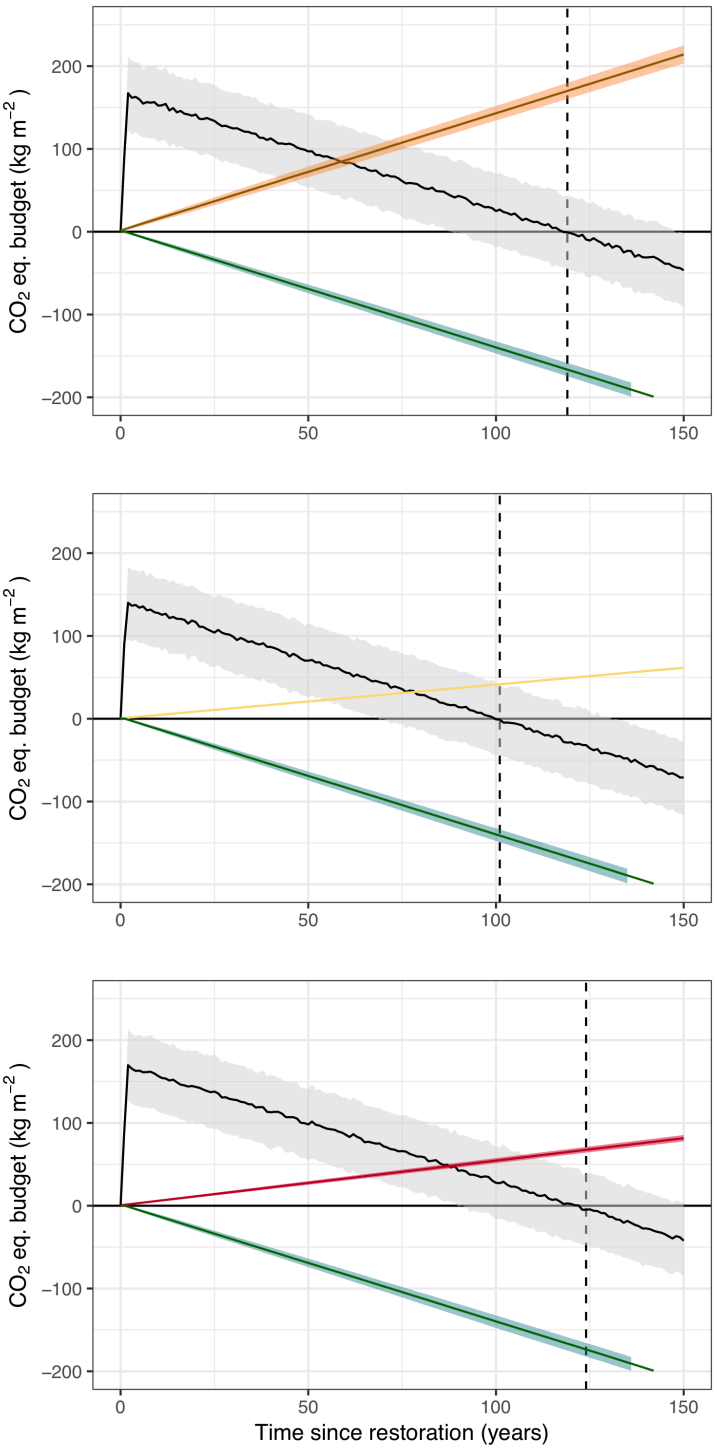


*Figure 3.6: Modeled cumulative wetland $CO_2$ uptake (green line) and cumulative net GHG emissions of $CO_2$ and $CH_4$ (black line) versus agricultural 'business as usual' cumulative $CO_2$ emissions for a. corn, b. pasture, and c. alfalfa. Emission rates based on mean annual land use fluxes reported above, using the GWP* metric of Allen et al, 2016, 2018. Grey area represents 95% uncertainty in switchover time.*

When transitioning from corn to wetland using the GWP* metric (Figure 3.6a), the two land uses become GHG equivalent sources after 60 ± 16 (mean ± 95% uncertainty interval of crossover) years. After this time, the restored wetland begins to accrue a net GHG benefit to the atmosphere, compared to its preceding land use. The wetland's large initial $CH_4$ burden, incurred when transitioning from a drained to a flooded land use, incurs a sizeable GHG 'debt' that is only neutralized by its cumulative $CO_2$ uptake after 119 ± 30 years. At this switchover time, the wetland land use has saved 169 kg $CO_2$eq $m^{-2}$ compared to continuous corn, and will continue to be GHG beneficial into the future assuming stable environmental conditions and no major disturbances.

A wetland restored from pasture, which is a much smaller net source than corn, will take 80 ± 24 years to begin accruing climate benefit. At the time the wetland switches over from a cumulative source to a cumulative sink (101 ± 31 years), it will have saved 42 kg $CO_2$eq $m^{-2}$ compared to continuous pasture land use (Figure 3.6b). Because the low-lying pasture is already a $CH_4$ emitter, the $\Delta CH_4$ 'debt' upon restoration is not as large, and thus the switchover time comes sooner than other land uses. Finally, a wetland restored from alfalfa will take 89 ± 22 years to begin accruing GHG benefits. After 124 ± 31 years, it will switchover to a net GHG sink, at which time it will have avoided 72 kg $CO_2$eq $m^{-2}$ compared to continuous alfalfa land use (Figure 3.6c).

Despite a large range of uncertainty due to the sizeable interannual variability in annual restored wetland $CO_2$ and $CH_4$ fluxes, we can see that depending on the preceding 'baseline' land use, restored wetlands will begin to accrue GHG benefits after a half century, and become net sinks from the atmosphere after a century. Because our simulation uses the same 'representative' wetland for each scenario, the differences in the switchover time and $CO_2$ savings are attributed to the emission burden of the 'business-as-usual' agricultural land use. Multi-decadal permanence of this kind of wetland restoration may not be sufficient to ensure GHG benefits, due to the time it takes for the incurred $CH_4$ debt to be neutralized by $CO_2$ uptake. On a multi-century timescale, however, these wetland land uses can be seen as largely climate-beneficial.

Common carbon crediting schemes compare GHG emissions of a low-emission land-use activity to a 'business as usual' baseline over a multi-decadal timescale, typically using a 100-year GWP. Wetland restoration, for example, would be compared to the agricultural land use that preceded it to compute emission reductions (Table 3.3). This framework generally assumes a static baseline – that the agricultural emissions are constant through time. In the Delta, with increasing subsidence and reductions in surface C stocks over time, high-value agriculture is often transitioned to lower-value agriculture as the soil quality is diminished. Future work could more explicitly capture this in long term projections.

Similarly, little is known about the long-term successional trajectory of restored wetlands, which can be considered novel systems due to their unique hydrological management and land use history. Although theory from natural terrestrial ecosystems suggests that in late ecological succession, NEE would tend towards zero (Chapin et al., 2012; Odum, 1969), this may not be the case in highly managed systems, especially given that the most mature restored wetland (West Pond, restored 1997) often took up the most $CO_2$ annually (Figure 3.2b). We assume that our sample of wetland site-years, which range from one to twenty years since restoration, is representative of the kinds of disturbance and interannual variability that may be encountered throughout a century. Our future projections are also limited due to uncertainties around future climate in California, which is likely to get hotter and drier throughout the century (Pathak et al., 2018). In addition to the biogeochemical considerations, commonly utilized quantification schemes rarely recognize the radiative and non-radiative impacts associated with biophysical changes due to restoration such as albedo, roughness, and evaporative efficiency (Baldocchi and Panuelas, 2018; Bonan, 2008; Perugini et al., 2017). In the case of wetlands, the net biophysical forcings cause a surface cooling effect and a reduction in the diurnal temperature range compared to an agricultural 'baseline' (Hemes et al., 2018b).

### *3.4.5 Scaling implications*

Using our 36 site-years of continuous ecosystem-scale measurements, we derived a relationship between GPP and ecosystem respiration ($R_{eco}$) in the Delta, aggregated by land use type (Figure 3.7; see Supplementary Figure 3.13 for disaggregated relationships). Wetland land use types and flooded periods of rice – together 'wet land cover' – inhibited $R_{eco}$ in a way that reduced the slope of the $R_{eco}$:GPP relationship by 23% compared to the 'dry' agricultural land covers, which did not generally have standing water. The background emissions in the absence of GPP were about half as much for the wet land covers ($52.6 \pm 1.9$ g C-$CO_2$ $m^{-2}$ $month^{-1}$; intercept ± standard error) compared to the dry ($94.8 \pm 4.5$ g C-$CO_2$ $m^{-2}$ $month^{-1}$). This flooding-induced inhibition of soil respiration reduced the C loss of the restored wetlands, led to C sequestration and in many cases, GHG emission reductions in transitions from degraded agricultural peat soils to managed restored wetlands (Table 3.3).

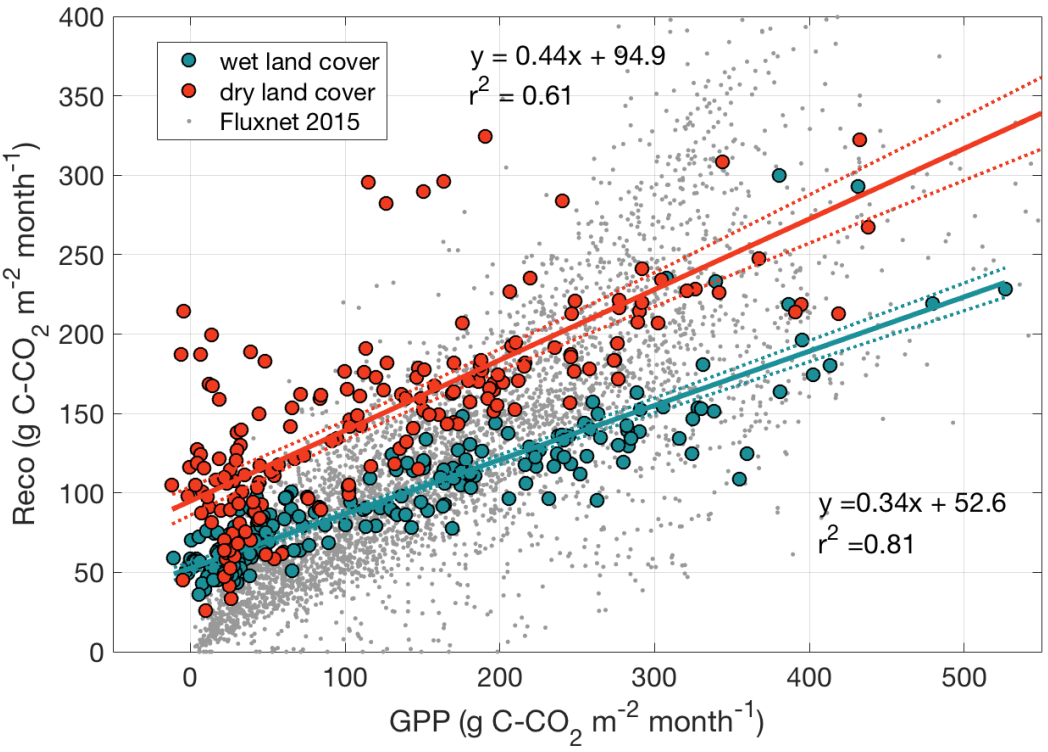


*Figure 3.7: Monthly sums of gross primary productivity (gC-$CO_2$ $m^{-2}$ $month^{-1}$) and ecosystem respiration (gC-$CO_2$ $m^{-2}$ $month^{-1}$) for aggregated land cover classes, with 95% uncertainty (dashed lines).*

Compared to the biogeochemical 'space' occupied by the range of biomes represented in the Fluxnet network of eddy covariance measurement sites across the world (Figure 3.7; grey points), we see that high-productivity wet land cover months occupy the lower right edge of the figure. The Delta's 'dry' land cover sites – irrigated agricultural sites on drained, organic peat soils, displayed some of the higher monthly $R_{eco}$:GPP ratios across the network, especially during shoulder season periods of exposed soil but little productivity. Our sites' highly organic soils and raised water levels add unique parameter space to the previous understandings of $R_{eco}$:GPP ratios. These high ratios are especially apparent at our rice site, when drained, and at our Bouldin corn site, which is on soil with especially high C content (~18% C) (Supplementary Figure 3.13). Conversion of these highly respiring sites to restored wetlands with vastly inhibited soil respiration can potentially achieve the greatest emission reductions. Observationally derived ratios of $R_{eco}$:GPP at a range of soil organic C content sites across the Delta could allow for spatial modeling of fluxes within a carbon accounting framework, as well as to identify restoration sites that would yield optimum GHG reductions.

While our network across the western and central Delta represents a range of dominant land uses over multiple years, scaling these field-level measurements to the broader Delta region will require a robust measurement-based modeling framework. Modeling frameworks that have been validated on measured observations and can capture emissions from restored wetlands could be an important tool to reduce costs associated with measurement and verification (Oikawa et al., 2016a). Methodologies that are not based on direct measurement, and instead use conservative emission factors, can underestimate the potential emission reductions achieved, and thus jeopardize funding for restoration projects. Recent analysis of one of the first carbon credit projects transacted for peatland restoration found that direct measurements, as opposed to conservative emission factors, resulted in a greater number of carbon credits the majority of the time (Günther et al., 2018). These benefits must be weighed against the costs to project proponents of undertaking and directly measuring the effects of a restoration project. Simple models that can be validated and calibrated for specific geographies and soil types, and rely on publicly available and remotely sensed data inputs, have the best chance of balancing cost and scientific rigor at scale to promote land use activities within a market or payment-for-ecosystem services program.

## *3.5 Conclusion*

Restoring drained and degraded peat soils to managed, impounded wetlands presents an attractive, but largely untested, climate change mitigation potential (Deverel et al., 2017; Griscom et al., 2017; Leifeld and Menichetti, 2018). Here, we synthesize 36 site-years of continuous $CO_2$ and $CH_4$ flux data from a mesonetwork of eddy covariance towers in the Sacramento-San Joaquin River Delta to compute C and GHG budgets for drained agricultural peatland sites and a chronosequence of four restored wetlands. Due to management practices that inhibit $R_{eco}$ and allow for robust GPP (Figure 3.7), we find that restored wetlands effectively sequester C, reversing soil loss that is associated with subsiding drained agricultural land uses (Figure 3.5). After the initial year of restoration, wetland land uses were, on average, sizeable sinks of C ($-339 \pm 55$ g C $m^{-2}$ $yr^{-1}$), while agricultural sites lost up to $1541 \pm 184$ g C $m^{-2}$ $yr^{-1}$ (Bouldin Corn, 2017; Table 3.2).

$CH_4$ emissions due to anaerobic decomposition and lack of $CH_4$ oxidation result in wetlands being near neutral to GHG sources (Hemes et al., 2018a), although the choice of GWP metric has an important impact on the magnitude of the total GHG budget (Table 3.2). Despite this, depending on the successional age and disturbance regime of the restored wetland, many land use conversions from agriculture to restored wetland would result in emission reductions over a 100-year timescale (Table 3.3). With a simple model of radiative forcing and atmospheric lifetimes, we show that restored wetlands will not begin to accrue GHG benefits for at least a half century, and become net sinks from the atmosphere after a century or more (Figure 3.6).

Policymakers and planners should take measures that promote the long-term restoration of these kinds of systems to maximize climatic benefit. Chronosequences of restored wetlands must be continuously measured to understand how their GHG sink or source nature changes as they mature.

Simple models, based on measured relationships between partitioned fluxes (Figure 3.7), could be instrumental in reducing costs and increasing implementation of GHG emission reduction projects like wetland restoration (Oikawa et al., 2016a). More robust integration of long-term $N_2O$ fluxes into the GHG budgets of the agricultural sites will likely increase the net benefit of wetland restoration. Active wetland management to reduce $CH_4$ evolution, through water table and/or redox manipulation, could also increase the benefit of restoration (Hemes et al., 2018a). Potential biogeochemical benefits of restoration should be considered in light of the other important co-benefits, such as habitat, water infrastructure, and microclimate impacts (Hemes et al., 2018b). Long term, continuous, ecosystem-scale measurements of land-atmosphere exchange over a range of managed land uses, disturbance regimes, and soil types will contribute to our understanding of how policies and programs could incentivize low emission land use management and climate change mitigation.

## *3.6 Supplemental figures*

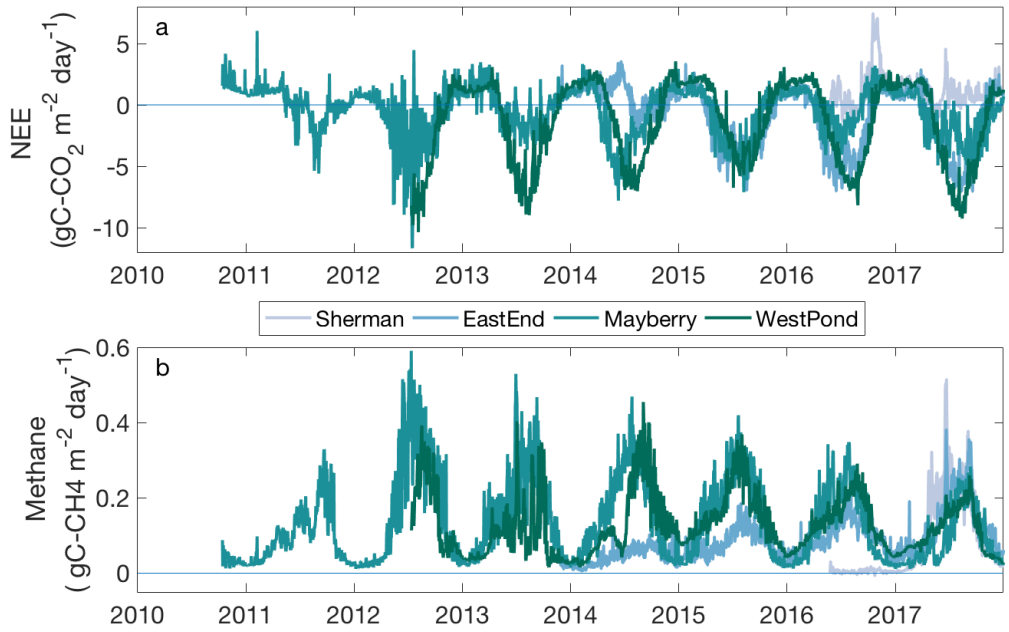


*Supplemental Figure 3.8: Timeseries of daily a.) net ecosystem exchange (gC-$CO_2$ $m^{-2}$ $day^{-1}$) and b.) methane flux (gC-$CH_4$ $m^{-2}$ $day^{-1}$) for wetland sites.*

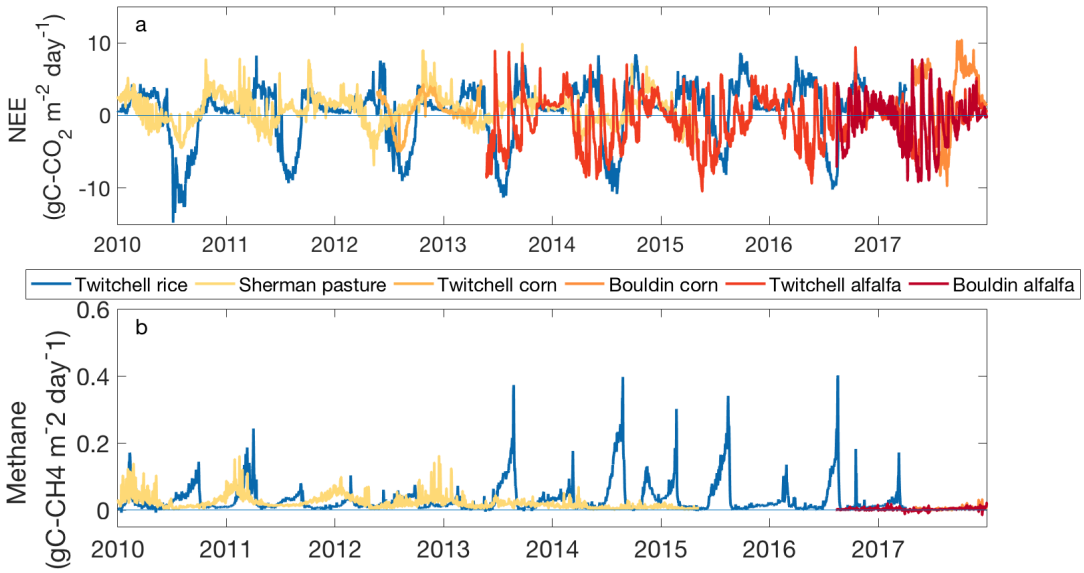


*Supplemental Figure 3.9: Timeseries of daily a) net ecosystem exchange (gC-$CO_2$ $m^{-2}$ $day^{-1}$) and b.) methane flux (gC-$CH_4$ $m^{-2}$ $day^{-1}$) for agricultural sites.*

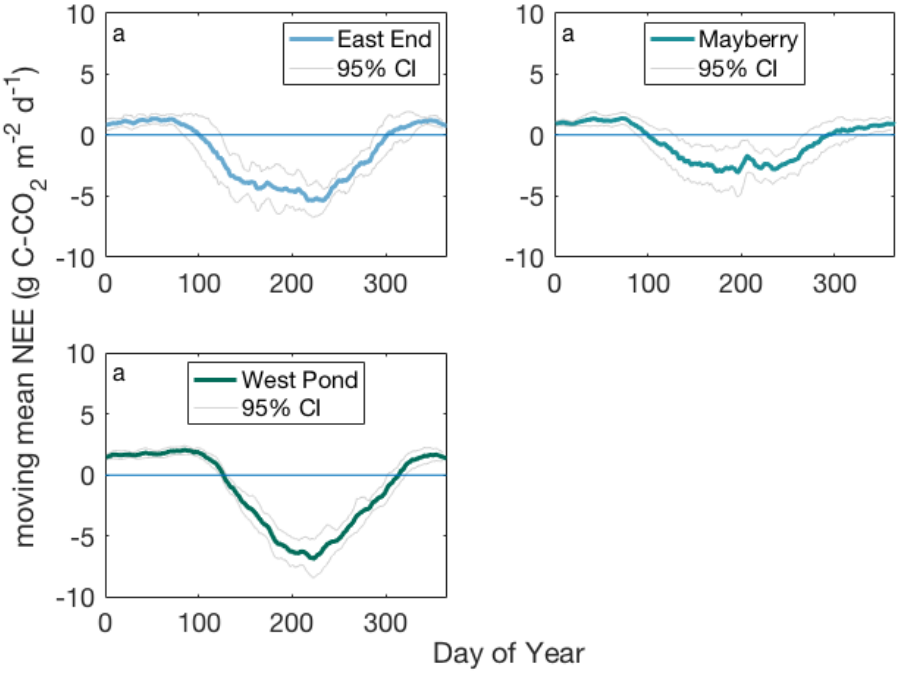


*Supplemental Figure 3.10: Mean annual (10 day moving mean) net ecosystem exchange (g C-$CO_2$ $m^{-2}$ $day^{-1}$) for wetland sites, as shown in Fig 1, with 95% uncertainty intervals (grey).*

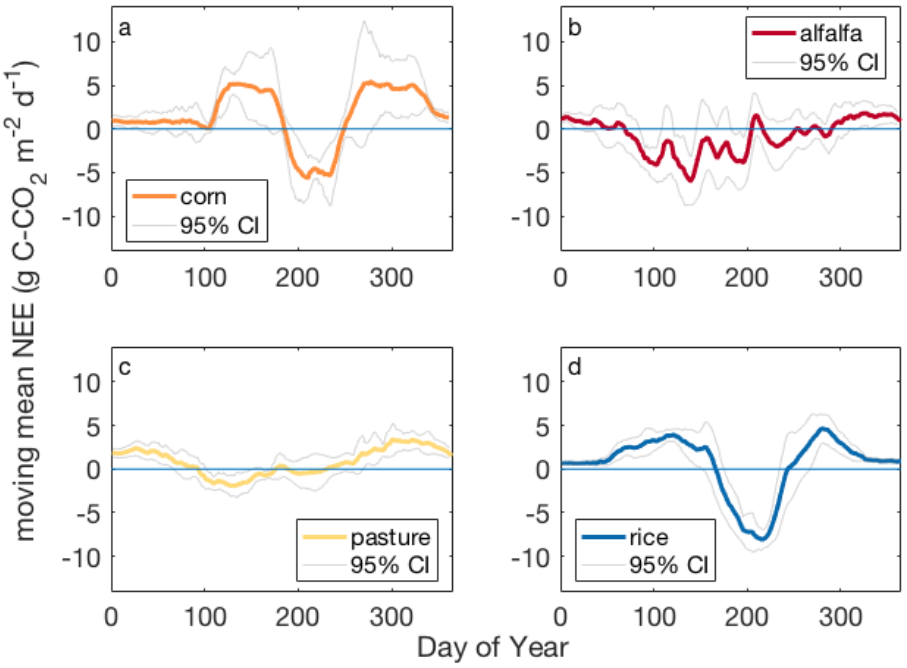


*Supplemental Figure 3.11: Mean annual (10 day moving mean) net ecosystem exchange (g C-$CO_2$ $m^{-2}$ $day^{-1}$) for agricultural sites, as shown in Fig 1, with 95% uncertainty intervals (grey).*

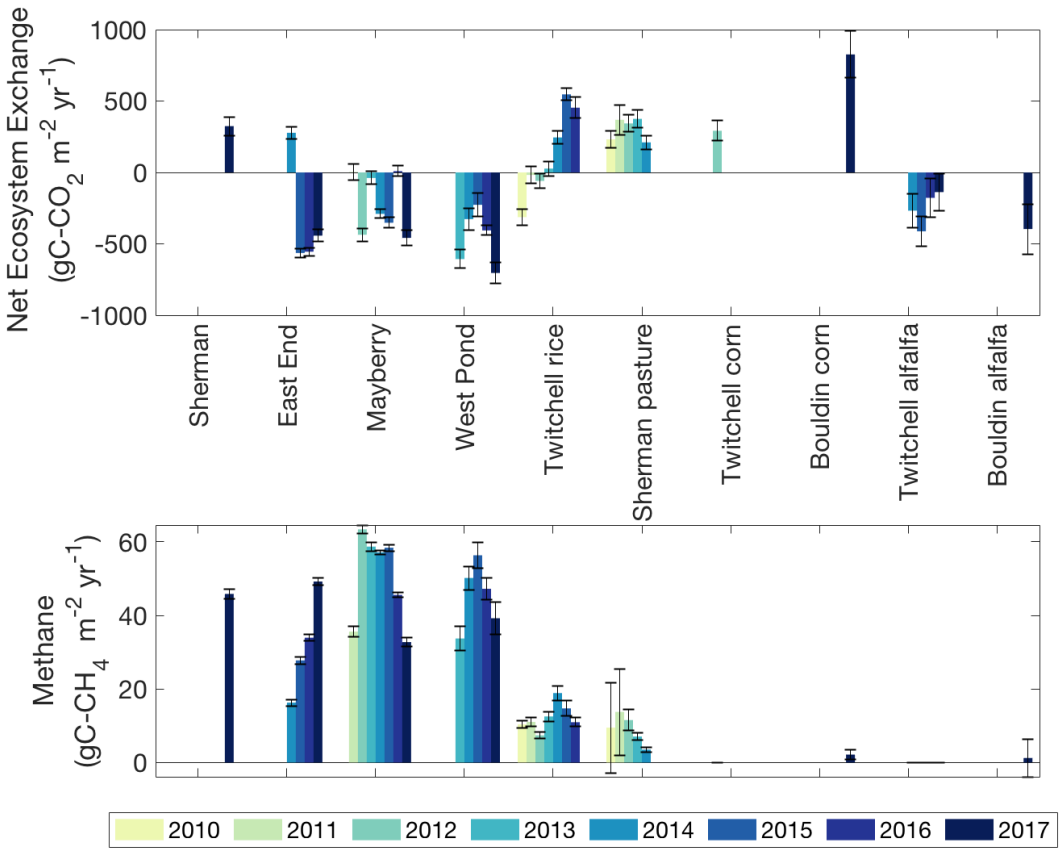


*Supplemental Figure 3.12: Annual carbon budget from $CO_2$ (top) ($gC\text{-}CO_2\ m^{-2}\ yr^{-1}$) and $CH_4$ (top) ($gC\text{-}CH_4\ m^{-2}\ yr^{-1}$) for each full year at each site ($CH_4$ not measured at Sherman Corn or Twitchell Alfalfa), with 95% uncertainty intervals.*

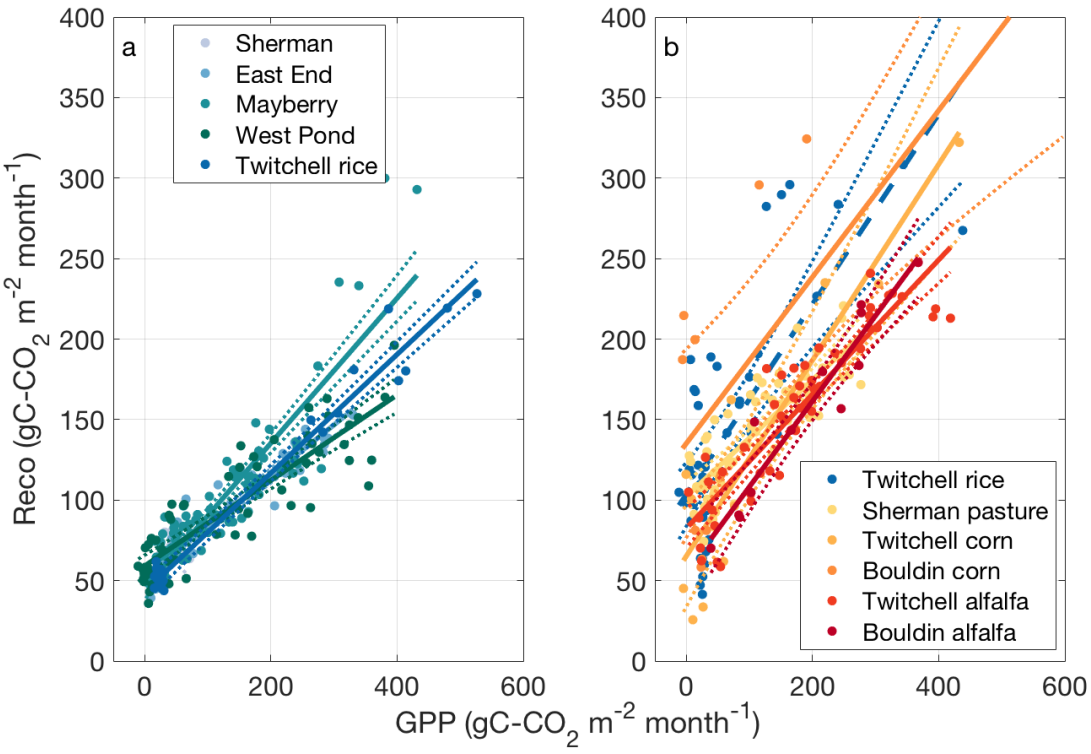


*Supplemental Figure 3.13: Monthly mean scaling of gross primary productivity (gC-$CO_2$ $m^{-2}$ $month^{-1}$) with ecosystem respiration (gC-$CO_2$ $m^{-2}$ $month^{-1}$) at a.) wet land covers, including flooded months at Twitchell Rice, and b.) 'dry' agricultural land covers including drained months at Twitchell Rice.*

# 4 A unique combination of aerodynamic and surface properties contribute to surface cooling in restored wetlands of the Sacramento-San Joaquin Delta, California[3]

## *4.1 Abstract*

Land use change and management affect climate by altering both the biogeochemical and biophysical interactions between the land and atmosphere. Whereas climate policy often emphasizes the biogeochemical impact of land use change, biophysical impacts, including changes in reflectance, energy partitioning among sensible and latent heat exchange, and surface roughness, can attenuate or enhance biogeochemical effects at local to regional scales. This study analyzes three years (2015-2017) of turbulent flux and meteorological data across three contrasting wetland restoration sites and one agricultural site, co-located in the Sacramento-San Joaquin Delta, California, USA, to understand if the biophysical impacts of freshwater wetland restoration can be expected to attenuate or enhance the potential biogeochemical benefits. We show that despite absorbing more net radiation, restored wetlands have the potential to cool daytime surface temperature by up to 5.1°C, as compared to a dominant drained agricultural land use. Wetland canopy structure largely determines the magnitude of surface temperature cooling, with wetlands that contain areas of open water leading to enhanced nighttime latent heat flux and reduced diurnal temperate range. Daytime surface cooling could be important in ameliorating physiological stress associated with hotter and drier conditions and could also promote boundary layer feedbacks at the local to regional scale. With a renewed focus on the mitigation and adaptation potential of natural and working lands, we must better understand the role of biophysical changes, especially in novel land use transitions like wetland restoration.

## *4.2 Introduction*

Land use change and management affect climate by altering both the biogeochemical and biophysical processes that govern the exchange of greenhouse gases (GHG) and energy between the land and atmosphere (Anderson et al., 2011; Bonan, 2008; Luyssaert et al., 2014). Biogeochemical impacts are caused by changes in GHG exchange rates between ecosystems and the atmosphere, with net atmospheric increases in GHG concentrations resulting in increased radiative forcing and climate change (Arneth et al., 2010; Tian et al., 2016). Biophysical impacts of land use change include changes in reflectance, the partitioning of energy into latent and sensible heat exchange, surface roughness, and ultimately surface and mixed-layer air temperature. These factors can attenuate or enhance biogeochemical effects at local to regional

[3] originally published as: Hemes, K.S., Eichelmann, E., Chamberlain, S.D., Knox, S.H., Oikawa, P.Y., Sturtevant, C., Verfaillie, J.G., Szutu, D., Baldocchi, D.D., 2018. A Unique Combination of Aerodynamic and Surface Properties Contribute to Surface Cooling in Restored Wetlands of the Sacramento-San Joaquin Delta, California. J. Geophys. Res. Biogeosciences 123, 2072–2090. https://doi.org/10.1029/2018JG004494

scales (Anderson et al., 2011; Bright et al., 2017; Jackson et al., 2008; Mahmood et al., 2014; Perugini et al., 2017; Rotenberg and Yakir, 2010; Zhao and Jackson, 2014).

Whereas much of the literature focuses exclusively on the biogeochemical impact of land use change (Mcalpine et al., 2010), the emphasis on biophysical impacts has been primarily limited to re- and deforestation scenarios (Alkama and Cescatti, 2016; Bonan, 2008; Burakowski et al., 2017; Juang et al., 2007; Lee et al., 2011; Lejeune et al., 2018; Perugini et al., 2017; Rotenberg and Yakir, 2010; Zhao and Jackson, 2014), woody vegetation encroachment (D'Odorico et al., 2010; He et al., 2015) and cropland management (Bonfils et al., 2007; Georgescu et al., 2011; Lobell et al., 2006; Lobell and Bonfils, 2008). With nascent policy mechanisms set to compensate landowners and farmers for low emission land use practices, it is essential that they take into consideration how the biophysical impacts of novel land use changes could drive local to regional-scale climatic perturbations, enhancing or attenuating the biogeochemical impacts. Beyond reforestation, few studies have explored the biophysical impacts of important types of land use change that have been proposed for climate change mitigation, such as restoring wetlands (Griscom et al., 2017; Paustian et al., 2016).

While flooded wetland systems have the potential to sequester carbon as photosynthesis outpaces oxygen-inhibited respiration, the highly reduced conditions can result in significant methane emissions (Bridgham et al., 2013; Dean et al., 2018; Petrescu et al., 2015). Restoring freshwater marshes has the potential to sequester significant amounts of carbon in accreted soil, as evidenced by the deep peatlands that have formed over thousands of years (Drexler et al., 2009), but come at the cost of significant methane emissions (Hatala et al., 2012; Knox et al., 2015). The biophysical changes inherent in the transition from drained peatland agriculture to restored wetland, however, are not well established.

The Sacramento-San Joaquin Delta (hereafter, 'Delta') provides an ideal system to understand the coupled biogeochemical and biophysical impacts of wetland restoration. The Delta has been subsiding dramatically since the mid-19th century, in large part due to agricultural conversion of the natural freshwater wetlands (Weir, 1950). As the carbon-rich peat soil was drained and tilled, levees were erected to protect the 'islands' from seasonal inundation. These processes exposed the previously flooded soil to oxygen and catalyzed aerobic oxidation, in some places leading to soil losses of up to 8 meters (Deverel et al., 2016; Drexler et al., 2009). Efforts to re-wet the peat soils through wetland restoration are attractive as climate mitigation activities, as well as to restore habitat and decrease hydrostatic pressure on levees that make up the Delta's fragile system of islands (Mount and Twiss, 2005). Measurements over a mesonetwork of restored wetlands in the Delta have shown that conversion of drained peatlands to wetlands can, in some cases, yield a net GHG benefit when compared to the original land use (Knox et al., 2015). Few studies have attempted to quantify the biophysical impacts of freshwater wetland restoration over such a network.

Part of the challenge in quantifying biophysical impacts of land use change stems from the fact that they consist of radiative (albedo) and non-radiative (evaporative efficiency and roughness) terms, often opposing in sign, that integrate to a net biophysical climatic impact (Bonan, 2008; Bright et al., 2017). Modification to the surface albedo changes the ratio of reflected to absorbed radiation, affecting the net radiation balance of the surface (Brovkin et al., 1999). The IPCC has included a term for radiative forcing associated with albedo changes due to anthropogenic land use and land cover change which partially offsets the net positive radiative forcing associated with anthropogenic changes in the atmosphere (Myhre et al., 2013). Changes in surface properties also affect surface temperature and emissivity, which govern the longwave emissions from the surface.

Evaporative efficiency, or the partitioning of available energy into latent and sensible heat fluxes, can affect near-surface temperature and planetary boundary layer processes (Davin and de Noblet-Ducoudre, 2010; Luyssaert et al., 2014). Water availability at the surface of an ecosystem, which can be expressed through bulk surface conductance, largely determines whether available energy is partitioned into latent or sensible heat. Surface roughness, which controls the transfer of energy, mass, and momentum between the canopy and atmosphere, plays an important role in transferring this sensible and latent heat away from the surface, into the atmosphere (Verma, 1989). Enhanced surface roughness will increase the degree to which a canopy is coupled to the atmosphere (Jarvis and McNaughton, 1986), and affect turbulent fluxes. In turn, this can cause a surface temperature effect determined by the evaporative efficiency. Due to large uncertainties around the signs and magnitudes of the integrated biophysical impacts to climate, and the fact that a simple metric does not exist to reconcile radiative and non-radiative impacts on a global scale, the IPCC has omitted these non-radiative effects of land use change (Myhre et al., 2013).

Studies of biophysical impacts of land use change have been largely focused on transitions from field to forest, where competing effects of ecophysiological aerodynamics and albedo have been found to drive cooling (Juang et al., 2007). In a Mediterranean system, the potential air temperature over a rougher and less reflective oak woodland savannah was warmer than an aerodynamically smoother annual grassland (Baldocchi and Ma, 2013). Other work points to a latitudinal dependence on the temperature difference between open land and forested measurement sites (Davin and de Noblet-Ducoudre, 2010; Lee et al., 2011). Compared to open lands, forests tend to reduce the diurnal temperature range (DTR) by cooling during the day (Lejeune et al., 2018) and warming at night (Lee et al., 2011), largely owing to roughness differences (Burakowski et al., 2017). Land use management associated with croplands has also been investigated at regional scales to understand near surface temperature impacts associated with irrigation (Bonfils et al., 2007), tilling, and crop productivity (Lobell et al., 2006). Other

important ecosystems beyond forests and irrigated croplands, like restored wetlands, have relatively few observations of biophysical climatic impacts.

This study analyzes three years (2015 - 2017) of eddy covariance flux and meteorological data across three wetland restoration sites and one drained peatland agriculture site co-located in the Delta. The restored wetland sites, all constructed with managed water tables, differ somewhat in their species mix, areal extent, bathymetry, and years since restoration, but are all subject to similar meteorological drivers due to their close spatial proximity (< 13 km). Using eddy covariance and associated meteorological and environmental measurements, we test the hypothesis that restored wetlands will have a cooling effect on surface temperature.

We expect low-albedo wetland surfaces to take up more net radiation which will be stored in the water column, or preferentially partitioned into latent heat flux, increasing evaporative efficiency. The wetlands' aerodynamically rougher canopy structure will enhance turbulent mixing of heat fluxes away from the canopy. We propose that wetland restoration, in the transition from an aerodynamically smooth and short-statured agricultural crop to dense, emergent wetland species may mimic some of the biophysical surface dynamics that characterize reforestation. Computations of aerodynamic surface temperature and energy balance differences, along with an assessment of canopy conductance properties will allow us to diagnose the biophysical differences between a drained agricultural peatland and the various restored wetlands. This study aims to understand if the biophysical impacts of restoration at the local scale can be expected to attenuate or enhance the potential biogeochemical benefits of freshwater wetland restoration. It also aims to understand the potential implications of regional-scale wetland restoration on plant physiology and mixed layer air temperature.

## *4.3 Data and methods*

### *4.3.1 Site characteristics*

The Sacramento-San Joaquin Delta lies at the confluence of two of California's major rivers and formed a historic 1400 $km^2$ freshwater wetland landscape at near-sea level (Atwater et al., 1979). In the mid 19th century, the wetland was diked and drained for agricultural purposes, exposing deep peat soils to oxygen. Today, more than 1700 km of dikes and levees hold back the rivers and sloughs that make up the modern Delta (Mount and Twiss, 2005). The Delta is critical to California's water storage and transport system; the rivers that feed the Delta provide at least a portion of the drinking water to more than two-thirds of Californians through the State Water Project and the Central Valley Project (Miller et al., 2008). The Delta's wetland soils are highly organic while the agricultural soils exhibit a degraded, oxidized peat surface layer underlain by a

deep peat horizon (Miller et al., 2008). The remaining peat is estimated to be 4,000-6,000 years old (Drexler et al., 2009; Weir, 1950).

To understand the biophysical impacts of land use change, the three restored wetland sites, designated young wetland, intermediate wetland, and old wetland (which refers to their age since restoration), are each compared to alfalfa, a drained agricultural peatland land use. While the Delta has supported a number of agricultural crops since drainage and 'reclamation' in the mid-19th century, alfalfa (Medicago sativa L.) shares a perennial life-cycle strategy with the dominant tule (Schoenoplectus acutus) and cattail (Typha spp.) wetland species and represents one of the most important agricultural crops in the five-county Delta region and California as a whole. In 2015, more than 80,000 acres were planted with alfalfa in the Delta region, representing 11.8% of the region's land cover (Medellín-Azuara et al., 2016). All sites have been described in previous studies and will be summarized here for brevity (Eichelmann et al., 2018; Knox et al., 2015).

The alfalfa (US-TW3, Twitchell Alfalfa) site is an alfalfa field on Twitchell Island, previously planted in corn. Alfalfa is sub-irrigated, harvested between 5 and 7 times a year, beginning in mid-March, and is periodically grazed with sheep. Alfalfa is California's largest agricultural water user and is, like the wetland systems, a perennial with a long growing season (Hanson et al., 2007). While the full record of the alfalfa crop was preserved to represent the actual state of the agro-ecosystem, the periodic cuttings did affect the surface energy balance. Tests excluding the 5-10 days after cutting to remove this effect had minor impacts on the results.

The young wetland (US-TW4, East End) was constructed in late 2013 after being under continuous corn cultivation. Since initial flooding, the wetland filled in with tule and cattail vegetation, and represents an early-intermediate stage of restoration, with limited patches of open water. The 90% average cumulative eddy covariance flux footprint spans 390 meters in the west-southwest direction (Eichelmann et al., 2018). The early years of the young wetland's restoration exhibited very dynamic changes in vegetation structure and extent as vegetation filled in. Due to a faulty wiring connection, horizontal wind speed and direction data over a period between July 2015 and Jan 2016 was corrupted and is thus omitted from the young wetland record.

The intermediate restored wetland (US-MYB, Mayberry) was constructed in 2010 on Sherman Island. With a water table as deep as 2 meters in open-water channels, the intermediate wetland is the most heterogeneous of the three restored wetland treatments in this study. The 90% average cumulative eddy covariance flux footprint spans 350 meters in the west-northwest direction capturing large areas of open water and patches of vegetation (Eichelmann et al., 2018).

Additionally, rising salinity levels during drought years and insect infestation in the wetland caused lowered productivity throughout the study period. This wetland is also vegetated with a mixture of tule and cattail.

The old restored wetland (US-TW1, West Pond) was constructed in 1997 as the pilot restored wetland for the ongoing study on Twitchell Island. We began eddy flux measurements in summer 2012. The old wetland, which is dominated by tall, emergent tule and cattail, represents a mature restored wetland and has no open water patches. The 90% average cumulative eddy covariance flux footprint spans 260 meters in the west-southwest direction (Eichelmann et al., 2018).

### *4.3.2 Eddy covariance measurements and processing*

#### *4.3.2.1 Site setup*

We used the eddy covariance method (Baldocchi et al., 1988) to measure continuous fluxes of $H_2O$, $CO_2$, and sensible heat at all sites. Fluxes were measured at a frequency of 20 Hz, using open-path infrared gas analyzers (LI-7500 or LI-7500A, LiCOR Inc., Lincoln, NE, USA) that are calibrated every 3 - 6 months in the lab (LI-7500). Sonic anemometers measure sonic temperature and three-dimensional wind speeds at 20 Hz (WindMaster Pro 1352, Gill Instruments Ltd, Lymington, Hampshire, England). All instruments are mounted on towers at a height of 2.9 to 5.1 meters above the surface (*Table 4.1*), in such an orientation as to prevent interference with winds from the dominant direction.

| Land use type | Site (Ameriflux ID) | Land use history | Location | Albedo (min/max) | Measurement height/mean canopy height** (m) |
|---|---|---|---|---|---|
| **'alfalfa'** | Alfalfa (US-TW3) | 30 ha Alfalfa since 2010, previously corn | Twitchell Island. 38.1159 N, -121.6467 W | 0.142/0.248 | 2.9/0.4*** |
| **'young wetland'** | East End (US-TW4) | 323 ha wetland restored in 2013 | Twitchell Island. 38.1030 N, -121.6414 W | 0.097/0.142 | 4.9/2.2 |

| | | | | | |
|---|---|---|---|---|---|
| **'intermediate wetland'** | Mayberry (US-MYB) | 121 ha wetland restored in 2010 | Sherman Island. 38.0498 N, -121.7651 W | 0.122/0.134* | 5.1/3.4 |
| **'old wetland'** | West Pond (US-TW1) | 3 ha wetland restored in 1997 | Twitchell Island. 38.1074 N, -121.6469 W | 0.108/0.142 | 4.5/2.6 |

*Table 4.1: Site characteristics. Maximum and minimum mean monthly midday shortwave albedo as measured with a tower-mounted four-way net radiometer (*intermediate wetland site albedo estimated from annual footprint averaged min/max values extracted from MODIS albedo product MCD43A; ** measurement height measured from water surface at wetland sites, mean canopy height computed from turbulent statistics; ***vegetation height varies from 0.1-0.6 cm depending on time since cutting).*

By most standards, the study sites provide near-ideal conditions for measuring turbulent fluxes using the eddy covariance method (Baldocchi et al., 1988). The study sites are exceedingly flat, have large fetches, and exhibit brisk daytime and nighttime winds. Sampling is at sufficiently high resolution to capture most of the flux-containing eddies and to minimize filtering of the flux signal by the separation of the instruments and the path separation of the transducers. The instrument setup (sampling rate, sensor separation, fetch and sensor height) was designed to optimize the measured cospectrum and minimize spectral filtering (Detto et al., 2010). Typical cospectra exhibit slopes that closely match the idealized slope from Kaimal et al. (1972). The main complication affecting the interpretation of our fluxes is the relative lack of homogeneity of the footprint of the restored wetlands, a mosaic of open water and vegetation.

Energy balance closure serves as a metric to evaluate scalar flux measurements when using the eddy covariance method over terrestrial ecosystems (Wilson et al., 2002). Ground heat flux (G) is not measured at the old or intermediate wetland sites but is expected to be small due to the water layer dampening the energy flux into the soil. Storage flux (S) in the water column of the wetlands is significant, due to the high heat capacity of water, especially in wetlands with open water surfaces. While multi-level temperature profiles are deployed at the towers, storage flux is challenging to accurately predict due to non-horizontally isothermal conditions, complex bathymetry at the sites, and variable vegetation shading and insulation. In addition, water table height changes depending on pumping, evaporation, and precipitation. The available measurements represent limited sample areas compared to the integrated footprint of latent and sensible heat fluxes provided by the eddy covariance measurements.

For these reasons, half hourly energy balance closure over the three-year study period is best at the alfalfa and old wetland sites with closed canopies (79.3% and 78.1%, respectively). The

young and intermediate wetlands, with large tracts of open water storing energy, are further from closure (55.8% and 65.2%, respectively), indicating the inability to measure the available energy terms (G and S) completely and representatively across the complex footprint (Eichelmann et al., 2018). To more adequately and consistently represent storage at all sites in our analysis, we use the residual of the energy balance to compute a combined soil and water storage term as:

$$S_{residual} = RNET - \lambda E - H \ \ (\text{W m}^{-2})$$

where RNET is the net radiation as measured by the radiometer, $\lambda E$ is the latent heat flux and H is the sensible heat flux, both measured by eddy covariance.

#### *4.3.2.2 Processing and gap filling*

Trace gas and energy fluxes were calculated using the 30-minute covariance of turbulent fluctuations in vertical wind speed and scalar of interest after applying a series of standard corrections and site-specific factors (Detto et al., 2010; Hatala et al., 2012; Knox et al., 2015). Coordinate rotations were performed so that mean wind speeds at each 30-minute averaging interval were zero in the cross-wind and vertical directions. To account for air density fluctuations, the Webb-Pearman-Leuning corrections were applied (Webb et al., 1980). To remove flux data measured over non-ideal conditions, half hourly fluxes were filtered for stability and turbulence, friction velocity, wind direction, spikes in mean densities, variances and covariances, and sensor window obstruction.

To integrate yearly budgets we gap filled fluxes by training an Artificial Neural Network (ANN) using measured meteorological variables (Moffat et al., 2007; Papale et al., 2006). Training, validation, and testing data was selected from a series of k-means clusters to avoid seasonal or diurnal bias (Mathworks, Inc. 2012). Network architecture with varying levels of complexity were tested, with the simplest architecture selected for which further increases in complexity yielded less than a 5% reduction in mean standard error (Knox et al., 2016, 2015). This entire ANN procedure was performed 20 times, producing 20 separate ANNs. The median prediction of the 20 ANNs was used to fill gaps in the annual data, with linear correlation fits of 94%, 91%, 88%, 98% (alfalfa, young wetland, intermediate wetland, and old wetland, respectively) for LE flux and 96%, 96%, 93%, 98% for H flux.

### *4.3.3 Temperature measurements*

Different temperature metrics can reveal various aspects of heat exchange between the landscape and the atmosphere. Near-surface air temperature is convenient for scaling observations with

basic meteorological data, but is influenced by measurement height, as well as local meteorological and atmospheric stability. Radiative temperature, derived from radiative longwave emission and knowledge of surface emissivity can reveal the temperature at the leaf. It can be biased if the canopy is open and the background surface temperature is much greater than the leaf temperature. Furthermore, the sampling area of the radiometer depends on its field of view, angle of observation and height above the surface, making it often unrepresentative of large heterogeneous footprints. Aerodynamic temperature, derived from canopy aerodynamic properties and sensible heat flux, yields the temperature of the surface that drives turbulent fluxes. It represents a large footprint, samples sunlit and shaded leaves, and may be the most representative measure of the temperature that organisms experience at the landscape scale (Verma, 1989). For these reasons, we used aerodynamic surface temperature ($T_{aero}$) as our metric for the integrated biophysical impacts of land use change. Aerodynamic surface temperature is defined as:

$$T_{aero} = \frac{H}{\rho C_p G_{aero}} + T_{air} \quad (°C)$$

where $T_{air}$ is measured with aspirated and wind-shielded humidity and temperature probes (HMP-60, Vaisala Inc., Helsinki, Finland) co-located with the gas analyzers (accuracy +/- 0.5 C). To remove inter-site $T_{air}$ calibration bias, $T_{air}$ was corrected to a co-located, recently factory calibrated sensor. H represents half-hourly sensible heat flux measurements, ρ is density of dry air, $C_p$ is the specific heat of air at a constant pressure, and $G_{aero}$ is the canopy aerodynamic conductance to heat exchange (as calculated below). Surface temperature differences, $\Delta T_{aero}$ (°C), are calculated as the half hour temperature difference between sites, averaged over a month or a specific half hour of the day to assess seasonal and diel trends, respectively. As a measure of uncertainty, $T_{aero}$ and energy flux differences are displayed with 95% confidence intervals.

To understand the importance of daytime $T_{aero}$ changes, we used a non-parametric binning approach to extract a functional pattern (Falge et al., 2001; Ma et al., 2017). We sorted the flux data by temperature and then binned successive pairs of net ecosystem productivity (NEP) and concurrent $T_s$ with a fixed sample size (n=50) per bin, to prevent skewness due to uneven numbers of samples per bin (Barr et al., 2013). Prior to binning, the data were filtered by light level (photosynthetically active radiation > 1500 $\mu$mol $m^{-2}$) to focus on high radiation midday growth periods. Although we recognize that this analytical method includes confounding effects such as phenological stage, vapor pressure deficit, and variable species mix, it capitalizes on the large sample sizes inherent to continuous eddy covariance measurements to effectively produce a response function.

### *4.3.4 Aerodynamic and surface conductance*

We diagnosed the biophysical controls on surface energy fluxes by evaluating the surface conductance from the Penman Monteith equation (Monteith, 1965). The Penman-Monteith equation describes evapotranspiration by reconciling the energy supply and stomatal demand for water, and at the canopy scale, acts as a weighted sum of the stomatal conductance of the measured flux footprint. By inverting the Penman-Monteith equation (Monteith, 1981), surface conductance can be derived as:

$$G_{sfc} = \frac{(\gamma * G_{aero} * \lambda E)}{(s*A)+\rho * C_\rho * VPD * G_{aero} - \lambda E * (s+\gamma)} \quad (\text{m s}^{-1})$$

where $\gamma$ is the psychometric constant, s is the slope of saturation vapor pressure-temperature curve, VPD is the atmospheric vapor pressure deficit, and A is the available energy defined as:

$$A = \lambda E + H \quad (\text{W m}^{-2})$$

Because S is challenging to measure across the heterogeneous bathymetry of a restored wetland's footprint, as explained above, λE and H were used to compute available energy in the inverted Penman-Monteith equation for all sites (Humphreys et al., 2006).

To account for the structural differences between land use types, we calculated the aerodynamic conductance, which, for an integrated canopy, is the inverse of the sum of the turbulent and laminar boundary layer resistance (Verma, 1989):

$$R_{aero} = R_{turbulent} + R_{boundary\ layer}$$

where

$$R_{turbulent} = \frac{\overline{u}}{ustar^2} \text{ (m/s)}$$

and

$$R_{boundary\ layer} = 6.2 * ustar^{-2/3} \quad (\text{m s}^{-1})$$

and

$$G_{aero} = \frac{1}{R_{aero}}$$

Where $\bar{u}$ is the average wind speed in the horizontal direction as measured by the tower-based sonic anemometer, ustar is the average friction velocity, a function of the Reynold's shear stress or average covariance between upward and horizontal instantaneous wind speeds, measured at the eddy covariance tower. Laminar boundary layer resistance ($R_{boundary\ layer}$) is modeled after Thom (1972); this empirical formulation has been shown to result in values sufficiently similar to a more complicated physically-based approach (Knauer et al., 2017). Due to noise in the observed data, raw conductance is filtered by cutting outliers in the percentile below 1% and above 99%, followed by omitting spurious negative values. As a measure of uncertainty, seasonal and diel $G_{sfc}$ are displayed with 95% confidence intervals.

Measurement height discrepancies between alfalfa (2.8m) and wetland sites (~5m) have minor effects on $T_{air}$ and $\bar{u}$. We performed sensitivity tests on the measurement height of alfalfa by computing $T_{aero}$ with modeled $\bar{u}$ at 5m based on the log wind profile. Taero at the measured (2.8m) and modeled (5m) heights differs by ~4% at the half hourly scale and ~0.2% at the daily scale; a simple two sample t-test does not reject the null hypothesis that the measured and modeled $T_{aero}$ have equal means. For these reasons, and to avoid unnecessary assumptions of the log wind profile, data presented here is from the measured 2.8m measurement height at alfalfa.

#### *4.3.5 Boundary layer feedbacks*

To understand the implications of $T_{aero}$ changes associated with different land use types studied, we employed a simple energy balance – planetary boundary layer (EB-PBL) model (Baldocchi and Ma, 2013). The model couples an analytical solution (Paw U and Gao, 1988) to the surface energy balance with a one-dimensional PBL growth model (Barr and Betts, 1997; McNaughton and Spriggs, 1986), considering a single column of air, and solves for moisture and heat fluxes into or out of the top and bottom. The model assumes infinite spatial homogeneity and returns surface and mixed layer air temperatures. It is run for a single clear-sky growing season day, with measured VPD and incoming radiation, where available. Initial boundary layer height is set at 100m (Bianco et al., 2011). Surface characteristics are proscribed (Supplemental Figure 4.5) with $G_{aero}$ and $G_{surface}$ computed from eddy covariance data, as presented in results below.

### *4.4 Results*

#### *4.4.1 Seasonal patterns of temperature, energy balance, and surface properties*

To understand the impact of land use change on local microclimate, we compare $T_{aero}$ and energy balance components of the restored wetland sites with the alfalfa site. Over a network of restored wetlands, we can address the question – what are the impacts of restoring a smooth statured, well irrigated perennial crop with a darker, taller, and rougher managed wetland? By convention, the

alfalfa land use is subtracted from each wetland land use, so that positive values indicate warmer temperatures or more heat flux to/from the wetland sites. Finally, we present $G_{sfc}$ and $G_{aero}$ dynamics to investigate how wetland structure impacts turbulent fluxes and ultimately, $T_{aero}$.

#### *4.4.1.1 Seasonal temperature and energy balance differences*

Monthly average wetland $T_{aero}$ was cooler than alfalfa $T_{aero}$ during the height of the growing season (Figure 4.1). During other times of the year, especially during the spring, the wetland's $T_{aero}$ was warmer than alfalfa's, by up to 2.3℃ (Supplemental Table 4.2). To understand how the underlying turbulent heat fluxes drive this observed seasonal $T_{aero}$ difference, we take an energy balance approach. Each term of the energy balance equation is compared by taking the difference between the respective wetland and the alfalfa land use (Supplemental Table 4.2).

The wetland sites receive more net radiation most months of the year, compared to alfalfa (Figure 4.1). Because incoming shortwave radiation is very comparable at all the sites due to proximity, net radiation differences are primarily a function of albedo and $T_{aero}$. Taller wetland vegetation is expected to have a lower albedo as it traps light more effectively than short, herbaceous vegetation (Cescatti et al., 2012; Stanhill, 1970). Additionally, the dark water surfaces at the restored wetland sites lower albedo to nearly half that at alfalfa (Table 4.1). An increase in net radiation at the wetland sites due to lowered albedo translates into increased available energy that can be partitioned into sensible heat, latent heat, and storage.

During June, July, and August, the young wetland's enhanced latent heat and diminished sensible heat compared to alfalfa is concurrent with nearly equivalent or cooler $T_{aero}$ at the wetland sites (Figure 4.1a). At the intermediate wetland site, we see a similar pattern. Excess radiation taken up by the wetland is almost completely emitted as latent energy during the growing season. This is concurrent with $T_{aero}$ up to 0.87°C cooler than those at alfalfa (Figure 4.1b). The old wetland exhibits significantly more sensible heat flux and less latent heat flux than alfalfa until early summer, when latent heat flux begins to outpace that at alfalfa (Figure 4.1c). Surface temperatures at the old wetland become cooler than those at alfalfa when the wetland latent energy enhancement is maximized, in July and August.

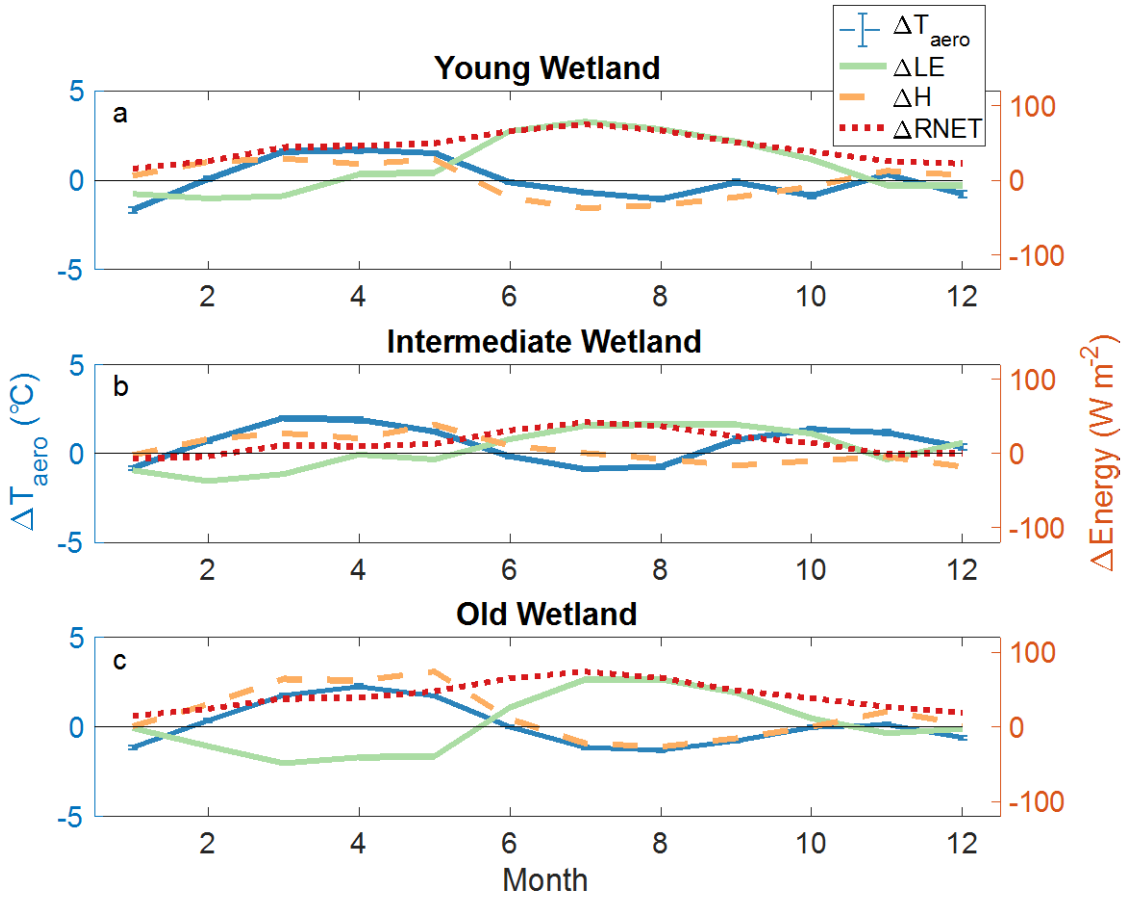


*Figure 4.1: Average monthly aerodynamic temperature and energy flux differences between the a. Young Wetland, b. Intermediate Wetland, and c. Old Wetland and the Alfalfa site. Error bars on the aerodynamic temperature difference line represent 95% confidence interval.*

#### *4.4.1.2 Seasonal aerodynamic and surface properties*

To further diagnose the mechanisms driving the observed temperature and energy balance discrepancies, we assessed the aerodynamic and surface properties of the land use types. Average seasonal cycles of $G_{aero}$ and $G_{sfc}$ reveal characteristic differences in the land uses that impact how energy and matter are exchanged with the atmosphere. At all sites, $G_{aero}$ is considerably larger than the $G_{sfc}$ (Figure 4.2, note scales of axes), indicating the importance of canopy structure and roughness on turbulent exchange, especially in the windy environment of the Sacramento-San Joaquin Delta.

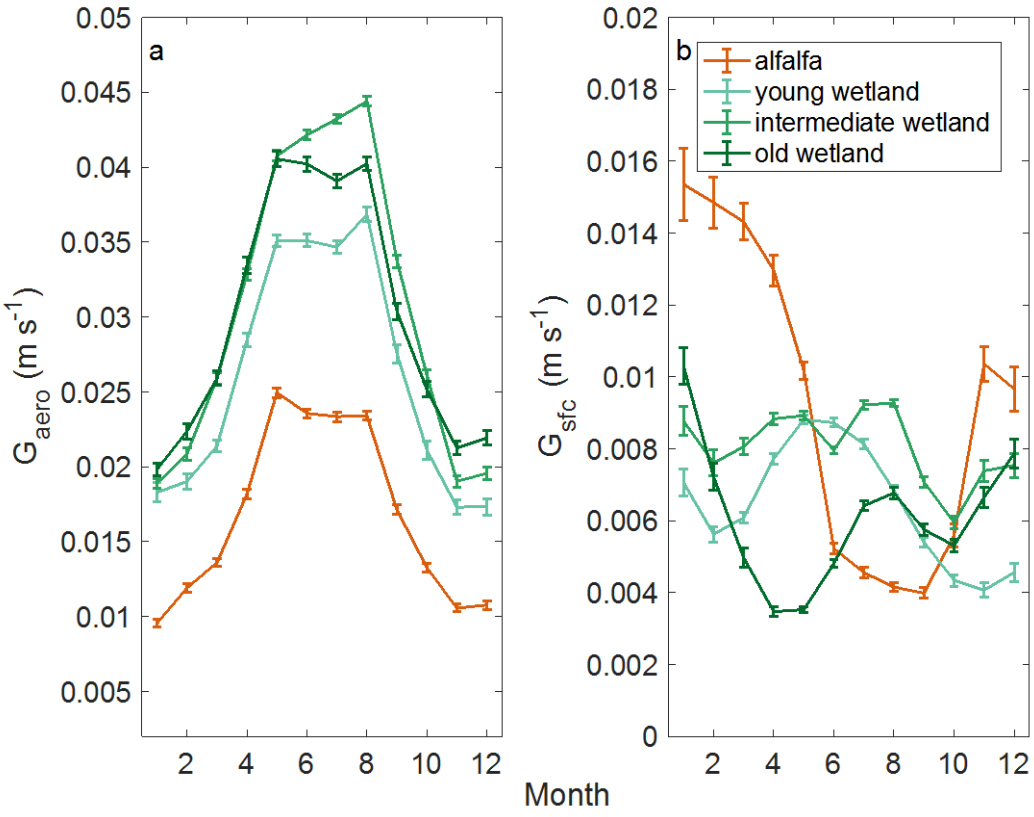


*Figure 4.2: Mean monthly a.) aerodynamic and b.) surface conductance at each of the four study sites (m $s^{-1}$). Error bars represent 95% confidence intervals of the conductance.*

Peak $G_{aero}$ at the old (0.041 m/s), intermediate (0.044 m/s), and young wetland (0.037 m/s) sites are nearly double the magnitude of the peak $G_{aero}$ at the short-statured and relatively smooth alfalfa site (0.025 m/s) (Figure 4.2a). At all sites, the seasonal cycle of $G_{aero}$ is similar. Alfalfa peaks early, in May, while the wetland crops peak towards the end of the summer growing season, when the wetlands are fully emergent with tule and cattail species extending 2-3 meters from the water level. Winter $G_{aero}$ of senescent vegetation hovers below 0.02 m/s at the wetland sites. Alfalfa's winter $G_{aero}$ drops to less than half that (Figure 4.2a).

While $G_{aero}$ reveals the impact of turbulent mixing conditions promoted by the canopy structure, $G_{sfc}$ tells us about the availability of water both through transpiration and evaporation (Jarvis and McNaughton, 1986; Raupach, 1998). Seasonal $G_{sfc}$ patterns exhibit markedly different dynamics among sites (Figure 4.2b). Alfalfa's $G_{sfc}$ peaks early in the year (0.015 m/s) and falls off throughout the main growing season to a minimum in September (0.004 m/s), recovering when

the cooler, wetter conditions of the winter return. Wet winter months, in which the perennial crop cover is spotty but the soil retains moisture, is likely contributing to the mid-winter maxima. The growing season decline is driven by high temperatures and uncertain access to ground water at the site throughout the summer (Supplemental Figure 4.3). The older wetland's $G_{sfc}$ exhibits a spring minimum, with maximum $G_{sfc}$ values in the winter months (0.01 m/s), and a secondary peak during green-up in mid-summer.

The young wetland, with decreasing contributions from open water throughout the study period, exhibits maximum $G_{sfc}$ (0.009 m/s) during May growth, with a gradual decline over the summer months. The intermediate wetland sustains a high $G_{sfc}$ throughout the growing season, falling off as the plants senesce in late summer. As $G_{sfc}$ represents an integrated footprint conductance value, the heterogeneous nature of these younger wetlands mean that $G_{sfc}$ is a combination of transpiration through stomata, and evaporation through open water surfaces, which have very different mechanistic controls (Goulden et al., 2007).

Direct comparisons of the magnitudes of $G_{sfc}$ between the alfalfa and the respective wetland sites show a seasonal bias towards higher values, especially at the more heterogenous young and intermediate wetlands (Supplemental Figure 4.4a,b). This contrasts with $G_{aero}$, which exhibits an annual bias towards significantly higher values at all of the wetland sites, with the largest magnitudes during the growing season (Supplemental Figure 4.4d,e,f). In general, the land use transition from drained alfalfa to flooded wetland is characterized by an increased growing season $G_{sfc}$ and an increased year-round $G_{aero}$.

### *4.4.2 Diel patterns of temperature, energy, and surface properties*

Mean monthly values are useful for understanding long-term seasonal trends but can mask important diel differences driven primarily by daily cycles of radiation. Here, we present patterns of $T_{aero}$, energy balance components, and $G_{sfc}$ and $G_{aero}$ at the diel scale, focusing on the growing season (May-September).

#### *4.4.2.1 Diel temperature and energy balance differences*

Diel $T_{aero}$ differences between the wetland sites and the alfalfa site vary considerably depending on the wetland structure. Each of the wetlands were significantly cooler than the alfalfa site during the day and warmer than the alfalfa site during the night. The young wetland was up to 3.4 ºC (occurring at 13:30) cooler than alfalfa during the daytime and up to 1.9 ºC warmer throughout the night. Similarly, the intermediate wetland was up to 5.1 ºC (13:30) cooler than alfalfa during the daytime and up to 3.6 ºC warmer during the night. The old wetland displays a similar, but more dampened diel cycle of temperature difference, with slightly cooler

temperatures of up to 2.1 ºC (14:30) during the day, and warmer temperatures of up to 0.7 ºC during the night (Figure 4.3). These differences suggest that the way incoming solar radiation is partitioned into turbulent heat fluxes at each of the sites affects the magnitude of the daytime cooling effect at the wetland sites.

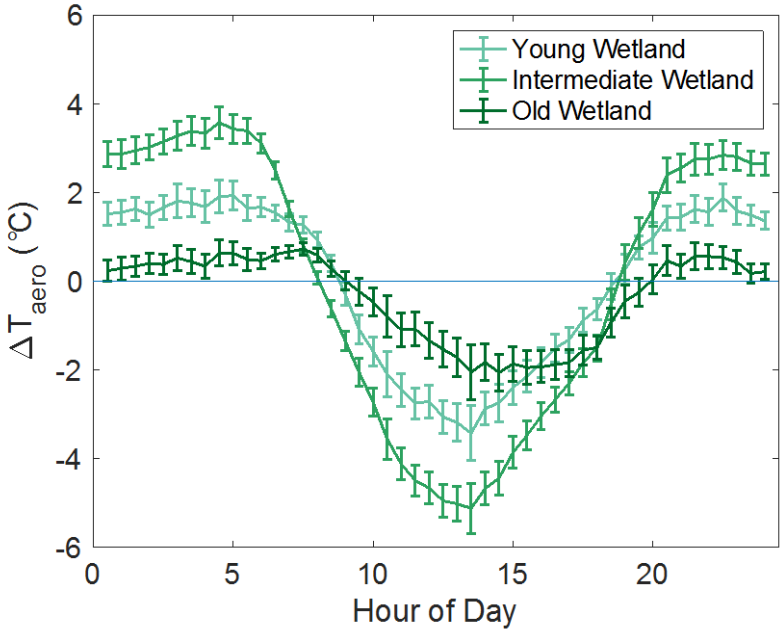


*Figure 4.3: Average diel aerodynamic temperature differences between the respective wetland sites and alfalfa during the growing season (May-September). Error bars represent 95% confidence intervals of the half-hourly mean growing season temperature difference.*

Diel patterns of sensible and latent energy flux differences between the site-pairs emphasize the importance of wetland canopy structure on biophysical properties (Figure 4.4c,d; Supplemental Figure 4.7). These structural characteristics include height, roughness, fraction of live and dead biomass, and the ratio of vegetation to open water. Owing to the decreased albedo of the dark vegetation and water surfaces, and increased leaf area index that can effectively trap photons, net radiation during the growing season was much larger at the wetland sites than at alfalfa (Figure 4.4a).

The young wetland receives up to 193 W $m^{-2}$ of additional daytime net radiation as compared to alfalfa during the growing season (Figure 4.4a). Much of this excess radiation is stored in the water column during the day; considerably more daytime storage than at alfalfa or the old wetland (Figure 4.4b). This storage results in cooler $T_{aero}$, and thus diminished sensible heat flux during the day compared to alfalfa, as less energy is available for partitioning into turbulent

fluxes (Figure 4.4c). The daytime $T_{aero}$ cooling effect at the wetlands with open water surfaces (Figure 4.3) is concurrent with a reduction in daytime sensible heat flux. Importantly, it also results in a release of the energy stored in the water as latent heat flux during the night (Figure 4.4d). The intermediate wetland exhibited similar patterns to the young wetland, with enhanced daytime storage flux and nighttime latent heat flux compared to the alfalfa site.

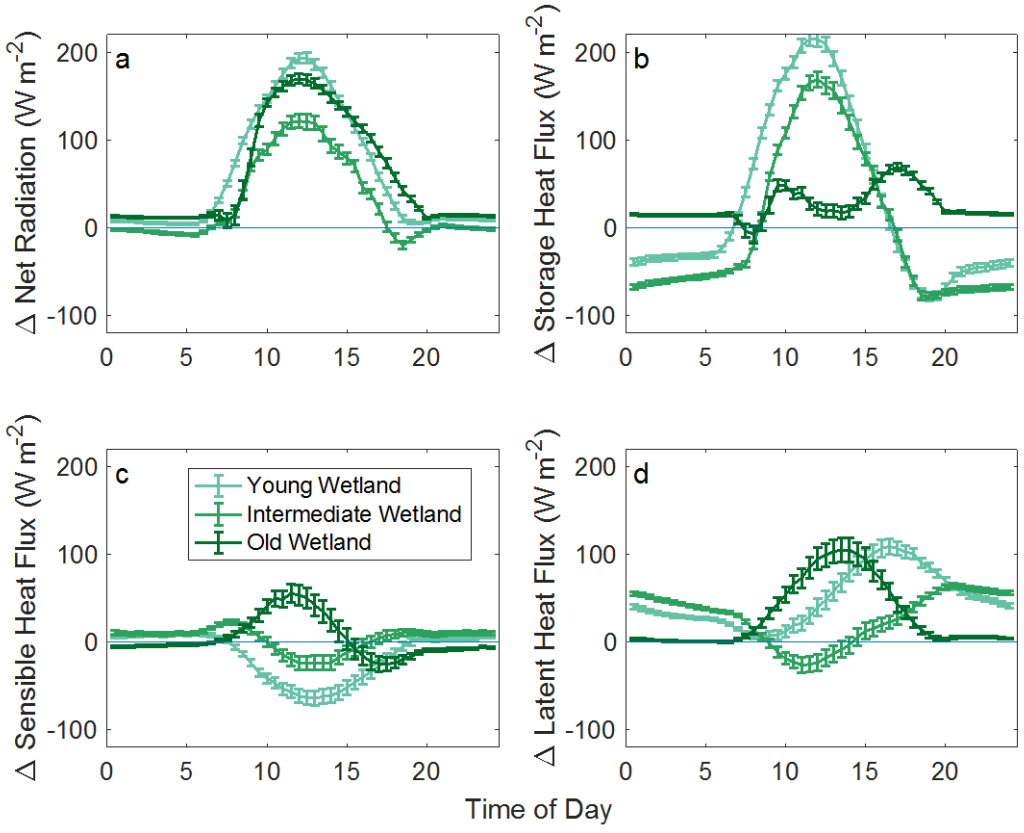


*Figure 4.4: Diel growing season differences in a.) net radiation, b.) residual storage flux, c.) sensible heat flux, and d.) latent heat flux between the respective wetland sites and alfalfa. Error bars represent 95% confidence intervals of the half-hourly mean growing season energy fluxes.*

The old wetland exhibited a different diel pattern of growing season energy balance differences. Much less of the old wetland's excess radiation was stored in the water column (Figure 4.4b). Instead of diminished daytime turbulent heat fluxes, as in the other wetlands, the old wetland's increased net radiation (Figure 4.4a) and high $G_{aero}$ (Figure 4.5b) drove enhanced daytime sensible and latent heat flux. This enhanced daytime sensible and latent heat flux heat removed heat from the surface, but less effectively than through water column storage, evidenced by less

of a daytime cooling effect at the old wetland (Figure 4.3). Nighttime turbulent heat fluxes were near zero at both the old wetland and alfalfa (Figure 4.4c,d) and storage heat flux showed little difference between the old wetland and the alfalfa site (Figure 4.4b).

#### *4.4.2.2 Diel aerodynamic and surface properties*

Average growing season diel trends reveal the reliance of $G_{sfc}$ on stomatal dynamics. Both alfalfa and the old wetland, with homogenous canopy cover and little open soil or water, had a distinct diel cycle of high $G_{sfc}$ during active photosynthesis in the daytime (0.011 and 0.010 m/s, respectively) and near zero $G_{sfc}$ at night (0.002 m/s) (Figure 4.5a). Both sites' diel cycles peaked around late morning, and dropped off throughout the day, likely a response to high growing season $T_{air}$ and vapor pressure deficit (VPD). While high VPD and $T_{air}$ would promote evaporation even after stomata close, a lack of open water surfaces result in dramatically declining $G_{sfc}$ during the afternoon and night. This is in contrast to the young and intermediate wetlands, which exhibit heightened $G_{sfc}$ throughout the diel period (Figure 4.5a). While the intermediate wetland's $G_{sfc}$ is reduced during the afternoon, likely due to stomatal closure on hot, dry growing season days, its $G_{sfc}$ appears to recover overnight. Nighttime stomatal conductance was confirmed to be near zero in a leaf-level measurement campaign (data not shown), indicating that heightened nighttime $G_{sfc}$ is largely a result of evaporation from the open water surfaces characteristic of the young and intermediate wetlands.

Diel growing season $G_{aero}$ at the wetland sites was close to 2 times those at the smooth, short-statured alfalfa site, reaching up to 0.047 m $s^{-1}$ at the old wetland (Figure 4.5b). $G_{aero}$ maxima follow the age of the wetland, suggesting that the more mature, taller structure promotes high $G_{aero}$ values. All sites follow a similar diel cycle, characterized by a daytime plateau.

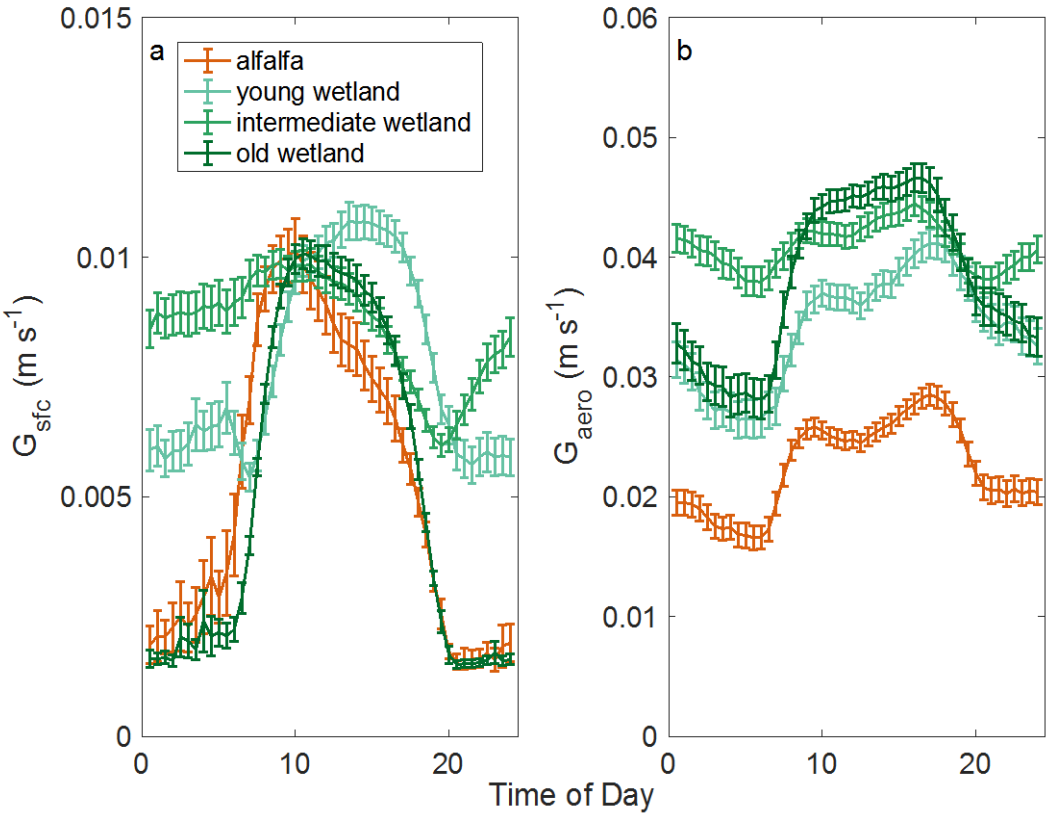


*Figure 4.5: Diel growing season surface and aerodynamic conductance at each site (m $s^{-1}$). (Note the scale of the y-axes differ). Error bars represent 95% confidence intervals of the half-hourly mean growing season conductance.*

## *4.5 Discussion*

### *4.5.1 Biophysical differences between sites*

Drained peatland agriculture is the dominant land use in the Delta region, and nascent policy mechanisms are aiming to incentivize restoration to an ecosystem resembling the pre-industrial inland freshwater wetlands. These policy mechanisms primarily focus on the biogeochemical benefit of the land use change. Here, we explore the biophysical impacts of wetland restoration; how this land use changes the surface properties to have an integrated impact on $T_{aero}$. Despite similar meteorological conditions, significant $T_{aero}$ differences emerged both seasonally (Figure 4.1) and diurnally (Figure 4.3) across the study sites due to the way that the ecosystems differentially exchange energy and momentum with the atmosphere.

At the seasonal scale, wetland $T_{aero}$ was up to 2.3°C warmer than alfalfa (Figure 4.1), mostly during the spring and autumn. High leaf area index and dark water surfaces at the wetland sites absorbed much more net radiation than the alfalfa land cover. During growing season periods, enhanced $G_{sfc}$ and $G_{aero}$, along with higher latent heat flux at the wetland sites drove monthly mean $T_{aero}$ lower than those at alfalfa. These results contrast with $T_{aero}$ dynamics from thaw-induced boreal wetland expansion, where a wetland cooling effect was observed to be maximum during late winter, and moderate in summer (Helbig et al., 2016). In that case, however, aerodynamically rough jack pine stands were being compared to relatively short-statured wetland ecosystems. Seasonal patterns alone are not sufficient to understand how biophysical properties affect $T_{aero}$, as they mask important diel variations driven by radiation.

On an average growing season day, during midday, the young, intermediate, and old wetlands cooled the surface by up to 3.4°C, 5.1°C, and 2.1°C respectively (Figure 4.3). Diel temperature differences revealed that in addition to the land cover transition itself, the structure of the restored wetland determined the magnitude of the $T_{aero}$ effect. The young and intermediate wetlands, with patches of open water interspersed between vegetation, provided more daytime cooling than the old wetland, with a mature, dense, closed canopy cover. Conversely, the open water wetlands were warmer during the night (Figure 4.3). By analyzing the differences in each energy balance term between the various wetlands and alfalfa, alongside the patterns of $G_{sfc}$ and $G_{aero}$, we can understand the drivers of the observed seasonal and diel $T_{aero}$ differences.

The young and intermediate wetlands store much of their enhanced net radiation during the day within the water column (Figure 4.4b). This storage reduces the latent and sensible heat flux during the day, temporarily decoupling the incoming radiation from the outgoing heat fluxes. This temporal decoupling results in a cooling effect of the $T_{aero}$ during the day, compared to alfalfa (Figure 4.3). Beginning in the early evening and throughout the night, much of this stored energy is released. With high $G_{aero}$ due to the tall, emergent properties of the wetland species (Figure 4.5b) and heightened $G_{sfc}$ despite closed stomata due to the surfaces of open water (Figure 4.5a), much of this nighttime heat flux is released in the form of latent energy, humidifying the low, stable boundary layer and contributing to enhanced nighttime $T_{aero}$ compared to alfalfa (Figure 4.3).

Aerodynamic conductance represents how well latent and sensible heat get transported away from the surface through turbulent mixing. Due to the tall, emergent canopy structures at the wetland sites, we see $G_{aero}$ almost twice that at the alfalfa site, which has a short, smooth, regular canopy. In the windy Delta landscape, with strong westerly gusts from the Pacific Ocean, $G_{aero}$ promotes turbulent fluxes, even at night (Figure 4.5b). Because $G_{aero}$ is instrumental in

transferring both latent and sensible heat to the atmosphere, the site's water availability is an important determinant of the relative partitioning of heat.

Alfalfa and the old wetland, with no exposed surface water, exhibit a regular diel cycle of $G_{sfc}$ (Figure 4.5a). A thick layer of dead litter and a closed, mature canopy at the old wetland decouples the atmosphere from the underlying water, eliminating daytime storage of net radiation in the water column (Figure 4.4b). This is reflected in old wetland water temperatures that are 15-25% cooler than the water temperatures at the other wetland sites (Eichelmann et al., 2018). Without daytime storage, enhanced radiation at the old wetland is dissipated as latent and sensible heat flux during the day, when stomata are open (Figure 4.4c,d), by high $G_{aero}$ (Figure 4.5b). In this way, the old wetland acts less as a flooded system, and more as a crop, with net radiation converted into daytime turbulent heat fluxes that result in a modest cooling effect compared to alfalfa.

These findings support work by Eichelmann et al. (2018), who found significant evapotranspiration differences between the more heterogeneous footprints of the young and intermediate wetlands and the closed-canopy old wetland, especially at night. The $G_{sfc}$ measurements presented here support the finding that with closed, dense, wetland canopies, even when water is present underneath, evapotranspiration is largely mediated through daytime stomatal transpiration with minimal contribution of free evaporation. In juxtaposition, heightened nighttime $G_{sfc}$ values at the more open young and intermediate wetlands, combined with ample energy storage in the water column, drive nighttime evaporation as latent energy - an important component of the energy balance for heterogeneous wetlands. Ongoing work to partition evaporation and transpiration in this system would provide a means to confirm these dynamics.

Impacts of the three critical biophysical properties that are affected by land use change - albedo, $G_{sfc}$, and $G_{aero}$ - have been shown to counteract each other. Often, in a transition from field to forest, lowered albedo causes warming while increased evaporative efficiency and $G_{aero}$ cause cooling (Davin and de Noblet-Ducoudre, 2010; Juang et al., 2007). The integrated balance of these effects over a year determine the net biophysical impact of land use change. In the Delta system, radiative biophysical mechanisms alone cannot explain the observed temperature differences – the wetlands consistently exhibited lower albedo as compared to alfalfa (Table 4.1). The non-radiative mechanisms driving the observed daytime cooling effect in the Delta – through changes to $G_{sfc}$, $G_{aero}$, and storage – are essential to understanding the energy dynamics in this system.

Despite a warming effect of wetland cover during some spring and autumn months, the integrated biophysical impacts of restoration can provide significant daytime surface cooling depending on structural features, such as the ratio of open water to vegetation and the coupling of the water surface with the atmosphere. These complex factors are missing from many assessments of climatic impact of land use change (Myhre et al., 2013), but may govern critical feedbacks to plant physiology and boundary layer processes, especially in scenarios of large-scale land conversion (Burakowski et al., 2017; Gerken et al., 2018). This result emphasizes the importance of diagnosing and modeling specific biophysical changes likely to take place in novel land use transitions, like re-flooding drained agricultural peatlands.

### *4.5.2 Implications for vegetation and boundary layer feedbacks*

To understand the interaction of daytime $T_{aero}$ reduction on productivity and plant physiology, we used a non-parametric binning approach to extract a response function from the three year data set (Barr et al., 2013; Ma et al., 2017).(Barr et al., 2013; Ma et al., 2017)(Barr et al., 2013; Ma et al., 2017)(Barr et al., 2013; Ma et al., 2017) The alfalfa site experienced higher $T_{aero}$, especially compared to the young and intermediate wetland sites. It's net ecosystem productivity (NEP) also responded most negatively to rising $T_{aero}$ (Figure 4.6a), even after removing the five days directly after harvest, when NEP is drastically reduced. The flooded wetland sites have more modulated responses to $T_{aero}$, each with an optimal between 25°C and 30°C, at which NEP is greatest (Figure 4.6b,c,d). This is a slightly higher optimal $T_{aero}$ than that recorded through isotopic cellulose measurements in trees covering a broad range of latitudes (Helliker and Richter, 2008). At higher than optimal $T_{aero}$ in the wetland sites, NEP plateaus without dramatic declines, as we see at Alfalfa.

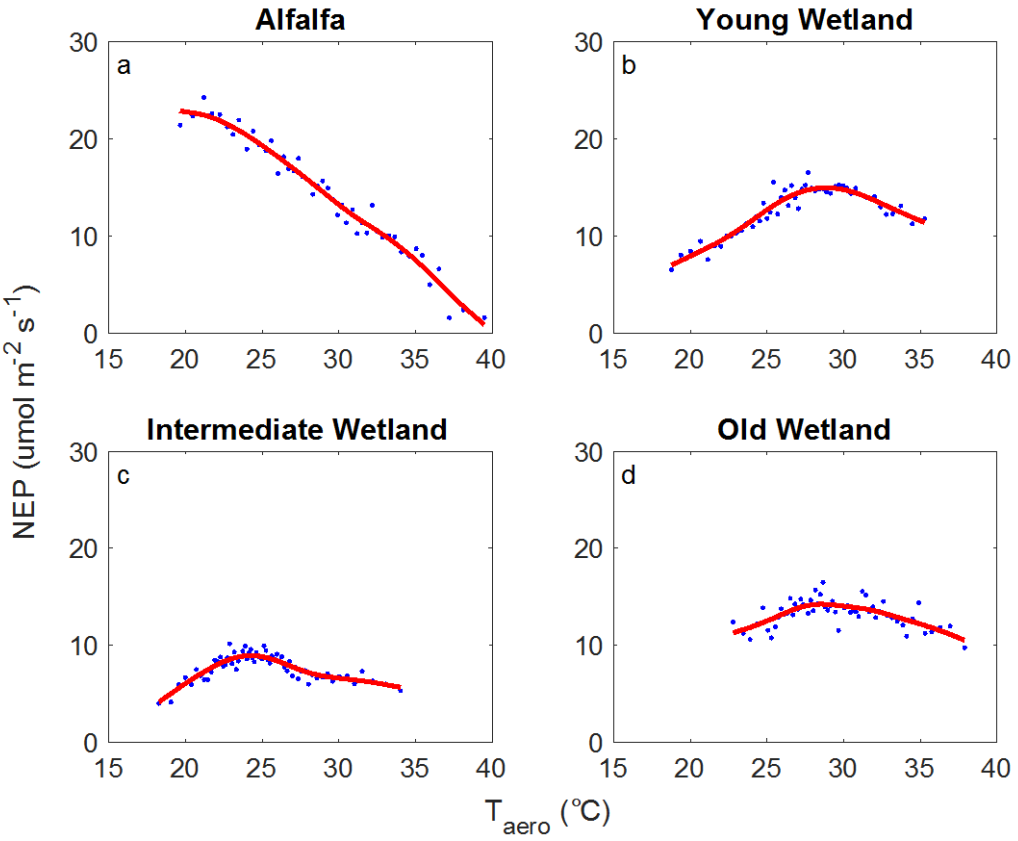


*Figure 4.6: Daytime aerodynamic temperature bins (n = 50) as a function of net ecosystem productivity (NEP). Excluded 5 days after harvest at Alfalfa site. Data is filtered for incoming photosynthetically active radiation (>1500 µmol $m^{-2}$ $s^{-1}$).*

The effect of climatic warming on wetlands, and especially freshwater restored wetlands, is not well understood. Differential responses of plant communities may mediate energy, carbon, and nutrient budgets (Weltzin et al., 2000), although other work has documented state changes associated with warming across salt marsh-mangrove gradients (Baldwin et al., 2014). Surface temperature and energy balance changes could affect thermal hydrodynamic convection, an important driver of diffusive $CH_4$ emission (Poindexter et al., 2016), as well as plant-mediated transfer of $CH_4$, which accounts for the majority of peatland $CH_4$ emissions (Dean et al., 2018). With California's climate projected to become warmer and drier into the future (Ficklin and Novick, 2017), wetland-induced surface cooling could be important in ameliorating physiological stress associated with high ambient air temperature and VPD, and potentially feedback to plant mediated biogeochemical cycling.

Surface modulation by the wetlands could produce feedbacks on the PBL as entrainment from above and modifications to the PBL depth and atmospheric volume influence daily evolution of air temperature in the mixed layer. Model computations, compared to tower-measured $T_{air}$, avoid confounding effects of temperature sensor calibration offsets, variable measurement height, and horizontal advection of heat. We used a simple EB-PBL model to understand the potential local atmospheric feedbacks to the surface properties at each of the study sites (Baldocchi and Ma, 2013). The model was run for cloudless growing season conditions, driven by measured diel VPD and incoming radiation ($Rg_{in}$), $S_{residual}$, and half hourly values of $G_{aero}$ and $G_{sfc}$ computed from flux data (Supplemental Figure 4.11).

The modeled $T_{aero}$ closely matches the daytime dynamics of $T_{aero}$, with the young and intermediate wetlands much cooler, and the old wetland slightly cooler, than the alfalfa site (Figure 4.7a). The young and intermediate wetlands, with open water surfaces and relatively high $G_{sfc}$ and $G_{aero}$ throughout the day, resulted in lower $T_{air}$ (Figure 4.7b) in the mixed layer by close to 5°C. This is consistent with the findings of Helbig et al. (2016) who also found a PBL cooling effect due to wetland expansion, primarily for reasons related to enhanced latent heat and diminished sensible heat flux. With suppressed sensible heat flux, heterogeneous restored wetlands may also result in a lower boundary layer.

In other systems, with much less available moisture, enhanced $G_{aero}$ could cause a mixed layer air temperature warming effect. In a nearby Mediterranean grassland and savannah system, the taller and rougher oak woodland caused a potential air temperature warming effect of 0.5°C (Baldocchi and Ma, 2013). Our results suggest that surface property differences inherent in transitions from drained agricultural peatland land uses to restored wetlands could have significant cooling impacts on local climate, especially under situations of widespread restoration. This cooling effect is dependent on wetland canopy structure, however. The old wetland's surface properties promoted higher boundary layers and $T_{air}$ slightly warmer than that over alfalfa by midday.

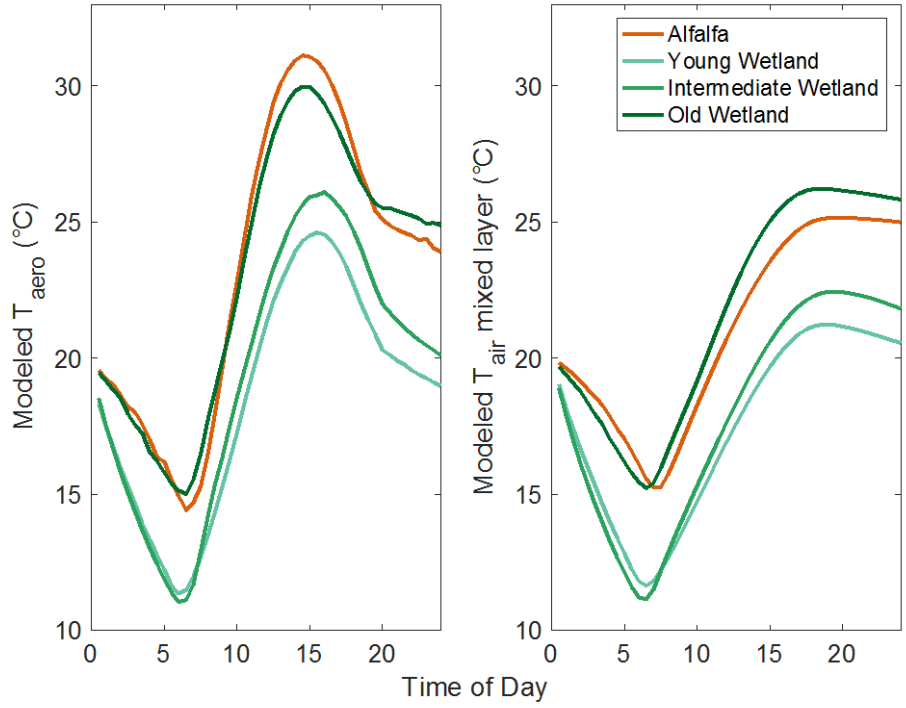


*Figure 4.7: Modeled (a) aerodynamic surface temperature and (b) mixed layer air temperature, given the surface properties at each of the study sites (Figure S5), for a clear-sky growing season day.*

### *4.5.3 Policy implications and future work*

Consideration of the biophysical impacts is critical to understanding how land use related policies and incentives will affect physiology and local to regional climate. While this is beginning to be recognized in forest land use transitions, other land use activities are being incentivized through methodologies as part of nascent climate change policies without a complete understanding of the biophysical impacts that could result. We hypothesized that the transition from drained agricultural peatlands planted with short-statured perennial alfalfa to managed wetlands with tall, emergent canopies is, in some ways, analogous to the biophysical impact of afforestation. In our analysis, the young and intermediate wetlands both exhibit cooler daytime and warmer nighttime surface conditions (Figure 4.3). Local tower-based air temperature measurements show a sizable (1.4 - 4.0°C) reduction in DTR at the young and intermediate wetland sites (Supplemental Figure 4.11), which is similarly reported as an impact of reforestation (Alkama and Cescatti, 2016; Burakowski et al., 2017; Lee et al., 2011; Lejeune et al., 2018).

Transition from a short-statured, smooth alfalfa crop to a tall, emergent, heterogeneous wetland has the potential to enhance biogeochemical benefits of wetland restoration (Knox et al., 2015) by causing a daytime surface cooling effect, counteracting the ongoing and predicted increases in temperature associated with global climate change. Wetland transition from other dominant Delta crops may have different, possibly more enhanced, cooling effects. When designing climate mitigation projects, ecosystem structure and time since restoration must be more explicitly considered. Older wetlands tend to accrue a dense mat of dead litter after multiple seasons of blowdowns and storm damage (Schile et al., 2013), which have been shown to decouple the canopy air space from the water below (Goulden et al., 2007), effectively turning a mature wetland into a well-watered crop (Eichelmann et al., 2018). Restored wetland designs that feature tracts of open water that will not rapidly fill in with vegetation may promote this cooling effect, which otherwise could be diminished as maturing wetlands fill in with vegetation and create a closed canopy structure. Future work should more explicitly quantify the storage term in restored wetlands with dynamic and varied bathymetry.

In addition to wetland design, wetland extent and scale will play an important role in the degree of local to regional cooling. Results from a wetlands-adjacent rice field in the Delta show that increasing the size of flooded land cover from ~1 $km^2$ to ~5 $km^2$ between 2009 and 2014 caused a decrease in evapotranspiration due to a decreasing oasis effect (Baldocchi et al., 2016). Where a mosaic of flooded patches in a semi-arid climate will promote entrainment of warm dry air from above the PBL (the 'oasis' effect) and enhance evaporation, larger tracts of flooded land could mitigate this feedback. Our study was performed during a time of relatively stable flooded land cover extent on the islands of interest, but future work should focus on modeling how much area and what kinds of orientations of flooded land cover will cause a meaningful effect across local to regional jurisdictions (Gerken et al., 2018).

These results are likely specific to restored, managed wetlands – with managed water tables and little current or outflow. Complete restoration to a more natural, tidal- and seasonally flood-influenced wetland is unlikely in California's highly managed water delivery system, especially given the policy goal to inhibit respiration and sequester carbon through permanent flooding. Connectivity with the pre-industrial, natural watershed would have hydrological impacts that we cannot adequately address here (Mitsch et al., 2005). Designing and managing restored wetlands to provide a cooling effect could increase water use (Eichelmann et al., 2018), conflicting with important urban, agricultural, and habitat water demand in a semi-arid California landscape characterized by large interannual variability in precipitation. This water cost must be considered in light of the integrated biophysical, biogeochemical, habitat, and levee stability benefits that are all associated with wetland restoration.

## *4.6 Conclusions*

While biogeochemical impacts of land use change are most often considered, our results emphasize the need to include an assessment of biophysical impacts to fully understand how a land use change, such as wetland restoration, affects the albedo, water availability, roughness, and ultimately the $T_{aero}$ of an ecosystem. Using twelve site-years of eddy covariance data across a network of restored wetland and agricultural sites in the Sacramento-San Joaquin Delta, we show significant $T_{aero}$ differences between restored wetlands and a dominant drained agricultural land use.

Heterogeneous wetlands with open water surfaces are characterized by increased daytime storage of energy, with reduced sensible heat during the day and enhanced latent heat during the night promoted by heightened $G_{sfc}$ and $G_{aero}$, compared to the alfalfa land cover. This daytime cooling effect, of up to 2.1°C to 5.1°C, could be important in ameliorating the physiological stress of increasing temperature associated with climate change at the local scale. Using a simple EB-PBL model, we show that the surface and aerodynamic properties that result in wetland $T_{aero}$ cooling at the young and intermediate wetlands also cause a reduction in $T_{air}$. Future studies should explore the potential teleconnection between large-scale wetland restoration and climate over broader regional scales. Along with habitat creation and levee stabilization, the biophysical daytime surface cooling effects of restored wetlands could enhance the biogeochemical sequestration benefits.

While this study was limited to the biophysical impacts of restored, managed wetlands under the scenario in which they are converted from a perennial field crop, future studies could expand this analysis to other crops and natural wetland systems. Despite the challenges with reconciling radiative and non-radiative impacts of land use change, especially in complex ecosystems such as wetlands, it is critical to understand the biophysical processes that will be affected under proposed land use change scenarios. With a renewed focus on the importance of natural and working lands in climate change mitigation, we must ensure that land use changes incentivized for their biogeochemical benefit do not have unforeseen negative consequences.

## *4.7 Supplemental figures and tables*

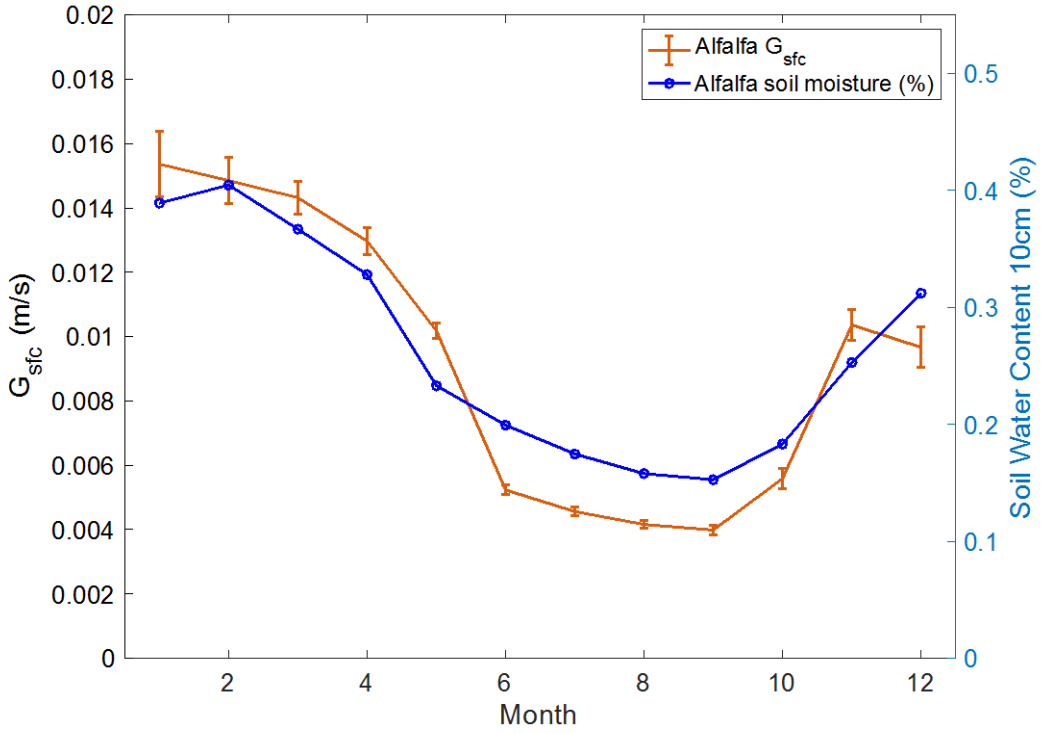


*Supplemental Figure 4.8: Alfalfa mean monthly surface conductance and soil water content at 10 cm.*

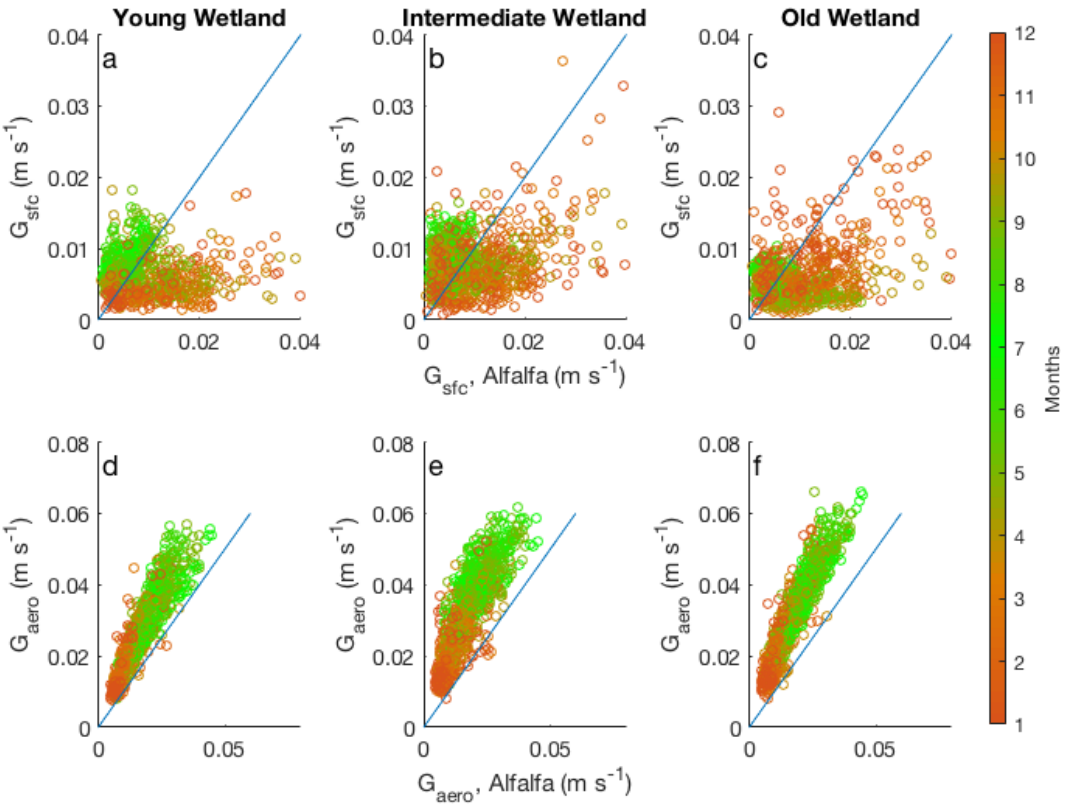


*Supplemental Figure 4.9: One to one plots of surface (a,b,c) and aerodynamic (d,e,f) conductance between the Alfalfa site on the x-axis and the three different restored wetland sites on the y-axis. Data is colored by seasonality, with growing season in green*

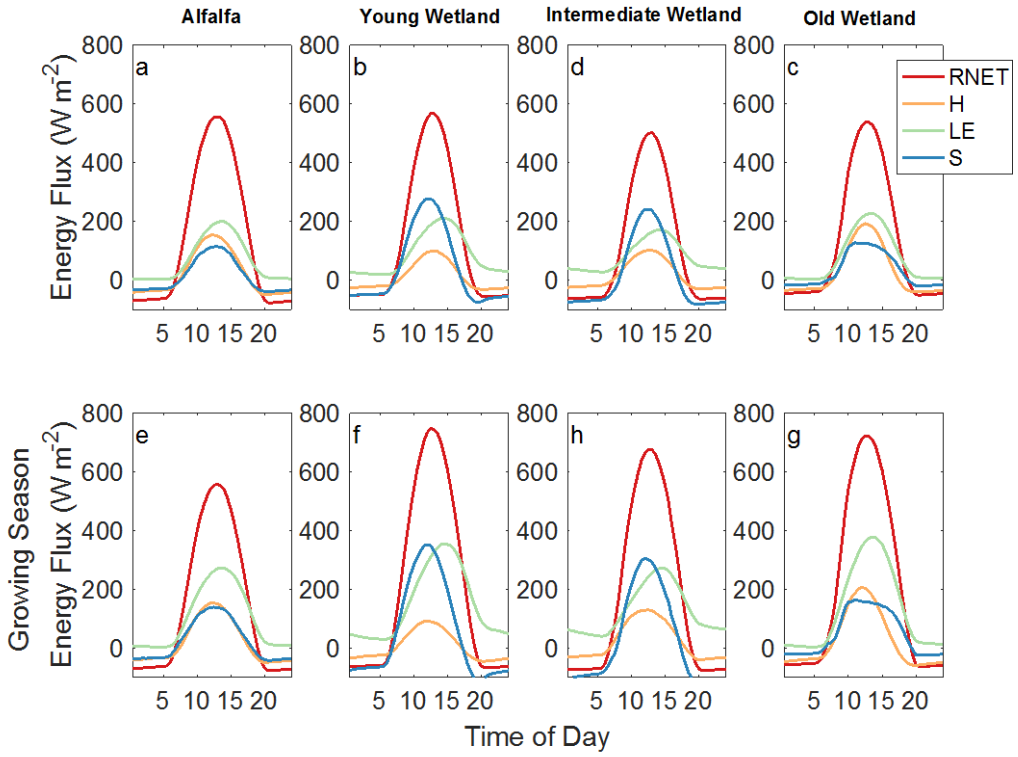


*Supplemental Figure 4.10: Yearly (a-d) and growing season (e-h) mean diel energy fluxes.*

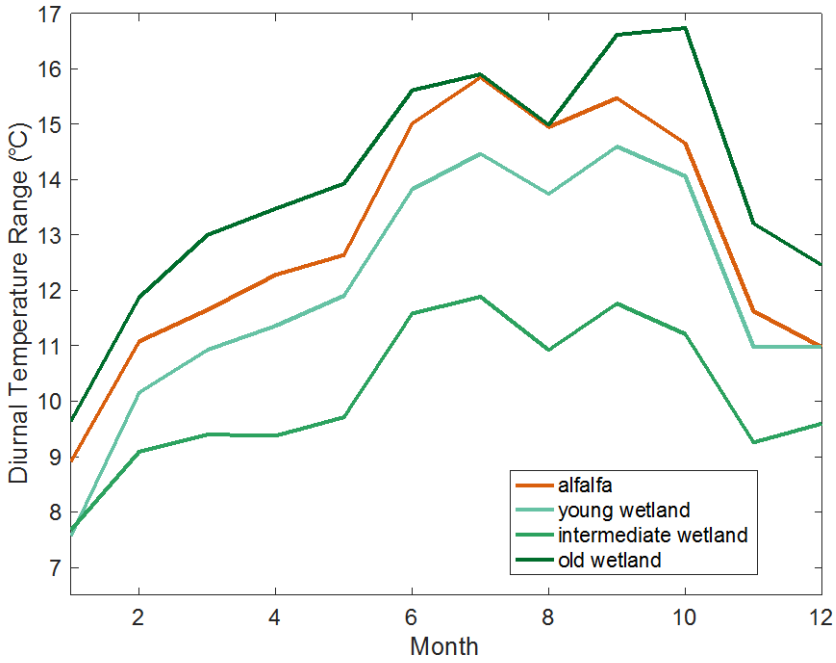


*Supplemental Figure 4.11: Mean diurnal air temperature range (DTR) for each site, as measured at eddy covariance towers.*

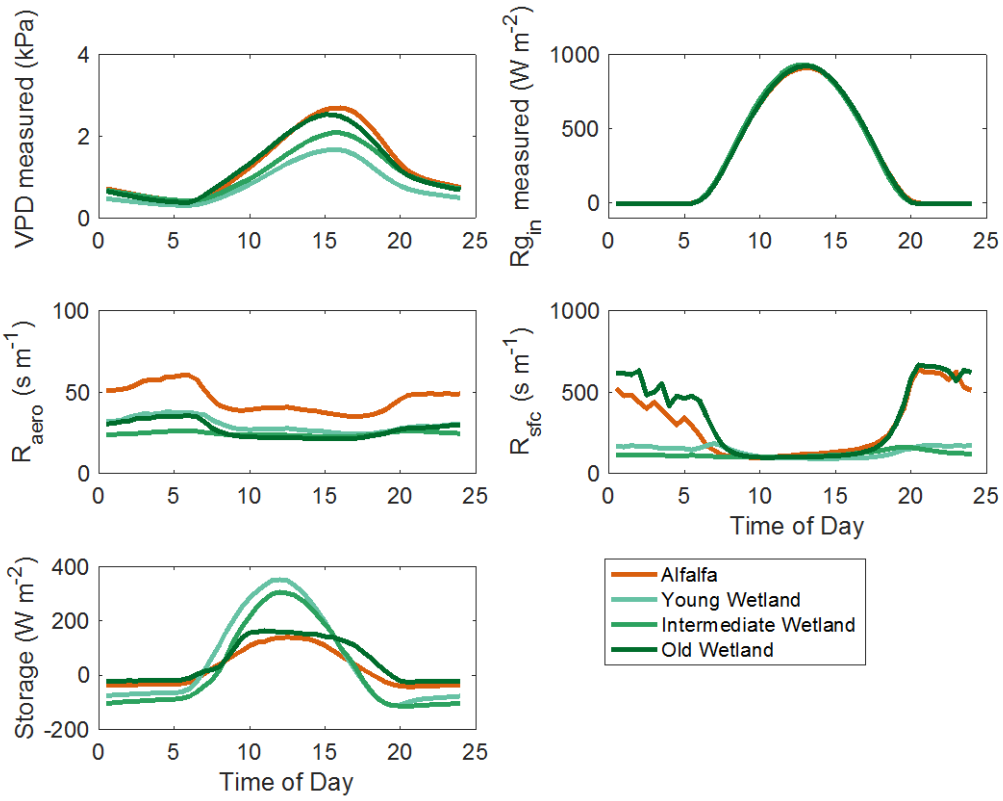


*Supplemental Figure 4.12: Energy balance – planetary boundary layer (EB-PBL) model inputs.*

| 2015-2017 | ΔSurface Temperature (°C) | | | ΔNet Radiation (W m$^{-2}$) | | | ΔLatent Heat Flux (W m$^{-2}$) | | | ΔSensible Heat Flux (W m$^{-2}$) | | |
|---|---|---|---|---|---|---|---|---|---|---|---|---|
| | Young Wetland | Intermediate Wetland | Old Wetland | Young Wetland | Intermediate Wetland | Old Wetland | Young Wetland | Intermediate Wetland | Old Wetland | Young Wetland | Intermediate Wetland | Old Wetland |
| Jan | -1.65 | -0.81 | -1.15 | 15.59 | -6.51 | 14.99 | -18.25 | -22.36 | -1.46 | 6.14 | -2.10 | 1.00 |
| Feb | 0.06 | 0.75 | 0.35 | 25.70 | -3.62 | 24.22 | -24.25 | -36.94 | -25.81 | 24.74 | 19.68 | 30.31 |

| | | | | | | | | | | | | |
|---|---|---|---|---|---|---|---|---|---|---|---|---|
| Mar | 1.60 | 2.00 | 1.76 | 44.05 | 11.49 | 38.30 | -21.18 | -27.53 | -48.73 | 29.08 | 27.31 | 64.42 |
| April | 1.70 | 1.91 | 2.25 | 46.29 | 9.76 | 39.48 | 8.09 | -1.23 | -40.75 | 21.82 | 20.66 | 62.11 |
| May | 1.52 | 1.25 | 1.74 | 49.53 | 13.24 | 47.90 | 10.40 | -7.88 | -39.30 | 28.06 | 38.99 | 74.47 |
| June | -0.11 | -0.15 | 0.00 | 66.20 | 31.26 | 65.10 | 65.98 | 19.49 | 26.21 | -23.74 | 10.80 | 10.63 |
| July | -0.68 | -0.87 | -1.15 | 74.92 | 42.44 | 74.32 | 78.68 | 37.52 | 63.81 | -37.45 | 0.74 | -22.00 |
| Aug | -1.04 | -0.73 | -1.30 | 67.07 | 37.32 | 66.05 | 68.55 | 39.61 | 63.73 | -33.53 | -7.13 | -26.52 |
| Sept | -0.12 | 0.77 | -0.77 | 50.75 | 23.02 | 49.02 | 51.95 | 38.95 | 46.05 | -22.63 | -15.98 | -15.17 |
| Oct | -0.86 | 1.36 | -0.02 | 38.56 | 14.73 | 38.72 | 28.06 | 26.97 | 11.50 | -8.43 | -9.69 | 0.20 |
| Nov | 0.33 | 1.18 | 0.13 | 25.81 | -0.59 | 26.91 | -6.75 | -7.76 | -8.38 | 12.74 | -4.41 | 20.85 |
| Dec | -0.77 | 0.36 | -0.60 | 22.38 | 0.56 | 19.16 | -6.80 | 14.58 | -2.60 | 7.09 | -17.50 | 4.20 |

*Supplemental Table 4.2: Mean monthly surface temperature and energy balance differences between alfalfa and each wetland. Negative values denote more temperature or energy flux at the wetland, compared to alfalfa.*

| Monthly mean conductance | | | | | | | | |
|---|---|---|---|---|---|---|---|---|
| | Twitchell Alfalfa | | Young Wetland | | Intermediate Wetland | | Old Wetland | |
| *Month* | *Gs (m s$^{-1}$)* | *Ga (m s$^{-1}$)* | *Gs (m s$^{-1}$)* | *Ga (m s$^{-1}$)* | *Gs (m s$^{-1}$)* | *Ga (m s$^{-1}$)* | *Gs (m s$^{-1}$)* | *Ga (m s$^{-1}$)* |
| Jan | 0.015 | 0.010 | 0.007 | 0.018 | 0.009 | 0.019 | 0.010 | 0.020 |
| Feb | 0.015 | 0.012 | 0.006 | 0.019 | 0.008 | 0.021 | 0.007 | 0.022 |
| Mar | 0.014 | 0.014 | 0.006 | 0.021 | 0.008 | 0.026 | 0.005 | 0.026 |
| Apr | 0.013 | 0.018 | 0.008 | 0.028 | 0.009 | 0.033 | 0.003 | 0.033 |
| May | 0.010 | 0.025 | 0.009 | 0.035 | 0.009 | 0.041 | 0.004 | 0.041 |
| Jun | 0.005 | 0.024 | 0.009 | 0.035 | 0.008 | 0.042 | 0.005 | 0.040 |
| Jul | 0.005 | 0.023 | 0.008 | 0.035 | 0.009 | 0.043 | 0.006 | 0.039 |
| Aug | 0.004 | 0.023 | 0.007 | 0.037 | 0.009 | 0.044 | 0.007 | 0.040 |
| Sep | 0.004 | 0.017 | 0.005 | 0.028 | 0.007 | 0.034 | 0.006 | 0.030 |
| Oct | 0.006 | 0.013 | 0.004 | 0.021 | 0.006 | 0.026 | 0.005 | 0.025 |
| Nov | 0.010 | 0.011 | 0.004 | 0.017 | 0.007 | 0.019 | 0.007 | 0.021 |
| Dec | 0.010 | 0.011 | 0.005 | 0.017 | 0.008 | 0.020 | 0.008 | 0.022 |

*Supplemental Table 4.3: Monthly mean surface and aerodynamic conductance.*

| Growing season mean diel conductance | | | | | | | | |
|---|---|---|---|---|---|---|---|---|
| | Twitchell Alfalfa | | Young Wetland | | Intermediate Wetland | | Old Wetland | |
| *Hour* | *Gs (m s$^{-1}$)* | *Ga (m s$^{-1}$)* | *Gs (m s$^{-1}$)* | *Ga (m s$^{-1}$)* | *Gs (m s$^{-1}$)* | *Ga (m s$^{-1}$)* | *Gs (m s$^{-1}$)* | *Ga (m s$^{-1}$)* |
| 0:00 | 0.002 | 0.019 | 0.006 | 0.031 | 0.008 | 0.042 | 0.002 | 0.033 |
| 0:30 | 0.002 | 0.020 | 0.006 | 0.031 | 0.009 | 0.041 | 0.002 | 0.032 |
| 1:00 | 0.002 | 0.019 | 0.006 | 0.030 | 0.009 | 0.041 | 0.002 | 0.031 |
| 1:30 | 0.002 | 0.019 | 0.006 | 0.029 | 0.009 | 0.041 | 0.002 | 0.031 |
| 2:00 | 0.002 | 0.018 | 0.006 | 0.028 | 0.009 | 0.040 | 0.002 | 0.030 |
| 2:30 | 0.002 | 0.018 | 0.006 | 0.027 | 0.009 | 0.040 | 0.002 | 0.029 |

| | | | | | | | | |
|---|---|---|---|---|---|---|---|---|
| 3:00 | 0.003 | 0.017 | 0.007 | 0.027 | 0.009 | 0.039 | 0.002 | 0.029 |
| 3:30 | 0.003 | 0.017 | 0.006 | 0.027 | 0.009 | 0.039 | 0.002 | 0.028 |
| 4:00 | 0.003 | 0.017 | 0.006 | 0.026 | 0.009 | 0.039 | 0.002 | 0.029 |
| 4:30 | 0.003 | 0.017 | 0.007 | 0.027 | 0.009 | 0.038 | 0.002 | 0.029 |
| 5:00 | 0.003 | 0.017 | 0.007 | 0.026 | 0.009 | 0.038 | 0.002 | 0.028 |
| 5:30 | 0.004 | 0.017 | 0.006 | 0.027 | 0.009 | 0.038 | 0.002 | 0.028 |
| 6:00 | 0.006 | 0.017 | 0.006 | 0.027 | 0.009 | 0.038 | 0.003 | 0.029 |
| 6:30 | 0.007 | 0.019 | 0.005 | 0.028 | 0.010 | 0.039 | 0.004 | 0.031 |
| 7:00 | 0.009 | 0.022 | 0.006 | 0.030 | 0.010 | 0.040 | 0.006 | 0.036 |
| 7:30 | 0.009 | 0.024 | 0.007 | 0.032 | 0.010 | 0.041 | 0.007 | 0.039 |
| 8:00 | 0.010 | 0.025 | 0.007 | 0.034 | 0.010 | 0.042 | 0.008 | 0.041 |
| 8:30 | 0.010 | 0.026 | 0.008 | 0.036 | 0.010 | 0.042 | 0.009 | 0.043 |
| 9:00 | 0.010 | 0.026 | 0.009 | 0.036 | 0.010 | 0.042 | 0.010 | 0.044 |
| 9:30 | 0.010 | 0.026 | 0.010 | 0.037 | 0.010 | 0.042 | 0.010 | 0.044 |
| 10:00 | 0.010 | 0.025 | 0.010 | 0.037 | 0.010 | 0.042 | 0.010 | 0.045 |
| 10:30 | 0.010 | 0.025 | 0.010 | 0.037 | 0.010 | 0.042 | 0.010 | 0.045 |
| 11:00 | 0.009 | 0.025 | 0.010 | 0.037 | 0.010 | 0.042 | 0.010 | 0.045 |
| 11:30 | 0.009 | 0.025 | 0.010 | 0.036 | 0.010 | 0.042 | 0.010 | 0.045 |
| 12:00 | 0.009 | 0.024 | 0.010 | 0.036 | 0.009 | 0.042 | 0.010 | 0.045 |
| 12:30 | 0.008 | 0.025 | 0.011 | 0.037 | 0.009 | 0.043 | 0.010 | 0.045 |
| 13:00 | 0.008 | 0.025 | 0.011 | 0.037 | 0.009 | 0.043 | 0.010 | 0.046 |
| 13:30 | 0.008 | 0.026 | 0.011 | 0.038 | 0.009 | 0.043 | 0.010 | 0.046 |
| 14:00 | 0.008 | 0.026 | 0.011 | 0.038 | 0.009 | 0.044 | 0.009 | 0.046 |
| 14:30 | 0.007 | 0.027 | 0.011 | 0.039 | 0.009 | 0.044 | 0.009 | 0.046 |
| 15:00 | 0.007 | 0.027 | 0.011 | 0.040 | 0.009 | 0.044 | 0.009 | 0.046 |
| 15:30 | 0.007 | 0.028 | 0.011 | 0.040 | 0.008 | 0.044 | 0.008 | 0.047 |

| | | | | | | | | |
|---|---|---|---|---|---|---|---|---|
| 16:00 | 0.007 | 0.028 | 0.010 | 0.041 | 0.008 | 0.044 | 0.008 | 0.047 |
| 16:30 | 0.006 | 0.029 | 0.010 | 0.041 | 0.008 | 0.044 | 0.007 | 0.046 |
| 17:00 | 0.006 | 0.028 | 0.010 | 0.041 | 0.007 | 0.043 | 0.007 | 0.045 |
| 17:30 | 0.005 | 0.028 | 0.009 | 0.041 | 0.007 | 0.042 | 0.006 | 0.043 |
| 18:00 | 0.004 | 0.027 | 0.008 | 0.040 | 0.007 | 0.041 | 0.004 | 0.042 |
| 18:30 | 0.003 | 0.026 | 0.008 | 0.039 | 0.006 | 0.040 | 0.003 | 0.040 |
| 19:00 | 0.003 | 0.024 | 0.007 | 0.038 | 0.006 | 0.039 | 0.002 | 0.038 |
| 19:30 | 0.002 | 0.022 | 0.007 | 0.036 | 0.006 | 0.038 | 0.002 | 0.037 |
| 20:00 | 0.002 | 0.021 | 0.006 | 0.035 | 0.006 | 0.038 | 0.001 | 0.036 |
| 20:30 | 0.002 | 0.021 | 0.006 | 0.035 | 0.007 | 0.038 | 0.002 | 0.036 |
| 21:00 | 0.002 | 0.021 | 0.006 | 0.034 | 0.007 | 0.038 | 0.002 | 0.035 |
| 21:30 | 0.002 | 0.020 | 0.006 | 0.035 | 0.008 | 0.039 | 0.002 | 0.035 |
| 22:00 | 0.002 | 0.021 | 0.006 | 0.034 | 0.008 | 0.039 | 0.002 | 0.035 |
| 22:30 | 0.002 | 0.020 | 0.006 | 0.033 | 0.008 | 0.040 | 0.002 | 0.034 |
| 23:00 | 0.002 | 0.021 | 0.006 | 0.033 | 0.008 | 0.040 | 0.002 | 0.033 |
| 23:30 | 0.002 | 0.020 | 0.006 | 0.033 | 0.008 | 0.041 | 0.002 | 0.033 |

*Supplemental Table 4.4: Diel mean surface and aerodynamic conductance*

## References


Alkama, R., Cescatti, A., 2016. Biophysical climate impacts of recent changes in global forest cover. Science (80-. ). 351.

Allen, M.R., Fuglestvedt, J.S., Shine, K.P., Reisinger, A., Pierrehumbert, R.T., Forster, P.M., 2016. New use of global warming potentials to compare cumulative and short-lived climate pollutants. Nat. Clim. Chang. https://doi.org/10.1038/nclimate2998

Allen, M.R., Shine, K.P., Fuglestvedt, J.S., Millar, R.J., Cain, M., Frame, D.J., Macey, A.H., 2018. A solution to the misrepresentations of CO2-equivalent emissions of short-lived climate pollutants under ambitious mitigation. npj Clim. Atmos. Sci. 1. https://doi.org/10.1038/s41612-018-0026-8

Anderson, C.M., DeFries, R.S., Litterman, R., Matson, P.A., Nepstad, D.C., Pacala, S., Schlesinger, W.H., Shaw, M.R., Smith, P., Weber, C., Field, C.B., 2019. Natural climate solutions are not enough. Science (80-. ). 363, 933–934. https://doi.org/10.1126/science.aaw2741

Anderson, F.E., Bergamaschi, B., Sturtevant, C., Knox, S.H., Hastings, L., Windham-Myers, L., Detto, M., Hestir, E.L., Drexler, J., Miller, R.L., Matthes, J.H., Verfaillie, J.G., Baldocchi, D.D., Snyder, R.L., Fujii, R., 2016. Variation of energy and carbon fluxes from a restored temperate freshwater wetland and implications for carbon market verification protocols. J. Geophys. Res. Biogeosciences n/a-n/a. https://doi.org/10.1002/2015JG003083

Anderson, M., Gao, F., Knipper, K., Hain, C., Dulaney, W., Baldocchi, D., Eichelmann, E., Hemes, K.S., Yang, Y., Medellin-Azuara, J., Kustas, W., 2018. Field-Scale Assessment of Land and Water Use Change over the California Delta Using Remote Sensing 10. https://doi.org/10.3390/rs10060889

Anderson, R.G., Canadell, J.G., Randerson, J.T., Jackson, R.B., Hungate, B.A., Baldocchi, D.D., Ban-Weiss, G.A., Bonan, G.B., Caldeira, K., Cao, L., Diffenbaugh, N.S., Gurney, K.R., Kueppers, L.M., Law, B.E., Luyssaert, S., O'Halloran, T.L., 2011. Biophysical considerations in forestry for climate protection. Front. Ecol. Environ. 9, 174–182. https://doi.org/10.1890/090179

Arneth, A., Harrison, S.P., Zaehle, S., Tsigaridis, K., Menon, S., Bartlein, P.J., Feichter, J., Korhola, A., Kulmala, M., O'Donnell, D., Schurgers, G., Sorvari, S., Vesala, T., 2010. Terrestrial biogeochemical feedbacks in the climate system. Nat. Geosci. 3, 525–532. https://doi.org/10.1038/ngeo905

Atwater, B.F., Conard, S.G., Dowden, J.N., Hedel, C.W., MacDonald, R.L., Savage, W., 1979. History, landforms, and vegetation of the estuary's tidal marshes, Pacific Division of the American Association for the Advancement of Science.

Aubinet, M., 2008. Eddy covariance CO2 flux measurements in nocturnal conditions: An analysis of the problem. Ecol. Appl. 18, 1368–1378. https://doi.org/10.1890/06-1336.1

Aubinet, M., Heinesch, B., Yernaux, M., 2003. Horizontal and vertical CO2 advection in a sloping forest. Boundary-Layer Meteorol. 108, 397–417. https://doi.org/10.1023/A:1024168428135

Balcombe, P., Speirs, J.F., Hawkes, A.D., Brandon, N.P., 2018. Methane emissions: choosing the right climate metric and time horizon. Environ. Sci. Process. Impacts. https://doi.org/2018/EM/C8EM00414E

Baldocchi, D., Sturtevant, C., 2015. Does day and night sampling reduce spurious correlation between canopy photosynthesis and ecosystem respiration? Agric. For. Meteorol. 207. https://doi.org/10.1016/j.agrformet.2015.03.010

Baldocchi, D.D., 2014. Measuring fluxes of trace gases and energy between ecosystems and the atmosphere - the state and future of the eddy covariance method. Glob. Chang. Biol. 20, 3600–3609. https://doi.org/10.1111/gcb.12649

Baldocchi, D.D., 2003. Assessing the eddy covariance technique for evaluating carbon dioxide exchange rates of ecosystems: past, present and future. Glob. Chang. Biol. 9, 479–492. https://doi.org/10.1046/j.1365-2486.2003.00629.x

Baldocchi, D.D., Falge, E., Gu, L., Olson, R., Hollinger, D., Running, S., Anthoni, P., Bernhofer, C., Davis, K., Evans, R., Fuentes, J., Goldstein, A., Katul, G., Law, B., Lee, X., Malhi, Y., Meyers, T., Munger, W., Oechel, W.C., Paw, U.K.T., Pilegaard, K., Schmid, H.P., Valentini, R., Verma, S.B., Vesala, T., Wilson, K., Wofsy, S.C., 2001. FLUXNET: A New Tool to Study the Temporal and Spatial Variability of Ecosystem-Scale Carbon Dioxide, Water Vapor, and Energy Flux Densities. Bull. Am. Meteorol. Soc. 82, 2415–2434. https://doi.org/10.1175/1520-0477(2001)082<2415:FANTTS>2.3.CO;2

Baldocchi, D.D., Hicks, B.B., Meyers, T.P., Hincks, B.B., Meyers, T.P., 1988. Measuring biosphere-atmosphere exchanges of biologically related gases with micrometeorological methods, Ecology. https://doi.org/10.2307/1941631

Baldocchi, D.D., Knox, S.H., Dronova, I., Verfaillie, J.G., Oikawa, P.Y., Sturtevant, C., Matthes, J.H., Detto, M., 2016. The impact of expanding flooded land area on the annual evaporation of rice. Agric. For. Meteorol. 223, 181–193. https://doi.org/10.1016/j.agrformet.2016.04.001

Baldocchi, D.D., Ma, S., 2013. How will land use affect air temperature in the surface boundary layer? Lessons learned from a comparative study on the energy balance of an oak savanna and annual grassland in California, USA. Tellus B 65. https://doi.org/10.3402/tellusb.v65i0.19994

Baldocchi, D.D., Panuelas, J., 2018. The Physics and Ecology of Mining Carbon Dioxide from the Atmosphere by Ecosystems. Glob. Chang. Biol. https://doi.org/10.1111/gcb.14559

Baldwin, A.H., Jensen, K., Schönfeldt, M., 2014. Warming increases plant biomass and reduces diversity across continents, latitudes, and species migration scenarios in experimental wetland communities. Glob. Chang. Biol. https://doi.org/10.1111/gcb.12378

Barr, A.G., Betts, A.K., 1997. Radiosonde boundary layer budgets above a boreal forest. J. Geophys. Res. 102, 29205–29212. https://doi.org/10.1029/97JD01105

Barr, J.G., Engel, V., Fuentes, J.D., Fuller, D.O., Kwon, H., 2013. Modeling light use efficiency in a subtropical mangrove forest equipped with CO2 eddy covariance. Biogeosciences 10, 2145–2158. https://doi.org/10.5194/bg-10-2145-2013

Bianco, L., Djalalova, I. V., King, C.W., Wilczak, J.M., 2011. Diurnal Evolution and Annual

Variability of Boundary-Layer Height and Its Correlation to Other Meteorological Variables in California's Central Valley. Boundary-Layer Meteorol. 140, 491–511. https://doi.org/10.1007/s10546-011-9622-4

Bonan, G.B., 2008. Forests and climate change: forcings, feedbacks, and the climate benefits of forests. Science 320, 1444–1449. https://doi.org/10.1126/science.1155121

Bonfils, C., Duffy, P.B., Santer, B.D., Wigley, T.M.L., Lobell, D.B., Phillips, T.J., Doutriaux, C., 2007. Identification of external influences on temperatures in California. Clim. Change 87. https://doi.org/10.1007/s10584-007-9374-9

Bridgham, S.D., Cadillo-Quiroz, H., Keller, J.K., Zhuang, Q., 2013. Methane emissions from wetlands: biogeochemical, microbial, and modeling perspectives from local to global scales. Glob. Chang. Biol. 19, 1325–1346. https://doi.org/10.1111/gcb.12131

Bridgham, S.D., Megonigal, J.P., Keller, J.K., Bliss, N.B., Trettin, C., 2006. The carbon balance of North American wetlands. Wetlands 26, 889–916. https://doi.org/10.1672/0277-5212(2006)26[889:TCBONA]2.0.CO;2

Bright, R.M., Davin, E.L., O'Halloran, T., Pongratz, J., Zhao, K., Cescatti, A., 2017. Local temperature response to land cover and management change driven by non-radiative processes. Nat. Clim. Chang. 7, 296–302. https://doi.org/10.1038/nclimate3250

Brovkin, V., Ganopolski, A., Claussen, M., Kubatzki, C., Petoukhov, V., 1999. Modelling climate response to historical land cover change. Glob. Ecol. Biogeogr. 8, 509–517. https://doi.org/10.1046/j.1365-2699.1999.00169.x

Brown, K.J., Pasternack, G.B., 2005. A palaeoenvironmental reconstruction to aid in the restoration of floodplain and wetland habitat on an upper deltaic plain, California, USA. Environ. Conserv. https://doi.org/10.1017/S037689290500216X

Burakowski, E., Tawfik, A., Ouimette, A., Lepine, L., Novick, K., Ollinger, S., Zarzycki, C., Bonan, G.B., 2017. The role of surface roughness, albedo, and Bowen ratio on ecosystem energy balance in the Eastern United States. Agric. For. Meteorol. https://doi.org/10.1016/j.agrformet.2017.11.030

Canadell, J.G., Schulze, E.D., 2014. Global potential of biospheric carbon management for climate mitigation. Nat. Commun. 5, 5282. https://doi.org/10.1038/ncomms6282

Cao, M., Marshall, S., Gregson, K., 1996. Global carbon exchange and methane emissions from natural wetlands: Application of a process-based model. J. Geophys. Res. Atmos. 101, 14399–14414.

Cathles, L.M., Brown, L., Taam, M., Hunter, A., 2012. A commentary on "The greenhouse-gas footprint of natural gas in shale formations" by R.W. Howarth, R. Santoro, and Anthony Ingraffea. Clim. Change. https://doi.org/10.1007/s10584-011-0333-0

Cescatti, A., Marcolla, B., Santhana Vannan, S.K., Pan, J.Y., Román, M.O., Yang, X., Ciais, P., Cook, R.B., Law, B.E., Matteucci, G., Migliavacca, M., Moors, E., Richardson, A.D., Seufert, G., Schaaf, C.B., 2012. Intercomparison of MODIS albedo retrievals and in situ measurements across the global FLUXNET network. Remote Sens. Environ. 121, 323–334. https://doi.org/10.1016/j.rse.2012.02.019

Chamberlain, S.D., Anthony, T.L., Silver, W.L., Eichelmann, E., Hemes, K.S., Oikawa, P.Y.,

Sturtevant, C., Szutu, D.J., Verfaillie, J.G., Baldocchi, D.D., 2018. Soil properties and sediment accretion modulate methane fluxes from restored wetlands. Glob. Chang. Biol. 24, 4107–4121. https://doi.org/10.1111/gcb.14124

Chamberlain, S.D., Gomez-Casanovas, N., Walter, M.T., Boughton, E.H., Bernacchi, C.J., Delucia, E.H., Groffman, P.M., Keel, E.W., Sparks, J.P., 2016. Influence of transient flooding on methane fluxes from subtropical pastures. J. Geophys. Res. Biogeosciences Biogeosciences 121, 965–977. https://doi.org/10.1002/2015JG003283

Chamberlain, S.D., Groffman, P.M., Boughton, E.H., Gomez-Casanovas, N., DeLucia, E.H., Bernacchi, C.J., Sparks, J.P., 2017a. The impact of water management practices on subtropical pasture methane emissions and ecosystem service payments. Ecol. Appl. 27, 1199–1209. https://doi.org/10.1002/eap.1514

Chamberlain, S.D., Verfaillie, J.G., Eichelmann, E., Hemes, K.S., Baldocchi, D.D., 2017b. Evaluation of Density Corrections to Methane Fluxes Measured by Open-Path Eddy Covariance over Contrasting Landscapes. Boundary-Layer Meteorol. 165, 197–210. https://doi.org/10.1007/s10546-017-0275-9

Chapin, F.S., Matson, P.A., Vitousek, P.M., 2012. Principles of terrestrial ecosystem ecology., 2nd ed. Springer, New York, NY.

Christensen, T.R., Prentice, I.C., Kaplan, J., Haxeltine, A., Sitch, S., 1996. Methane flux from northern wetlands and tundra: An ecosystem source modelling approach. Tellus, Ser. B Chem. Phys. Meteorol. https://doi.org/10.1034/j.1600-0889.1996.t01-4-00004.x

Chu, H., Gottgens, J.F., Chen, J., Sun, G., Desai, A.R., Ouyang, Z., Shao, C., Czajkowski, K., 2015. Climatic variability, hydrologic anomaly, and methane emission can turn productive freshwater marshes into net carbon sources. Glob. Chang. Biol. 21, 1165–1181. https://doi.org/10.1111/gcb.12760

Cloern, J.E., Jassby, A.D., 2012. Drivers of change in estuarine - coastal ecosystems: discoveries from four decades of study in San Francisco Bay. Rev. Geophys. 50, 1–33. https://doi.org/10.1029/2012RG000397.1.INTRODUCTION

D'Odorico, P., Fuentes, J.D., Pockman, W.T., Collins, S.L., He, Y., Medeiros, J.S., DeWekker, S., Litvak, M.E., 2010. Positive feedback between microclimate and shrub encroachment in the northern Chihuahuan desert. Ecosphere 1, art17. https://doi.org/10.1890/ES10-00073.1

Davin, E.L., de Noblet-Ducoudre, N., 2010. Climatic impact of global-scale Deforestation: Radiative versus nonradiative processes. J. Clim. 23, 97–112. https://doi.org/10.1175/2009JCLI3102.1

Dean, J.F., Middelburg, J.J., Röckmann, T., Aerts, R., Blauw, L.G., Egger, M., Jetten, M.S.M., de Jong, A.E.E., Meisel, O.H., Rasigraf, O., Slomp, C.P., in 't Zandt, M.H., Dolman, A.J., 2018. Methane feedbacks to the global climate system in a warmer world. Rev. Geophys. https://doi.org/10.1002/2017RG000559

Dengel, S., Zona, D., Sachs, T., Aurela, M., Jammet, M., Parmentier, F.J.W., Oechel, W., Vesala, T., 2013. Testing the applicability of neural networks as a gap-filling method using CH4flux data from high latitude wetlands. Biogeosciences 10, 8185–8200. https://doi.org/10.5194/bg-10-8185-2013

Desai, A.R., Xu, K., Tian, H., Weishampel, P., Thom, J., Baumann, D., Andrews, A.E., Cook, B.D., King, J.Y., Kolka, R., 2015. Landscape-level terrestrial methane flux observed from a very tall tower. Agric. For. Meteorol. https://doi.org/10.1016/j.agrformet.2014.10.017

Detto, M., Baldocchi, D.D., Katul, G.G., 2010. Scaling Properties of Biologically Active Scalar Concentration Fluctuations in the Atmospheric Surface Layer over a Managed Peatland. Boundary-Layer Meteorol. 136, 407–430. https://doi.org/10.1007/s10546-010-9514-z

Deverel, S.J., Ingrum, T., Leighton, D., 2016. Present-day oxidative subsidence of organic soils and mitigation in the Sacramento-San Joaquin Delta, California, USA. Hydrogeol. J. 24, 569–586. https://doi.org/10.1007/s10040-016-1391-1

Deverel, S.J., Ingrum, T., Lucero, C., Drexler, J.Z., 2014. Impounded Marshes on Subsided Islands: Simulated Vertical Accretion, Processes, and Effects, Sacramento-San Joaquin Delta, CA USA. San Fr. Estuary Watershed Sci. 12.

Deverel, S.J., Jacobs, P., Lucero, C., Dore, S., Kelsey, T.R., 2017. Implications for Greenhouse Gas Emission Reductions and Economics of a Changing Agricultural Mosaic in the Sacramento – San Joaquin Delta. San Fr. Estuary Watershed Sci. 15. https://doi.org/10.5811/westjem.2011.5.6700

Deverel, S.J., Leighton, D.A., 2010. Historic, Recent, and Future Subsidence, Sacramento-San Joaquin Delta, California, USA. San Fr. Estuary Watershed Sci. 8.

Drexler, J.Z., de Fontaine, C., Knifong, D.L., 2007. Age Determination of the Remaining Peat in the Sacramento-San Joaquin Delta, California, USA. USGS.

Drexler, J.Z., Fontaine, C.S., Deverel, S.J., 2009. The legacy of wetland drainage on the remaining peat in the Sacramento — San Joaquin Delta, California, USA. Wetlands 29, 372–386. https://doi.org/10.1672/08-97.1

Eichelmann, E., Hemes, K.S., Knox, S.H., Oikawa, P.Y., Chamberlain, S.D., Sturtevant, C., Verfaillie, J.G., Baldocchi, D.D., 2018. The effect of land cover type and structure on evapotranspiration from agricultural and wetland sites in the Sacramento–San Joaquin River Delta, California. Agric. For. Meteorol. 256–257. https://doi.org/10.1016/j.agrformet.2018.03.007

Erb, K.H., Kastner, T., Plutzar, C., Bais, A.L.S., Carvalhais, N., Fetzel, T., Gingrich, S., Haberl, H., Lauk, C., Niedertscheider, M., Pongratz, J., Thurner, M., Luyssaert, S., 2018. Unexpectedly large impact of forest management and grazing on global vegetation biomass. Nature 553, 73–76. https://doi.org/10.1038/nature25138

Erb, K.H., Luyssaert, S., Meyfroidt, P., Pongratz, J., Don, A., Kloster, S., Kuemmerle, T., Fetzel, T., Fuchs, R., Herold, M., Haberl, H., Jones, C.D., Marín-Spiotta, E., McCallum, I., Robertson, E., Seufert, V., Fritz, S., Valade, A., Wiltshire, A., Dolman, A.J., 2017. Land management: data availability and process understanding for global change studies. Glob. Chang. Biol. 23, 512–533. https://doi.org/10.3945/ajcn.116.130518

Estes, L., Elsen, P.R., Treuer, T., Ahmed, L., Caylor, K., Chang, J., Choi, J.J., Ellis, E.C., 2018. The spatial and temporal domains of modern ecology. Nat. Ecol. Evol. 2, 819–826. https://doi.org/10.1038/s41559-018-0524-4

Falge, E., Baldocchi, D.D., Olson, R., Anthoni, P., Aubinet, M., Bernhofer, C., Burba, G.,

Ceulemans, R., Clement, R., Dolman, H., Granier, A., Gross, P., Grünwald, T., Hollinger, D., Jensen, N.O., Katul, G., Keronen, P., Kowalski, A., Ta Lai, C., Law, B.E., Meyers, T., Moncrieff, J., Moors, E., William Munger, J., Pilegaard, K., Rannik, Ü., Rebmann, C., Suyker, A., Tenhunen, J., Tu, K., Verma, S.B., Vesala, T., Wilson, K., Wofsy, S.C., 2001. Short communication: Gap filling strategies for long term energy flux data sets. Agric. For. Meteorol. 107, 71–77. https://doi.org/10.1016/S0168-1923(00)00235-5

Fargione, J., Bassett, S., Boucher, T., Bridgham, S., Conant, R.T., Cook-Patton, S., Ellis, P.W., Falcucci, A., Fourqurean, J., Gopalakrishna, T., Gu, H., Henderson, B., Hurteau, M.D., Kroeger, K.D., Kroeger, T., Lark, T.J., Leavitt, S.M., Lomax, G., McDonald, R., Megonigal, P.J., Miteva, D.A., Richardson, C., Sanderman, J., Shoch, D., Spawn, S.A., Veldman, J.W., Williams, C.A., Woodbury, P.B., Zganjar, C., Baranski, M., Elias, P., Houghton, R.A., Landis, E., McGlynn, E., Schlesinger, W.H., Siikamaki, J. V., Sutton-Grier, A.E., Griscom, B.W., 2018. Natural Climate Solutions for the United States. Sci. Adv. In Press, 1–15. https://doi.org/10.1126/sciadv.aat1869

Feldman, D.R., Collins, W.D., Biraud, S.C., Risser, M.D., Turner, D.D., Gero, P.J., Tadić, J., Helmig, D., Xie, S., Mlawer, E.J., Shippert, T.R., Torn, M.S., 2018. Observationally derived rise in methane surface forcing mediated by water vapour trends. Nat. Geosci. 11, 238–243. https://doi.org/10.1038/s41561-018-0085-9

Ficklin, D.L., Novick, K.A., 2017. Historic and projected changes in vapor pressure deficit suggest a continental-scale drying of the United States atmosphere. J. Geophys. Res. Atmos. 122, 2061–2079. https://doi.org/10.1002/2016JD025855

Firestone, M.K., Davidson, E.A., 1989. Microbiologial Basis of NO and N20 production and consumption in soil, in: Exchange of Trace Gases between Terrestrial Ecosystems and the Atmosphere. pp. 7–21.

Flanagan, L.B., Syed, K.H., 2011. Stimulation of both photosynthesis and respiration in response to warmer and drier conditions in a boreal peatland ecosystem. Glob. Chang. Biol. https://doi.org/10.1111/j.1365-2486.2010.02378.x

Friborg, T., Christensen, T.R., Hansen, B.U., Nordstroem, C., Soegaard, H., 2000. Trace gas exchange in a high-Arctic valley: 2. Landscape CH4 fluxes measured and modeled using eddy correlation data. Global Biogeochem. Cycles. https://doi.org/10.1029/1999GB001136

Friborg, T., Soegaard, H., Christenen, T.R., Lloyd, C.R., Panikov, N.S., 2003. Siberian wetlands: Where a sink is a source. Geophys. Res. Lett. 30. https://doi.org/10.1029/2003GL017797

Friedlingstein, P., Meinshausen, M., Arora, V.K., Jones, C.D., Anav, A., Liddicoat, S.K., Knutti, R., 2014. Uncertainties in CMIP5 climate projections due to carbon cycle feedbacks. J. Clim. 27, 511–526. https://doi.org/10.1175/JCLI-D-12-00579.1

Frolking, S., Roulet, N., Fuglestvedt, J., 2006. How northern peatlands influence the Earth's radiative budget: Sustained methane emission versus sustained carbon sequestration. J. Geophys. Res. Biogeosciences. https://doi.org/10.1029/2005JG000091

Frolking, S., Roulet, N.T., 2007. Holocene radiative forcing impact of northern peatland carbon accumulation and methane emissions. Glob. Chang. Biol. https://doi.org/10.1111/j.1365-2486.2007.01339.x

Frolking, S., Talbot, J., Jones, M.C., Treat, C.C., Kauffman, J.B., Tuittila, E.-S., Roulet, N.,

2011. Peatlands in the Earth's 21st century climate system. Environ. Rev. https://doi.org/10.1139/a11-014

Gauci, V., Dise, N., Blake, S., 2005. Long-term suppresion of wetland methane flux following a pulse of simulated acid rain. Geophys. Res. Lett. https://doi.org/10.1029/2005GL022544

Georgescu, M., Lobell, D.B., Field, C.B., 2011. Direct climate effects of perennial bioenergy crops in the United States. Proc. Natl. Acad. Sci. U. S. A. 108, 4307–4312. https://doi.org/10.1073/pnas.1008779108

Gerken, T., Bromley, G.T., Stoy, P.C., 2018. Surface Moistening Trends in the Northern North American Great Plains Increase the Likelihood of Convective Initiation. J. Hydrometeorol. https://doi.org/10.1175/JHM-D-17-0117.1

Goulden, M.L., Litvak, M., Miller, S.D., 2007. Factors that control Typha marsh evapotranspiration. Aquat. Bot. 86, 97–106. https://doi.org/10.1016/j.aquabot.2006.09.005

Griscom, B.W., Adams, J., Ellise, P.W., Houghton, R.A., Lomax, G., 2017. Natural Climate Solutions. Proc. Natl. Acad. Sci. 11–12. https://doi.org/10.1073/pnas.1710465114

Günther, A., Böther, S., Couwenberg, J., Hüttel, S., Jurasinski, G., 2018. Profitability of Direct Greenhouse Gas Measurements in Carbon Credit Schemes of Peatland Rewetting. https://doi.org/10.1016/j.ecolecon.2017.12.025

Hanson, B., Putnam, D., Snyder, R., 2007. Deficit irrigation of alfalfa as a strategy for providing water for water-short areas. Agric. Water Manag. 93, 73–80. https://doi.org/10.2495/SI080121

Hatala, J.A., Detto, M., Sonnentag, O., Deverel, S.J., Verfaillie, J.G., Baldocchi, D.D., 2012. Greenhouse gas (CO2, CH4, H2O) fluxes from drained and flooded agricultural peatlands in the Sacramento-San Joaquin Delta. Agric. Ecosyst. Environ. 150, 1–18. https://doi.org/10.1016/j.agee.2012.01.009

He, C., Tian, J., Gao, B., Zhao, Y., 2015. Differentiating climate- and human-induced drivers of grassland degradation in the Liao River Basin, China. Environ. Monit. Assess. 187, 4199. https://doi.org/10.1007/s10661-014-4199-2

Helbig, M., Chasmer, L.E., Kljun, N., Quinton, W.L., Treat, C.C., Sonnentag, O., 2016. The positive net radiative greenhouse gas forcing of increasing methane emissions from a thawing boreal forest-wetland landscape. Glob. Chang. Biol. 2413–2427. https://doi.org/10.1111/gcb.13520

Helliker, B.R., Richter, S.L., 2008. Subtropical to boreal convergence of tree-leaf temperatures. Nature 454, 511–514. https://doi.org/10.1038/nature07031

Hemes, K.S., Chamberlain, S.D., Eichelmann, E., Anthony, T., Valach, A., Kasak, K., Szutu, D., Verfaillie, J., Silver, W.L., Baldocchi, D.D., 2019. Assessing the carbon and climate benefit of restoring degraded agricultural peat soils to managed wetlands. Agric. For. Meteorol. 268, 202–214. https://doi.org/10.1016/j.agrformet.2019.01.017

Hemes, K.S., Chamberlain, S.D., Eichelmann, E., Knox, S.H., Baldocchi, D.D., 2018a. A Biogeochemical Compromise: The High Methane Cost of Sequestering Carbon in Restored Wetlands. Geophys. Res. Lett. https://doi.org/10.1029/2018GL077747

Hemes, K.S., Eichelmann, E., Chamberlain, S.D., Knox, S.H., Oikawa, P.Y., Sturtevant, C., Verfaillie, J.G., Szutu, D., Baldocchi, D.D., 2018b. A Unique Combination of Aerodynamic and Surface Properties Contribute to Surface Cooling in Restored Wetlands of the Sacramento-San Joaquin Delta, California. J. Geophys. Res. Biogeosciences 123, 2072–2090. https://doi.org/10.1029/2018JG004494

Herbst, M., Friborg, T., Schelde, K., Jensen, R., Ringgaard, R., Vasquez, V., Thomsen, A.G., Soegaard, H., 2013. Climate and site management as driving factors for the atmospheric greenhouse gas exchange of a restored wetland. Biogeosciences 10, 39–52. https://doi.org/10.5194/bg-10-39-2013

Heskel, M. a, Atkin, O.K., Turnbull, M.H., Griffin, K.L., 2013. Bringing the Kok effect to light: A review on the integration of daytime respiration and net ecosystem exchange. Ecosphere 4, 1–14. https://doi.org/10.1890/Es13-00120.1

Himes-Cornell, A., Pendleton, L., Atiyah, P., 2018. Valuing ecosystem services from blue forests: A systematic review of the valuation of salt marshes, sea grass beds and mangrove forests. Ecosyst. Serv. https://doi.org/10.1016/j.ecoser.2018.01.006

Holm, G.O., Perez, B.C., McWhorter, D.E., Krauss, K.W., Johnson, D.J., Raynie, R.C., Killebrew, C.J., 2016. Ecosystem Level Methane Fluxes from Tidal Freshwater and Brackish Marshes of the Mississippi River Delta: Implications for Coastal Wetland Carbon Projects. Wetlands 36, 401–413. https://doi.org/10.1007/s13157-016-0746-7

Hoper, H., Augustin, J., Cagampan, J.P., Drosler, M., Lundin, L., Moors, E., Vasander, H., Waddington, J.M., Wilson, D., 2008. Restoration of Peatlands and Greenhouse Gas Balances, in: Strack, M.J. (Ed.), Peatlands and Climate Change.

Howarth, R.W., Santoro, R., Ingraffea, A., 2011. Methane and the greenhouse-gas footprint of natural gas from shale formations. Clim. Change. https://doi.org/10.1007/s10584-011-0061-5

Humphreys, E.R., Lafleur, P.M., Flanagan, L.B., Hedstrom, N., Syed, K.H., Glenn, A.J., Granger, R., 2006. Summer carbon dioxide and water vapor fluxes across a range of northern peatlands. J. Geophys. Res. Biogeosciences 111. https://doi.org/10.1029/2005JG000111

Jackson, R.B., Randerson, J.T., Canadell, J.G., Anderson, R.G., Avissar, R., Baldocchi, D.D., Bonan, G.B., Caldeira, K., Diffenbaugh, N.S., Field, C.B., Hungate, B.A., Jobbágy, E.G., Kueppers, L.M., Nosetto, M.D., Pataki, D.E., 2008. Protecting climate with forests. Environ. Res. Lett. 3, 044006. https://doi.org/10.1088/1748-9326/3/4/044006

Jammet, M., Dengel, S., Kettner, E., Parmentier, F.J.W., Wik, M., Crill, P., Friborg, T., 2017. Year-round CH4 and CO2flux dynamics in two contrasting freshwater ecosystems of the subarctic. Biogeosciences. https://doi.org/10.5194/bg-14-5189-2017

Jarvis, P.G., McNaughton, K.G., 1986. Stomatal control of transpiration: Scaling up from leaf to region. Adv. Ecol. Res. 15, water relations, canopy coupling.

Johnson, C.R., Chabot, R.H., Marzloff, M.P., Wotherspoon, S., 2017. Knowing when (not) to attempt ecological restoration. Restor. Ecol. 25, 140–147. https://doi.org/10.1111/rec.12413

Juang, J.Y., Katul, G., Siqueira, M., Stoy, P., Novick, K., 2007. Separating the effects of albedo

from eco-physiological changes on surface temperature along a successional chronosequence in the southeastern United States. Geophys. Res. Lett. 34, 1–5. https://doi.org/10.1029/2007GL031296

Kaimal, J.C., Wyngaard, J.C., Izumi, Y., Cot??, O.R., 1972. Spectral characteristics of surface-layer turbulence. Q. J. R. Meteorol. Soc. 98, 563–589. https://doi.org/10.1002/qj.49709841707

Kandel, T.P., Laerke, P.E., Hoffmann, C.C., Elsgaard, L., 2018. Complete annual CO2 , CH4 , and N2O balance of a temperate riparian wetland 12 years after rewetting. Ecol. Eng. https://doi.org/10.1016/j.ecoleng.2017.12.019

Kirschke, S., Bousquet, P., Ciais, P., Saunois, M., Canadell, J.G., Dlugokencky, E.J., Bergamaschi, P., Bergmann, D., Blake, D.R., Bruhwiler, L., Cameron-Smith, P., Castaldi, S., Chevallier, F., Feng, L., Fraser, A., Heimann, M., Hodson, E.L., Houweling, S., Josse, B., Fraser, P.J., Krummel, P.B., Lamarque, J.-F., Langenfelds, R.L., Le Quéré, C., Naik, V., O'Doherty, S., Palmer, P.I., Pison, I., Plummer, D., Poulter, B., Prinn, R.G., Rigby, M., Ringeval, B., Santini, M., Schmidt, M., Shindell, D.T., Simpson, I.J., Spahni, R., Steele, L.P., Strode, S.A., Sudo, K., Szopa, S., van der Werf, G.R., Voulgarakis, A., van Weele, M., Weiss, R.F., Williams, J.E., Zeng, G., 2013. Three decades of global methane sources and sinks. Nat. Geosci. 6, 813–823. https://doi.org/10.1038/ngeo1955

Knauer, J., Zaehle, S., Medlyn, B.E., Reichstein, M., Williams, C.A., Migliavacca, M., De Kauwe, M.G., Werner, C., Keitel, C., Kolari, P., Limousin, J.-M., Linderson, M.-L., 2017. Towards physiologically meaningful water-use efficiency estimates from eddy covariance data. Glob. Chang. Biol. https://doi.org/10.1111/gcb.13893

Knox, S.H., Matthes, J.H., Sturtevant, C., Oikawa, P.Y., Verfaillie, J.G., Baldocchi, D.D., 2016. Biophysical controls on interannual variability in ecosystem scale CO 2 and CH 4 exchange in a California rice paddy. J. Geophys. Res. Biogeosciences n/a-n/a. https://doi.org/10.1002/2015JG003247

Knox, S.H., Sturtevant, C., Matthes, J.H., Koteen, L., Verfaillie, J.G., Baldocchi, D.D., 2015. Agricultural peatland restoration: effects of land-use change on greenhouse gas (CO2 and CH4) fluxes in the Sacramento-San Joaquin Delta. Glob. Chang. Biol. 21, 750–65. https://doi.org/10.1111/gcb.12745

Knox, S.H., Windham-Myers, L., Anderson, F.E., Sturtevant, C., Bergamaschi, B., 2018. Direct and indirect effects of tides on ecosystem-scale CO2 exchange in a brackish tidal marsh in Northern California. J. Geophys. Res. Biogeosciences. https://doi.org/10.1002/2017JG004048

Krauss, K.W., Holm, G.O., Perez, B.C., McWhorter, D.E., Cormier, N., Moss, R.F., Johnson, D.J., Neubauer, S.C., Raynie, R.C., 2016. Component greenhouse gas fluxes and radiative balance from two deltaic marshes in Louisiana: Pairing chamber techniques and eddy covariance. J. Geophys. Res. Biogeosciences 121, 1503–1521. https://doi.org/10.1002/2015JG003224

Krauss, K.W., Noe, G.B., Duberstein, J.A., Conner, W.H., Stagg, C.L., Cormier, N., Jones, M.C., Bernhardt, C.E., Graeme Lockaby, B., From, A.S., Doyle, T.W., Day, R.H., Ensign, S.H., Pierfelice, K.N., Hupp, C.R., Chow, A.T., Whitbeck, J.L., 2018. The Role of the Upper Tidal Estuary in Wetland Blue Carbon Storage and Flux. Global Biogeochem. Cycles 32,

817–839. https://doi.org/10.1029/2018GB005897

Kroeger, K.D., Crooks, S., Moseman-Valtierra, S., Tang, J., 2017. Restoring tides to reduce methane emissions in impounded wetlands: A new and potent Blue Carbon climate change intervention. Sci. Rep. 7, 11914. https://doi.org/10.1038/s41598-017-12138-4

Laguë, M.M., Swann, A.L.S., 2016. Progressive midlatitude afforestation: Impacts on clouds, global energy transport, and precipitation. J. Clim. 29, 5561–5573. https://doi.org/10.1175/jcli-d-15-0748.1

Lee, S.C., Christen, A., Black, A.T., Johnson, M.S., Jassal, R.S., Ketler, R., Nesic, Z., Merkens, M., 2016. Annual greenhouse gas budget for a bog ecosystem undergoing restoration by rewetting. Biogeosciences Discuss. 1, 1–26. https://doi.org/10.5194/bg-2016-446

Lee, X., Goulden, M.L., Hollinger, D.Y., Barr, A.G., Black, T.A., Bohrer, G., Bracho, R., Drake, B., Goldstein, A., Gu, L., Katul, G., Kolb, T., Law, B.E., Margolis, H., Meyers, T., Monson, R., Munger, W., Oren, R., Paw U, K.T., Richardson, A.D., Schmid, H.P., Staebler, R., Wofsy, S.C., Zhao, L., 2011. Observed increase in local cooling effect of deforestation at higher latitudes. Nature 479, 384–387. https://doi.org/10.1038/nature10588

Leifeld, J., Menichetti, L., 2018. The underappreciated potential of peatlands in global climate change mitigation strategies. Nat. Commun. 9, 1071. https://doi.org/10.1038/s41467-018-03406-6

Lejeune, Q., Davin, E.L., Gudmundsson, L., Winckler, J., Seneviratne, S.I., 2018. Historical deforestation locally increased the intensity of hot days in northern mid-latitudes. Nat. Clim. Chang. 8, 386–390. https://doi.org/10.1038/s41558-018-0131-z

Leuning, R., van Gorsel, E., Massman, W.J., Isaac, P.R., 2012. Reflections on the surface energy imbalance problem. Agric. For. Meteorol. 156, 65–74. https://doi.org/10.1016/j.agrformet.2011.12.002

Lobell, D.B., Bala, G., Duffy, P.B., 2006. Biogeophysical impacts of cropland management changes on climate. Geophys. Res. Lett. 33, 4–7. https://doi.org/10.1029/2005GL025492

Lobell, D.B., Bonfils, C., 2008. The effect of irrigation on regional temperatures: A spatial and temporal analysis of trends in California, 1934-2002. J. Clim. 21, 2063–2071. https://doi.org/10.1175/2007JCLI1755.1

Long, K.D., Flanagan, L.B., Cai, T., 2010. Diurnal and seasonal variation in methane emissions in a northern Canadian peatland measured by eddy covariance. Glob. Chang. Biol. https://doi.org/10.1111/j.1365-2486.2009.02083.x

Luyssaert, S., Jammet, M., Stoy, P.C., Estel, S., Pongratz, J., Ceschia, E., Churkina, G., Don, A., Erb, K., Ferlicoq, M., Gielen, B., Grünwald, T., Houghton, R. a., Klumpp, K., Knohl, A., Kolb, T., Kuemmerle, T., Laurila, T., Lohila, A., Loustau, D., McGrath, M.J., Meyfroidt, P., Moors, E.J., Naudts, K., Novick, K., Otto, J., Pilegaard, K., Pio, C. a., Rambal, S., Rebmann, C., Ryder, J., Suyker, A.E., Varlagin, A., Wattenbach, M., Dolman, a. J., 2014. Land management and land-cover change have impacts of similar magnitude on surface temperature. Nat. Clim. Chang. 4, 389–393. https://doi.org/10.1038/nclimate2196

Luyssaert, S., Marie, G., Valade, A., Chen, Y.Y., Njakou Djomo, S., Ryder, J., Otto, J., Naudts, K., Lansø, A.S., Ghattas, J., McGrath, M.J., 2018. Trade-offs in using European forests to

meet climate objectives. Nature 562, 259–262. https://doi.org/10.1038/s41586-018-0577-1

Ma, S., Osuna, J.L., Verfaillie, J.G., Baldocchi, D.D., 2017. Photosynthetic responses to temperature across leaf–canopy–ecosystem scales: a 15-year study in a Californian oak-grass savanna. Photosynth. Res. 0, 1–15. https://doi.org/10.1007/s11120-017-0388-5

Mahmood, R., Pielke, R.A., Hubbard, K.G., Niyogi, D., Dirmeyer, P.A., Mcalpine, C., Carleton, A.M., Hale, R., Gameda, S., Beltr??n-Przekurat, A., Baker, B., Mcnider, R., Legates, D.R., Shepherd, M., Du, J., Blanken, P.D., Frauenfeld, O.W., Nair, U.S., Fall, S., 2014. Land cover changes and their biogeophysical effects on climate. Int. J. Climatol. 34, 929–953. https://doi.org/10.1002/joc.3736

Mastepanov, M., Sigsgaard, C., Dlugokencky, E.J., Houweling, S., Ström, L., Tamstorf, M.P., Christensen, T.R., 2008. Large tundra methane burst during onset of freezing. Nature 456, 628–630. https://doi.org/10.1038/nature07464

Mcalpine, C.A., Ryan, J.G., Seabrook, L., Thomas, S., Dargusch, P.J., Syktus, J.I., Sr, R.A.P., Etter, A.E., Fearnside, P.M., Laurance, W.F., 2010. More than CO 2 : a broader paradigm for managing climate change and variability to avoid ecosystem collapse. Curr. Opin. Environ. Sustain. 1–13. https://doi.org/10.1016/j.cosust.2010.10.001

McNaughton, K.G., Spriggs, T.W., 1986. A mixed-layer model for regional evaporation. Boundary-Layer Meteorol. 34, 243–262. https://doi.org/10.1007/BF00122381

McNicol, G., Sturtevant, C.S., Knox, S.H., Dronova, I., Baldocchi, D.D., Silver, W.L., 2016. Effects of seasonality, transport-pathway, and spatial structure on greenhouse gas fluxes in a restored wetland. Glob. Chang. Biol. 1–15. https://doi.org/10.1111/gcb.13580

Medellín-Azuara, J., Paw U, K.T., Jin, Y., Hart, Q., Kent, E., Clay, J., Wong, A., Bell, A., Anderson, M., Howes, D., Melton, F., Kadir, T., Orang, M., Leinfelder-Miles, M., Lund, J.R., 2016. Estimation of Crop Evapotranspiration in the Sacramento San Joaquin Delta for the 2014-2015 Water Year, Interim Report.

Melton, J.R., Wania, R., Hodson, E.L., Poulter, B., Ringeval, B., Spahni, R., Bohn, T., Avis, C.A., Chen, G., Eliseev, A. V., Hopcroft, P.O., Riley, W.J., Subin, Z.M., Tian, H., Van Bodegom, P.M., Kleinen, T., Yu, Z.C., Singarayer, J.S., Zürcher, S., Lettenmaier, D.P., Beerling, D.J., Denisov, S.N., Prigent, C., Papa, F., Kaplan, J.O., 2013. Present state of global wetland extent and wetland methane modelling: Methodology of a model inter-comparison project (WETCHIMP). Geosci. Model Dev. 6, 617–641. https://doi.org/10.5194/gmd-6-617-2013

Meng, L., Roulet, N., Zhuang, Q., Christensen, T.R., Frolking, S., 2016. Focus on the impact of climate change on wetland ecosystems and carbon dynamics. Environ. Res. Lett. https://doi.org/10.1088/1748-9326/11/10/100201

Miller, R.L., Fram, M., Fujii, R., Wheeler, G., 2008. Subsidence Reversal in a Re-established Wetland in the Sacramento-San Joaquin Delta, California, USA. San Fr. Estuary Watershed Sci. 6.

Mitsch, W.J., Bernal, B., Nahlik, A.M., Mander, Ü., Zhang, L., Anderson, C.J., Jørgensen, S.E., Brix, H., 2013. Wetlands, carbon, and climate change. Landsc. Ecol. 28, 583–597. https://doi.org/10.1007/s10980-012-9758-8

Mitsch, W.J., Mander, Ü., 2018. Wetlands and carbon revisited. Ecol. Eng. 114, 1–6. https://doi.org/10.1016/j.ecoleng.2017.12.027

Mitsch, W.J., Zhang, L., Anderson, C.J., Altor, A.E., Hernández, M.E., 2005. Creating riverine wetlands: Ecological succession, nutrient retention, and pulsing effects. Ecol. Eng. 25, 510–527. https://doi.org/10.1016/j.ecoleng.2005.04.014

Moffat, A.M., Papale, D., Reichstein, M., Hollinger, D.Y., Richardson, A.D., Barr, A.G., Beckstein, C., Braswell, B.H., Churkina, G., Desai, A.R., Falge, E., Gove, J.H., Heimann, M., Hui, D., Jarvis, A.J., Kattge, J., Noormets, A., Stauch, V.J., 2007. Comprehensive comparison of gap-filling techniques for eddy covariance net carbon fluxes. Agric. For. Meteorol. 147, 209–232. https://doi.org/10.1016/j.agrformet.2007.08.011

Monteith, J.L., 1981. Evaporation and Surface Temperature. Q. J. R. Meteorol. Soc. 107, 1–27.

Monteith, J.L., 1965. Evaporation and environment. Symp. Soc. Exp. Biol. 19.

Moomaw, W.R., Chmura, G.L., Davies, G.T., Finlayson, C.M., Middleton, B.A., Natali, S.M., Perry, J.E., Roulet, N., Sutton-Grier, A.E., 2018. Wetlands In a Changing Climate: Science, Policy and Management. Wetlands 38, 183–205. https://doi.org/10.1007/s13157-018-1023-8

Mooney, H.A., Dunn, E.L., Harrison, A.T., Morrow, P.A., Bartholomew, B., Hays, R.L., 1971. Mobile laboratory for gas exchange measurements. Photosynthetica.

Moreno-Mateos, D., Barbier, E.B., Jones, P.C., Jones, H.P., Aronson, J., López-López, J.A., McCrackin, M.L., Meli, P., Montoya, D., Rey Benayas, J.M., 2017. Anthropogenic ecosystem disturbance and the recovery debt. Nat. Commun. 8, 8–13. https://doi.org/10.1038/ncomms14163

Moreno-Mateos, D., Power, M.E., Comín, F.A., Yockteng, R., 2012. Structural and functional loss in restored wetland ecosystems. PLoS Biol. 10. https://doi.org/10.1371/journal.pbio.1001247

Mount, J., Twiss, R., 2005. Subsidence, Sea Level Rise, and Seismicity in the Sacramento–San Joaquin Delta. San Fr. Estuary Watershed Sci. 3. https://doi.org/10.5811/westjem.2011.5.6700

Myhre, G., Shindell, D., Bréon, F.-M., Collins, W., Fuglestvedt, J., Huang, J., Koch, D., Lamarque, J.-F., Lee, D., Mendoza, B., Nakajima, T., Robock, A., Stephens, G., Takemura, T., Zhang, H., 2013. 2013: Anthropogenic and Natural Radiative Forcing. In: Climate Change 2013: The Physical Science Basis. Contribution of Working Group I to the Fifth Assessment Report of the Intergovernmental Panel on Climate Change.

Neubauer, S.C., 2014. On the challenges of modeling the net radiative forcing of wetlands: Reconsidering Mitsch et al. 2013. Landsc. Ecol. 29, 571–577. https://doi.org/10.1007/s10980-014-9986-1

Neubauer, S.C., Megonigal, J.P., 2015. Moving Beyond Global Warming Potentials to Quantify the Climatic Role of Ecosystems. Ecosystems. https://doi.org/10.1007/s10021-015-9879-4

Nisbet, E.G., Dlugokencky, E.J., Manning, M.R., Lowry, D., Fisher, R.E., France, J.L., Michel, S.E., Miller, B., White, J.W.C., Vaughn, B., Bousquet, P., Pyle, J.A., Warwick, N.J., Cain, M., Brownlow, R., Zazzeri, G., Lanoisell, M., Manning, A.C., Gloor, E., Worthy, D.E.J.,

Brunke, E.-G., Labuschagne, C., Wolff, E.W., Ganesan, A.L., 2016. Rising atmospheric methane: 2007–2014 growth and isotopic shift. Glob. Biogeochem. Cycles 30, 1–15. https://doi.org/10.1002/2015GB005326.Received

Nisbet, E.G., Manning, M.R., Platt, S.M., Hossaini, R., Bousquet, P., Hermansen, O., Vaughn, B., Brownlow, R., White, J.W.C., Fisher, R.E., Myhre, C.L., Michel, S.E., Levin, I., France, J.L., Pyle, J.A., Manning, A.C., Jones, A.E., Lowry, D., Allen, G., Dlugokencky, E.J., Cain, M., Myhre, G., Warwick, N.J., 2019. Very strong atmospheric methane growth in the four years 2014-2017: Implications for the Paris Agreement. Global Biogeochem. Cycles. https://doi.org/10.1029/2018gb006009

Novick, K.A., Desai, A.R., Biederman, J.A., Moore, D.J.P., Scott, R.L., Litvak, M.E., Torn, M.S., 2018. The AmeriFlux network: A coalition of the willing. Agric. For. Meteorol. 249, 444–456. https://doi.org/10.1016/j.agrformet.2017.10.009

Nunez, F., Pavley, F., 2006. AB 32 California Global Warming Solutions Act of 2006.

Odum, E.., 1969. The Strategy of Ecosystem Development. Science (80-. ). 164, 262–270.

Oikawa, P.Y., Jenerette, G.D., Knox, S.H., Sturtevant, C., Verfaillie, J.G., Dronova, I., Poindexter, C.M., Eichelmann, E., Baldocchi, D.D., 2016a. Evaluation of a hierarchy of models reveals importance of substrate limitation for predicting carbon dioxide and methane exchange in restored wetlands. J. Geophys. Res. Biogeosciences. https://doi.org/10.1002/2016JG003438

Oikawa, P.Y., Sturtevant, C., Knox, S.H., Verfaillie, J.G., Huang, Y., Baldocchi, D.D., 2016b. Revisiting the Partitioning of Net Ecosystem Exchange of CO2 into Photosynthesis and Respiration with Simultaneous Flux Measurements of 13CO2 and CO2, Soil Respiration and a Biophysical Model, CANVEG. Agric. For. Meteorol. 234–235, in press. https://doi.org/10.1016/j.agrformet.2016.12.016

Olson, D.M., Griffis, T.J., Noormets, A., Kolka, R., Chen, J., 2013. Interannual, seasonal, and retrospective analysis of the methane and carbon dioxide budgets of a temperate peatland. J. Geophys. Res. Biogeosciences 118, 226–238. https://doi.org/10.1002/jgrg.20031

Papale, D., Reichstein, M., Aubinet, M., Canfora, E., Bernhofer, C., Kutsch, W., Longdoz, B., Rambal, S., Valentini, R., Vesala, T., Yakir, D., 2006. Towards a standardized processing of Net Ecosystem Exchange measured with eddy covariance technique: algorithms and uncertainty estimation. Biogeosciences 3, 571–583. https://doi.org/10.5194/bg-3-571-2006

Parmentier, F.J.W., Van Huissteden, J., Van Der Molen, M.K., Schaepman-Strub, G., Karsanaev, S.A., Maximov, T.C., Dolman, A.J., 2011. Spatial and temporal dynamics in eddy covariance observations of methane fluxes at a tundra site in northeastern Siberia. J. Geophys. Res. Biogeosciences. https://doi.org/10.1029/2010JG001637

Pathak, T., Maskey, M., Dahlberg, J., Kearns, F., Bali, K., Zaccaria, D., 2018. Climate Change Trends and Impacts on California Agriculture: A Detailed Review. Agronomy 8, 25. https://doi.org/10.3390/agronomy8030025

Paustian, K., Lehmann, J., Ogle, S., Reay, D., Robertson, G.P., Smith, P., 2016. Climate-smart soils. Nature 532, 49–57. https://doi.org/10.1038/nature17174

Paw U, K.T., Gao, W., 1988. Applications of solutions to non-linear energy budget equations.

Agric. For. Meteorol. 43, 121–145. https://doi.org/10.1016/0168-1923(88)90087-1

Perugini, L., Caporaso, L., Marconi, S., Cescatti, A., Quesada, B., de Noblet, N., House, J., Arneth, A., 2017. Biophysical effects on temperature and precipitation due to land cover change. Environ. Res. Lett. https://doi.org/10.1088/1748-9326/aa6b3f

Petrescu, A.M.R., Lohila, A., Tuovinen, J.-P., Baldocchi, D.D., Desai, A.R., Roulet, N.T., Vesala, T., Dolman, A.J., Oechel, W.C., Marcolla, B., Friborg, T., Rinne, J., Matthes, J.H., Merbold, L., Meijide, A., Kiely, G., Sottocornola, M., Sachs, T., Zona, D., Varlagin, A., Lai, D.Y.F., Veenendaal, E., Parmentier, F.-J.W., Skiba, U., Lund, M., Hensen, A., van Huissteden, J., Flanagan, L.B., Shurpali, N.J., Grünwald, T., Humphreys, E.R., Jackowicz-Korczyński, M., Aurela, M.A., Laurila, T., Grüning, C., Corradi, C.A.R., Schrier-Uijl, A.P., Christensen, T.R., Tamstorf, M.P., Mastepanov, M., Martikainen, P.J., Verma, S.B., Bernhofer, C., Cescatti, A., 2015. The uncertain climate footprint of wetlands under human pressure. Proc. Natl. Acad. Sci. U. S. A. 112, 4594–9. https://doi.org/10.1073/pnas.1416267112

Poindexter, C.M., Baldocchi, D.D., Matthes, J.H., Knox, S.H., Variano, E.A., 2016. The contribution of an overlooked transport process to a wetland's methane emissions. Geophys. Res. Lett. 1–9. https://doi.org/10.1002/2016GL068782.Received

Poulter, B., et al, 2017. Global wetland contribution to 2000–2012 atmospheric methane growth rate dynamics. Environ. Res. Lett. 12. https://doi.org/https://doi.org/10.1088/1748-9326/aa8391

Psarras, P., Krutka, H., Fajardy, M., Zhang, Z., Liguori, S., Dowell, N. Mac, Wilcox, J., 2017. Slicing the pie: how big could carbon dioxide removal be? Wiley Interdiscip. Rev. Energy Environ. 6, e253. https://doi.org/10.1002/wene.253

Pugh, C.A., Reed, D.E., Desai, A.R., Sulman, B.N., 2017. Wetland flux controls: how does interacting water table levels and temperature influence carbon dioxide and methane fluxes in northern Wisconsin? Biogeochemistry. https://doi.org/10.1007/s10533-017-0414-x

Raupach, M.R., 1998. Influences of local feedbacks on land-air exchanges of energy and carbon. Glob. Chang. Biol. 4, 477–494.

Rey-Sanchez, A.C., Morin, T.H., Stefanik, K.C., Wrighton, K., Bohrer, G., 2017. Determining total emissions and environmental drivers of methane flux in a Lake Erie estuarine marsh. Ecol. Eng. https://doi.org/10.1016/j.ecoleng.2017.06.042

Richardson, A.D., Hollinger, D.Y., 2007. A method to estimate the additional uncertainty in gap-filled NEE resulting from long gaps in the CO2 flux record. Agric. For. Meteorol. 147, 199–208. https://doi.org/10.1016/j.agrformet.2007.06.004

Rinne, J., Riutta, T., Pihlatie, M., Aurela, M., Haapanala, S., Tuovinen, J.P., Tuittila, E.S., Vesala, T., 2007. Annual cycle of methane emission from a boreal fen measured by the eddy covariance technique, in: Tellus, Series B: Chemical and Physical Meteorology. pp. 449–457. https://doi.org/10.1111/j.1600-0889.2007.00261.x

Rogelj, J., Popp, A., Calvin, K. V., Luderer, G., Emmerling, J., Gernaat, D., Fujimori, S., Strefler, J., Hasegawa, T., Marangoni, G., Krey, V., Kriegler, E., Riahi, K., Van Vuuren, D.P., Doelman, J., Drouet, L., Edmonds, J., Fricko, O., Harmsen, M., Havlík, P., Humpenöder, F., Stehfest, E., Tavoni, M., 2018a. Scenarios towards limiting global mean

temperature increase below 1.5 °c. Nat. Clim. Chang. 8, 325–332. https://doi.org/10.1038/s41558-018-0091-3

Rogelj, J., Shindell, D., Jiang, S., Fifita, P., Forster, B., Ginzburg, C., Handa, H., Kheshgi, S., Kobayashi, E., Kriegler, L., Mundaca, R., Seferian, M., Vilarino, V., 2018b. Mitigation pathways compatible with 1.5°C in the context of sustainable development.

Rotenberg, E., Yakir, D., 2010. Contributions of semi-arid forests to the climate system. Science (80-. ).

Roulet, N.T., 2000. Peatlands, carbon storage, greenhouse gases, and the Kyoto Protocol: Prospects and significance for Canada. Wetlands 20, 605–615. https://doi.org/10.1672/0277-5212(2000)020[0605:PCSGGA]2.0.CO;2

Roulet, N.T., Lafleur, P.M., Richard, P.J.H., Moore, T.R., Humphreys, E.R., Bubier, J., 2007. Contemporary carbon balance and late Holocene carbon accumulation in a northern peatland. Glob. Chang. Biol. https://doi.org/10.1111/j.1365-2486.2006.01292.x

Sachs, T., Giebels, M., Boike, J., Kutzbach, L., 2010. Environmental controls on CH4 emission from polygonal tundra on the microsite scale in the Lena river delta, Siberia. Glob. Chang. Biol. https://doi.org/10.1111/j.1365-2486.2010.02232.x

Sachs, T., Wille, C., Boike, J., Kutzbach, L., 2008. Environmental controls on ecosystem-scale CH 4 emission from polygonal tundra in the Lena River Delta, Siberia. J. Geophys. Res. 113, G00A03. https://doi.org/10.1029/2007JG000505

Sanderman, J., Hengl, T., Fiske, G.J., 2017. Soil carbon debt of 12,000 years of human land use. Proc. Natl. Acad. Sci. 2017, 201706103. https://doi.org/10.1073/PNAS.1706103114

Saunois, M., Bousquet, P., Poulter, B., Peregon, A., Ciais, P., Canadell, J.G., Dlugokencky, E.J., Etiope, G., Bastviken, D., Houweling, S., Janssens-Maenhout, G., Tubiello, F.N., Castaldi, S., Jackson, R.B., Alexe, M., Arora, V.K., Beerling, D.J., Bergamaschi, P., Blake, D.R., Brailsford, G., Brovkin, V., Bruhwiler, L., Crevoisier, C., Crill, P., Covey, K., Curry, C., Frankenberg, C., Gedney, N., Höglund-Isaksson, L., Ishizawa, M., Ito, A., Joos, F., Kim, H.S., Kleinen, T., Krummel, P., Lamarque, J.F., Langenfelds, R., Locatelli, R., Machida, T., Maksyutov, S., McDonald, K.C., Marshall, J., Melton, J.R., Morino, I., Naik, V., O'Doherty, S., Parmentier, F.J.W., Patra, P.K., Peng, C., Peng, S., Peters, G.P., Pison, I., Prigent, C., Prinn, R., Ramonet, M., Riley, W.J., Saito, M., Santini, M., Schroeder, R., Simpson, I.J., Spahni, R., Steele, P., Takizawa, A., Thornton, B.F., Tian, H., Tohjima, Y., Viovy, N., Voulgarakis, A., Van Weele, M., Van Der Werf, G.R., Weiss, R., Wiedinmyer, C., Wilton, D.J., Wiltshire, A., Worthy, D., Wunch, D., Xu, X., Yoshida, Y., Zhang, B., Zhang, Z., Zhu, Q., 2016. The global methane budget 2000-2012. Earth Syst. Sci. Data 8, 697–751. https://doi.org/10.5194/essd-8-697-2016

Schaefer, H., Fletcher, S.E.M., Veidt, C., Lassey, K.R., Brailsford, G.W., Bromley, T.M., Dlugokencky, E.J., Michel, S.E., Miller, J.B., Levin, I., Lowe, D.C., Martin, R.J., Vaughn, B.H., White, J.W.C., 2016. A 21st century shift from fossil-fuel to biogenic methane emissions indicated by 13CH4. Science 352, 80–84. https://doi.org/10.1126/science.aad2705

Schile, L.M., Byrd, K.B., Windham-Myers, L., Kelly, M., 2013. Accounting for non-photosynthetic vegetation in remote-sensing-based estimates of carbon flux in wetlands.

Remote Sens. Lett. 4, 542–551. https://doi.org/10.1080/2150704X.2013.766372

Schlesinger, W.H., Amundson, R., 2018. Managing for soil carbon sequestration: Let's get realistic. Glob. Chang. Biol. 20–23. https://doi.org/10.1111/gcb.14478

Schrier-Uijl, A.P., Kroon, P.S., Hendriks, D.M.D., Hensen, A., Van Huissteden, J., Berendse, F., Veenendaal, E.M., 2014. Agricultural peatlands: Towards a greenhouse gas sink - A synthesis of a Dutch landscape study. Biogeosciences. https://doi.org/10.5194/bg-11-4559-2014

Shurpali, N.J., Verma, S.B., Clement, R.J., Billesbach, D.P., 1993. Seasonal Distribution of Methane Flux in a Minnesota Peatland Measured by Eddy Correlation. J. Geophys. Res. 98655, 649–20.

Spahni, R., Wania, R., Neef, L., Van Weele, M., Pison, I., Bousquet, P., Frankenberg, C., Foster, P.N., Joos, F., Prentice, I.C., Van Velthoven, P., 2011. Constraining global methane emissions and uptake by ecosystems. Biogeosciences 8, 1643–1665. https://doi.org/10.5194/bg-8-1643-2011

Stanhill, G., 1970. Some results of helicopter measurements of the albedo of different land surfaces. Sol. Energy 13, 59–66. https://doi.org/10.1016/0038-092X(70)90007-1

Sturtevant, C., Ruddell, B.L., Knox, S.H., Verfaillie, J.G., Matthes, J.H., Oikawa, P.Y., Baldocchi, D.D., 2016. Identifying scale-emergent, nonlinear, asynchronous processes of wetland methane exchange. J. Geophys. Res. Biogeosciences 121, 188–204. https://doi.org/10.1002/2015JG003054

Suding, B.K., Higgs, E., Palmer, M., Callicott, J.B., Anderson, C.B., Gutrich, J.J., Hondula, K.L., Lafevor, M.C., Larson, B.M.H., Randall, A., 2015. Committing to ecological restoration. Science (80-. ). 348, 638–640.

Swann, A., Lague, M., 2018. Continental-scale consequences of tree die-offs in North America: identifying where forest loss matters most. Environ. Res. Lett. 13. https://doi.org/10.1088/1748-9326/aa727f

Syvitski, J.P.M., Kettner, A.J., Overeem, I., Hutton, E.W.H., Hannon, M.T., Brakenridge, G.R., Day, J., Vörösmarty, C., Saito, Y., Giosan, L., Nicholls, R.J., 2009. Sinking deltas due to human activities. Nat. Geosci. 2, 681–686. https://doi.org/10.1038/ngeo629

Teh, Y.A., Silver, W.L., Sonnentag, O., Detto, M., Kelly, M., Baldocchi, D.D., 2011. Large Greenhouse Gas Emissions from a Temperate Peatland Pasture. Ecosystems 14, 311–325. https://doi.org/10.1007/s10021-011-9411-4

Thom, A.S., 1972. Momentum, mass and heat exchange of vegetation. Q. J. R. Meteorol. Soc. 98, 124–134. https://doi.org/10.1002/qj.49709841510

Tian, H., Lu, C., Ciais, P., Michalak, A.M., Canadell, J.G., Saikawa, E., Huntzinger, D.N., Gurney, K.R., Sitch, S., Zhang, B., Yang, J., Bousquet, P., Bruhwiler, L., Chen, G., Dlugokencky, E., Friedlingstein, P., Melillo, J., Pan, S., Poulter, B., Prinn, R., Saunois, M., Schwalm, C.R., Wofsy, S.C., 2016. The terrestrial biosphere as a net source of greenhouse gases to the atmosphere. Nature 531, 225–228. https://doi.org/10.1038/nature16946

Tiedie, J.M., 1988. Ecology of denitrification and dissimilatory nitrate reduction to ammonium, in: Biology of Anaerobic Microorganisms. Wiley-Interscience Publication, Canada, pp.

179–244.

Tiemeyer, B., 2013. Klimarelevanz von Mooren und Anmooren in Deutschland: Ergebnisse aus dem Verbundprojekt "Organische Böden in der Emissionsberichterstattung" [Climate impact of peatlands and bogs in Germany: Results from the joint project“Organic soils in emissi, Thünen Working Paper 15 (Johann Heinrich von Thünen-Institut, Braunschweig, Germany).

Turner, A.J., Frankenberg, C., Wennberg, P.O., Jacob, D.J., 2017. Ambiguity in the causes for decadal trends in atmospheric methane and hydroxyl. Proc. Natl. Acad. Sci. 114, 5367–5372. https://doi.org/10.1073/pnas.1616020114

UNFCCC, 2015. Paris Agreement.

UNFCCC, 1997. Kyoto Protocol.

Veber, G., Kull, A., Villa, J.A., Maddison, M., Paal, J., Oja, T., Iturraspe, R., Pärn, J., Teemusk, A., Mander, Ü., 2017. Greenhouse gas emissions in natural and managed peatlands of America: Case studies along a latitudinal gradient. Ecol. Eng. https://doi.org/10.1016/j.ecoleng.2017.06.068

Verma, S.B., 1989. Aerodynamic resistances to transfers of heat, mass and momentum, in: Black, T.A., Spittlehouse, D.L., Novak, M.D., Price, D.T. (Eds.), Estimation of Areal Evapotranspiration. p. 13-.

Webb, E.K., Pearman, G.I., Leuning, R., 1980. Correction of flux measurements for density effects due to heat and water vapour transfer. Q. J. R. Meteorol. Soc. 106, 85–100. https://doi.org/10.1002/qj.49710644707

Weir, W.W., 1950. Subsidence of Peatlands of the Sacramento-San Joaquin Delta, California. Hilgardia 20.

Weltzin, J.F., Pastor, J., Harth, C., Bridgham, S.D., Updegraff, K., Chapin, C.T., Chapin6, C.T., 2000. Response of Bog and Fen Plant Communities to Warming and Water-Table Manipulations. Source Ecol. Ecol. 81, 3464–3478.

Whiting, G.J., Chanton, J.P., 2001. Greenhouse carbon balance of wetlands: Methane emission versus carbon sequestration. Tellus, Ser. B Chem. Phys. Meteorol. 53, 521–528. https://doi.org/10.3402/tellusb.v53i5.16628

Whittaker, R.H., Bormann, F.H., Likens, G.E., Siccama, T.G., 1974. The Hubbard Brook Ecosystem Study: Forest Biomass and Production. Ecol. Monogr. 44, 233–254. https://doi.org/10.2307/1942313

Wilson, D., Blain, D., Couwenberg, J., Evans, C.D., Murdiyarso, D., Page, S.E., Renou-Wilson, F., Rieley, J.O., Sirin, A., Strack, M., Tuittila, E.-S., 2016a. Greenhouse gas emission factors associated with rewetting of organic soils. Mires Peat 17, 1–28. https://doi.org/10.19189/MaP.2016.OMB.222

Wilson, D., Farrell, C.A., Fallon, D., Moser, G., Müller, C., Renou-Wilson, F., 2016b. Multi-year greenhouse gas balances at a rewetted temperate peatland. Glob. Chang. Biol. https://doi.org/10.1111/gcb.13325

Wilson, K., Goldstein, A., Falge, E., Aubinet, M., Baldocchi, D.D., Berbigier, P., Bernhofer, C.,

Ceulemans, R., Dolman, H., Field, C., Grelle, A., Ibrom, A., Law, B.E., Kowalski, A., Meyers, T., Moncrieff, J., Monson, R., Oechel, W.C., Tenhunen, J., Valentini, R., Verma, S.B., 2002. Energy balance closure at FLUXNET sites. Agric. For. Meteorol. 113, 223–243. https://doi.org/10.1016/S0168-1923(02)00109-0

Windham-Myers, L., Bergamaschi, B., Anderson, F., Knox, S., Miller, R., Fujii, R., 2018. Potential for negative emissions of greenhouse gases (CO2, CH4 and N2O) through coastal peatland re-establishment: Novel insights from high frequency flux data at meter and kilometer scales. Environ. Res. Lett. 13. https://doi.org/10.1088/1748-9326/aaae74

Worden, J.R., Bloom, A.A., Pandey, S., Jiang, Z., Worden, H.M., Walker, T.W., Houweling, S., Röckmann, T., 2017. Reduced biomass burning emissions reconcile conflicting estimates of the post-2006 atmospheric methane budget. Nat. Commun. https://doi.org/10.1038/s41467-017-02246-0

Wu, J., Roulet, N.T., 2014. Climate change reduces the capacity of northern peatlands to absorb the atmospheric carbon dioxide: The different responses of bogs and fens. Global Biogeochem. Cycles. https://doi.org/10.1002/2014GB004845

Yarwood, S.A., 2018. The role of wetland microorganisms in plant-litter decomposition and soil organic matter formation: a critical review. FEMS Microbiol. Ecol. 1–17. https://doi.org/10.1093/femsec/fiy175

Yu, Z.C., 2012. Northern peatland carbon stocks and dynamics: A review. Biogeosciences 9, 4071–4085. https://doi.org/10.5194/bg-9-4071-2012

Zhang, B., Tian, H., Lu, C., Chen, G., Pan, S., Anderson, C., Poulter, B., 2017. Methane emissions from global wetlands: An assessment of the uncertainty associated with various wetland extent data sets. Atmos. Environ. 165, 310–321. https://doi.org/10.1016/j.atmosenv.2017.07.001

Zhang, Y., Sachs, T., Li, C., Boike, J., 2012. Upscaling methane fluxes from closed chambers to eddy covariance based on a permafrost biogeochemistry integrated model. Glob. Chang. Biol. https://doi.org/10.1111/j.1365-2486.2011.02587.x

Zhang, Z., Zimmermann, N.E., Stenke, A., Li, X., Hodson, E.L., Zhu, G., Huang, C., Poulter, B., 2017. Emerging role of wetland methane emissions in driving 21st century climate change. Proc. Natl. Acad. Sci. U. S. A. 201618765. https://doi.org/10.1073/pnas.1618765114

Zhao, K., Jackson, R.B., 2014. Biophysical forcings of land-use changes from potential forestry activities in North America. Ecol. Monogr. 84, 329–353. https://doi.org/10.1890/12-1705.1

Zona, D., Oechel, W.C., Kochendorfer, J., Paw U, K.T., Salyuk, A.N., Olivas, P.C., Oberbauer, S.F., Lipson, D.A., 2009. Methane fluxes during the initiation of a large-scale water table manipulation experiment in the Alaskan Arctic tundra. Global Biogeochem. Cycles. https://doi.org/10.1029/2009GB003487